Calhoun
Institutional Archive of the Naval Postgraduate School

Calhoun: The NPS Institutional Archive

DSpace Repository

Theses and Dissertations | 1. Thesis and Dissertation Collection, all items

1968

Experimental investigation of turbulent jet attachment to a convex wall.

Johnson, Larry Dean

Monterey, California. Naval Postgraduate School

http://hdl.handle.net/10945/12147

Downloaded from NPS Archive: Calhoun

http://www.nps.edu/library

Calhoun is the Naval Postgraduate School's public access digital repository for research materials and institutional publications created by the NPS community. Calhoun is named for Professor of Mathematics Guy K. Calhoun, NPS's first appointed -- and published -- scholarly author.

Dudley Knox Library / Naval Postgraduate School
411 Dyer Road / 1 University Circle
Monterey, California USA 93943

NPS ARCHIVE
1968
JOHNSON, L.

EXPERIMENTAL INVESTIGATION OF TURBULENT JET ATTACHMENT TO A CONVEX WALL

by

Larry Dean Johnson

DUDLEY KNOX LIBRARY
NAVAL POSTGRADUATE SCHOOL
MONTEREY CA 93943-5101

UNITED STATES
NAVAL POSTGRADUATE SCHOOL

THESIS

EXPERIMENTAL INVESTIGATION OF TURBULENT

JET ATTACHMENT TO A CONVEX WALL

by

Larry Dean Johnson

September 1968

[redacted]

EXPERIMENTAL INVESTIGATION OF TURBULENT JET ATTACHMENT TO A CONVEX WALL

by

Larry Dean Johnson
Lieutenant, United States Navy
B.S.E.E., University of New Mexico, 1960

Submitted in partial fulfillment of the
requirements for the degree of

MASTER OF SCIENCE IN MECHANICAL ENGINEERING

from the

NAVAL POSTGRADUATE SCHOOL
September 1968

NPS ARCHIVE
1968
JOHNSON, L.
Rid J6235 c1

ABSTRACT

The effects of geometry and Reynolds number on the attachement of an air jet to a circular convex wall and the mechanism of high pressure recovery in convex-walled amplifiers are investigated. The results are presented in terms of normalized parameters suitable for comparison with theoretical predictions. Extremely high pressure recoveries are possible in convex-walled amplifiers due to the particular velocity distribution and entrainment characteristics exhibited by flow attached to a convex wall. The wall setback and the condition of the control port have very little influence on the flow downstream of the initial attachment region.

TABLE OF CONTENTS

LIST OF ILLUSTRATIONS

LIST OF SYMBOLS

A_c	cross sectional area of power jet
CF(P)	pressure correction factor
CF(T)	temperature correction factor
J	momentum per unit width
P_a	atmospheric pressure
P_s	wall pressure
P_o	average stagnation pressure in the power jet
P_t	local stagnation pressure
Q	volumetric flow rate
r	radius of convex wall
Rew	Reynolds number based on width of power jet
U	local velocity
U_m	maximum fluid velocity in a given profile
U_o	average velocity in the power jet
w	power jet width
x	downstream distance measured from origin of jet
y	distance from the boundary to the local velocity
y_m	distance from the boundary to the maximum local velocity
$y_{m/2}$	distance from the boundary to the point where the local velocity in the upper half of the jet is equal to one half of the maximum velocity
θ	convex wall angular position
ν	kinematic viscosity
ρ	fluid density

ACKNOWLEDGEMENT

The work described herein was made possible through the sponsorship of the Harry Diamond Laboratories of the United States Material Command, Washington, D. C. The author wishes to express his appreciation to Professor T. Sarpkaya for his guidance and encouragement during the course of the investigation. A special note of appreciation is also given to Messrs. K. Mothersell, J. Beck, and J. McKay, of the Mechanical Engineering Machine Shop, for their efforts in the construction of the experimental apparatus.

1. Introduction.

It is a matter of common observation that jets, particularly plane, two-dimensional jets, show a strong tendency to become attached to, and flow around, a nearby solid surface. This phenomenom, commonly referred to as the Coanda effect, has been widely used in the past decade as the basic principle of operation of fluid amplifier elements. Most of the research in the field of fluidics has been devoted to the study of straight-walled devices. Investigations by Kesler [1] and Sarpkaya and Kirshner [2] have suggested that a vented, convex-walled amplifier, Fig. 1, exhibits performance characteristics superior to those of a straight-walled amplifier.

The most critical parameters affecting the performance of a fluid amplifier are the sidewall setback, the splitter location, receiving aperture width, location of vents, splitter-cusp radius, and the geometry of the Coanda-walls. For a complete understanding of the reasons for the superiority of the curved wall amplifiers it is obvious that a systematic investigation of the curved-wall attachment, including the effects of the critical parameters, both singular and composite, must be made. Previous studies include those by Kadosch [3] on the separation of jets from curved surfaces, by Norman [4] on turbulent jet flow around a circular cylinder, by McGlaughlin and Greber [5] on curved wall attachment and separation for Reynolds numbers below the critical range, and by Kesler [1] on the deflection of turbulent jets by convex walls. All but the latter considered only the case of tangential jet impingement on the curved wall, i.e., employing neither a control port nor a setback.

It should be noted at this point that although the above investigations were primarily conducted for the purpose of developing suitable

fluidic devices, part of the attention stemmed from the possibility of obtaining thrust-vector control for applications on V/STOL aircraft.

Some of the lifting devices on V/STOL vehicles such as the jet-augmented flap exhibit behavior similar to that of Coanda flow around curved surfaces. It is therefore apparent that the information derived from a comprehensive study of the flow over a curved surface would have broad applications not only to fluidic devices but also to related fields such as the development of V/STOL aircraft.

At present, definitive analysis of the turning of laminer or turbulent jets is rather incomplete. At low Reynolds numbers, McGlaughlin and Greber [5] reported that a laminar jet separates from the curved surface at a relatively short distance from the jet exit. The separated jet becomes turbulent some distance downstream of this separation point and, at some critical Reynolds number, reattaches to the surface. This separation and reattachment results in an enclosed separation bubble. If the Reynolds number is further increased, the reattachment point moves upstream but the separation point does not change significantly. Increasing the Reynolds number further results in a size decrease, and eventual disappearance, of the separation bubble.

The transition zone in a turbulent jet is defined as the region where the jet becomes similiar in appearance to a flow of fluid from a source or pole of infinitely small thickness. In other words, it is the zone where the effect of the specific velocity distribution at the exit has vanished. According to the measurements of Liepman and Laufer [6], transition in a free jet occurs at a distance of $7 \times 10^4 \nu/U_o$ from the exit. Newman [4], in the case of a jet flow around a cylinder, found that transition in the outer portion of the flow occurred at a distance of about

$3 \times 10^4 \ \nu/U_o$ from the exit and in the inner boundary layer occasional bursts of turbulence were detected at $2 \times 10^4 \ \nu/U_o$ and transition was completed by about $7 \times 10^4 \ \nu/U$. For all of these measurements, transition was completed by approximately 25 degrees along the curved-wall.

Newman compared his data with the theoretical studies of Gortler [7] and Glauert [8]. Gortler's analysis of a free jet assumed that the eddy viscosity is constant across the flow at all downstream positions and thereby obtained a solution for the local mean velocity in a two-dimensional free turbulent jet as

$$U = U_m \operatorname{sech}^2 \frac{0.88\, y}{y_{m/2}} = \left[\frac{3\, J\sigma}{4\rho x}\right]^{\frac{1}{2}} \operatorname{sech}^2 \frac{y\sigma}{x} \qquad (1)$$

where σ was assumed to be a constant. Injecting a word of caution at this point, Lamb [9] noted that Gortler's similar profiles are achieved only after the effect of the initial profile has vanished. Also the measurements of Reichardt [10] and Forthmann [11] indicated a value of $\sigma = 12$ near the jet exit, decreasing to about 7.7 for large values of x/w.

Glauert obtained an approximate solution for the plane turbulent wall jet. His notation is shown in Fig. 2. The mean velocity profile consists of an inner boundary layer ($Y < Y_m$) and an outer half jet. The boundary layer, in which the eddy viscosity varies with y, was matched to the outer flow, in which the eddy viscosity was assumed constant as in Gortler's analysis of a free jet.

The inner profile of the jet was computed numerically by Glauert. The outer profile was taken to be similar to that of a free jet and given by

$$U = U_m \operatorname{sech}^2 \left[0.88 \left(\frac{y - y_m}{y_{m/2} - y_m} \right) \right] \qquad (2)$$

This solution assumes U_m proportional to x^{β} and $y_{m/2}$ proportional to x^{α}. Measurements of the plane turbulent wall jet by Forthamann [11] and Sigalla [12] yielded values of β and α as $-\frac{1}{2}$ and 1 respectively. These investigators also reported a constant value of $y_m / y_{m/2}$ of approximately 0.15.

Newman's experimentally obtained non-dimensional mean velocity profiles fell convincingly on a single curve. This curve was in extremely good agreement with Glauert's theory except for low values of U/U_m in the outer half jet. These profiles were all at positions corresponding to 45 degrees or greater and at a ratio of w/r of 0.027. Kesler's investigation [1], incorporating a control part, various values of setback, and a w/r ratio of 0.05, yielded velocity profiles showing, as would be expected, very poor correlation with Glauert's theory for angles of less than 66 degrees.

Newman's measured growth of $y_{m/2}$ around the cylinder resulted in a linear relationship between $y_{m/2}$ and x. This relationship was empirically represented as

$$\frac{y_{m/2}}{r\theta} = 0.11 \left(1 + 1.5 \frac{y_{m/2}}{r} \right) \tag{3}$$

where $(r + 1.5y_{m/2})$ represents the downstream distance. His comparison of the results obtained from equation (3) with those obtained for a wall jet indicated that the flow around a cylinder spreads more rapidly than that of a wall jet. Next, Newman derived an equation relating the non-dimensional surface static pressure distribution as a function of $y_{m/2}$, making the assumption that the flow streamlines were circles with centers at the center of the cylinder.

$$\left(\frac{P_a - P_s}{P_o - P_a}\right)\frac{r}{w} = \frac{8 \ln\left(\frac{4\, y_{m/2}}{3\, r}\right)}{\left(\frac{4\, y_{m/2}}{3\, r} + 1\right)^2 - 1 + 2 \ln \left(\frac{4\, y_{m/2}}{3\, r} + 1\right)^2} \qquad (4)$$

The actual level of the pressure distribution was about 30% lower than that predicted indicating that the underlying assumptions were not entirely correct. More will be said about this in a subsequent section.

In concluding his investigation, Newman derived an equation relating the dimensionless maximum velocity parameter

$$\frac{U_m^{\,2}\, r\, \rho\, \theta}{\left(P_o - P_a\right) w}$$

to $y_{m/2}$ and r as

$$\frac{U_m^{\,2}\, r\, \rho}{\left(P_o - P_a\right) w} = \frac{128}{9}\left[\left(\frac{4\, y_{m/2}}{3\, r} + 1\right)^2 - 1 + 2 \ln\left(\frac{4\, y_{m/2}}{3\, r} + 1\right)\right]^{-1} \qquad (5)$$

The following assumptions were made: (1) that the effect of skin friction on momentum was negligible; (2) that the streamlines were circles with centers at the center of the cylinder; and (3) that all velocity profiles were similiar. The comparison of his measured values with this theoretical relationship appeared to be satisfactory.

Sarpkaya and Kirshner [2] have reported pressure recoveries in convex-walled vented amplifiers which are in excess of those obtained by a one-dimensional isentropic flow analysis. In order to account for the excess energy (per unit mass) recovered at the load port above and beyond that at the source, the necessity of additional outputs such as a vent and/or a splitter plate, at which the average energy (per unit mass) is lower than the input was recognized. Kesler's experimental investigation [1] has shown

that, at low Reynolds numbers, the flow along a convex Coanda-wall rapidly undergoes an energy distribution with high-energy flow near the core and low-energy flow at the two sides of the core.

The first phase of the present investigation was the accumulation of velocity and pressure data for flow around a convex wall, with control port and setback, at high (but still subsonic) Reynolds numbers. The second phase consisted of the addition of a cusped splitter plate. The third phase was the study of the characteristics of the geometry consisting of a splitter plate and a vent. The geometry of all experimental apparatus utilized was similiar to that described by Sarpkaya and Kirschner [2].

2. Experimental Equipment and Procedures.

Three different arrangements of experimental apparatus, as shown in Figs. 3, 4, and 5, were utilized. The basic test assembly containing the steel tubing, transition piece, sliding panels, and side plates was common to all three arrangements.

Air, at approximately 200 psig, was supplied to the basic assembly through a one inch stop valve and then fed into a pressure regulator (maximum input of 400 psig and maximum output of 125 psig). From the regulator the air was directed into a Fisher-Porter rotameter and finally into the steel tubing of the basic assembly through a long length of plastic tubing.

All pressures were monitored by a differential-pressure transducer (either a Sanborn or Pace depending upon the magnitude of the pressure) connected to a Hewlett-Packard Model 7712 two channel strip recorder with a Sanborn 350-1100 C carrier preamplifier. To ensure maintenance of a reference zero on the recorder readout, individual pressure readings were taken through a common manifold which could be vented to the atmosphere between readings.

Velocity profiles were obtained through the use of either an impact tube or a pitot tube coupled with a micrometer barrel. The impact tube was made of a brass tubing of 0.058 inches O.D. and 0.026 inches I.D. The pitot tube O.D. was 0.063 inches and the I.D. was 0.021 inches. Four static holes were arranged around the perimeter of the shank 0.25 inches from the end. The micrometer barrel carriage moved along slots in the side panels in order that velocities could be measured at various angular positions along the convex wall.

Test Section #1 - 90 Degree Convex Wall.

Construction. The basic test assembly was fabricated from a sheet of 1"

plexiglass placed between two ½" sheets of plexiglass. Particulars of construction concerning the basic test section and the 90 degree convex wall may be found in Kesler's investigation [1].

To reiterate a few of the more important points, fourteen pressure taps were placed every 6 degrees around the convex wall. Observing the quadrant from downstream the taps, starting of 6 degrees, were located as follows: centerline, 1/16" to left of centerline, 1/16" to right of centerline, centerline, etc. The convex wall section was firmly attached to the side panels through the use of reference dowels and the sliding panels were moved to effect various values of setback. All flow surfaces were carefully hand-polished with rouge.

Procedure.

Each run consisted of selecting a proper setback, flow rate, and control port condition (open or closed). During operation the following parameters were recorded: (1) atmospheric pressure and temperature; (2) rotameter outlet pressure; (3) power jet wall pressure; (4) wall pressures along the convex wall; (5) velocity readings every 0.025" from the convex wall, in a plane normal to the wall, and every 12 degrees along the wall starting at 6 degrees; and (6) velocity at the center of the power jet immediately downstream of the power jet exit.

The three setbacks used, 0.025", 0.050", and 0.075", were set into the test section by means of a depth micrometer. Gage blocks, ¼", were inserted into the control port and the power jet opening to maintain parallelism.

The flow rates were established with the use of a calibrated rotameter. In measuring velocities, three flow rates were used for each setback and control port condition. These flow rates correspond to Reynolds

numbers (based on the power jet width) of 21,700, 32,700, and 51,500. In measuring wall pressures, six flow rates were used, corresponding to Reynolds numbers of 21,700, 28,000, 32,700, 43,000, 51,500, and 63,000.

Two pressure transducers were utilized during the investigation; a Sanborn differential pressure transducer (maximum pressure of 43 inches of HG) for static and stagnation pressure measurements at flows corresponding to Reynolds numbers of 33,000 and less, and a Pace differential pressure transducer (maximum pressure of 50 psig) for Reynolds numbers of greater than 33,000.

The calibration of the system was accomplished by connecting the pressure transducer and a micromanometer to the pressure manifold. The manifold was then vented to the atmosphere and the manometer zeroed. Next the manifold vent was closed and the valve connecting the power jet pressure tap to the manifold was opened. The flow rate was varied until the manometer level was raised to a position indicating 1" of water. The gain of the amplifier was then adjusted until a convenient deflection on the readout chart was achieved with attenuation on position #1. With the Sanborn transducer a full scale deflection of 50mm was used and with the Pace transducer a deflection of 25mm. The linearity of the recording system was regularly checked and no deviation from the straight calibration curve was detected.

After selecting the setback and control-port condition and balancing and calibrating the recorder, a typical run was made as follows:

(1) The flow rate was set with the rotameter;

(2) The manifold atmospheric vent was opened and the recorder reading positioned to zero;

(3) The manifold vent was closed and the rotameter outlet pressure valve was opened;

(4) After the pressure was recorded, the valve was closed and the vent valve again opened and the recorder reading checked to ensure it was zeroed;

(5) This procedure was repeated for the power jet wall pressure and the fourteen pressure taps along the convex wall;

(6) Again using the same zeroing procedure, velocity profiles were taken at 6, 18, 30, 42, 54, 66, and 78 degree positions along the convex wall and a single velocity measurement at the center of the power jet immediately downstream of the power jet exit.

Test Section #2 - 90 Degree Convex Wall and Splitter Plate.

Construction. A cusped splitter plate, as depicted in Fig. 6, was constructed of 1" plexiglass. To accommodate the Pitot tube, three holes, 3/16" in diameter, were drilled in the midplane of the splitter plate and each inclined to such an angle that velocity measurements could be taken normal to the curved wall at approximately 30, 42, and 54 degree positions. All surfaces of the plate, including the cusp, were carefully hand polished and extreme care was employed to keep the leading edges of the cusp as sharp as possible (edge radius was approximately 0.001").

The test section described previously was utilized with no change in dimensions. The splitter plate was installed in this test section by means of two reference dowels and one nut and bolt.

Procedure.

The same procedures to ensure zero reference were again utilized. Static pressures at the fourteen convex wall taps and at the power jet wall tap were recorded for eight flow rates between Reynolds numbers of 15,000 and 70,000, each at a setback of 0.025" and for both open and closed control port conditions.

It was noted that the flow would attach to the curved wall, the splitter wall, or oscillate between the two, depending upon the flow rate and the condition of the control port. This observation precipitated an attempt to define these flow "regimes" as a function of the Reynolds number. To accomplish this, small tufts of thread were attached to the trailing edge of the splitter plate, to the 90 degree position of the convex wall, and to a wire between the two walls, to provide visual observation of the flow position. The flow rate was slowly increased from zero to the maximum capacity of the rotameter and flow rates corresponding to transition points (transition from attachment to curved wall to attachment to the splitter wall, etc.) were recorded. Next the flow rate was decreased from the maximum and transition points again recorded. As this visual technique is especially vulnerable to human fallability, identical runs were made on three different days and the results compared. No appreciable variance was noted. This investigation was conducted for setbacks of 0.025" and 0.075" together with both open and closed control port conditions.

Velocity profiles were measured at the 30 degree position on the convex wall for two flow rates (Reynolds numbers of 21,700 and 51,500) corresponding to two different flow "regimes." Each profile was taken at a setback of 0.025" for both open and closed control port conditions. Due to the unstable flow between the convex wall and the splitter plate, no velocity measurements were taken in this region.

Test Section #3 - 24 Degree Convex Wall, Vent, and Splitter Plate.

Construction. For the final phase of this investigation a 24 degree convex wall segment and a straight-walled load port panel were fabricated to replace the 90 degree convex wall. The basic test assembly and the splitter plate used in test section #3 were again employed for this test section.

The 24 degree wall segment was constructed of 1" plexiglass as shown in Fig. 7. Pressure taps were drilled in this segment, with a number 67 drill bit, every 6 degrees following the same staggering sequence as used in the 90 degree convex wall. One additional tap was drilled on the segment centerline approximately 2 degrees from the leading edge. As before, the walls were carefully polished.

The load port panel, as pictured in Fig. 7, was also fabricated of 1" plexiglass. Again using a number 67 drill bit, six pressure taps were drilled in the rounded and straight walls of the panel. The three taps on the rounded section lie on the centerline of the panel and the three on the straight section were staggered as follows; centerline, 1/16" to the left of centerline, and 1/16" to the right of centerline.

The only change to the splitter plate was the plugging of the impact tube across holes with Castoglass and subsequent repolishing of the surfaces.

To attain the configuration shown in Fig. 5, the 24 degree segment was installed in the basic test assembly and positioned by means of reference dowels. Next the splitter plate and load port panel were installed and positioned with dowels using the 24 degree segment as a reference. Finally, using a ¼" gage block for the power jet opening and a 1/8" gage block for the control port to retain parallelism, the sliding panels were adjusted to achieve a setback of 0.025."

Procedure.

Again following the measuring techniques outlined for test section #1, static pressures on the convex wall, the load port panel wall, and the power jet wall were recorded for flow rates corresponding to Reynolds numbers of 10,100, 21,700, 32,700, 51,500, and 63,000, each with setback of 0.025" and with control port both open and closed.

Velocity profiles normal to the convex wall at 21 degrees (i.e., with the impact tube as far downstream as the splitter plate would allow) and at the center of the power jet exit were recorded for the same five flow rates, setback, and control port conditions listed above.

Both the Pitot tube and the impact tube were utilized to obtain velocity profiles at 16 degrees in order to ascertain the error associated with ignoring the static pressure. The 16 degree position was the maximum downstream position possible due to the necessarily large shank length of the Pitot tube.

Next the Pitot tube was placed at the 16 degree position approximately 0.2 inches above the wall and slowly transversed across the width of the flow. Various flow rates were utilized. No change was noted in the measured pressures up to 3/8 inches to either side of the centerline.

Data Reduction. The following procedure was followed in the reduction of test data.

The flow rate in standard cubic feet per minute was calculated as

$$Q = \text{Rotameter reading} \times 100\% \text{ full flow} \times CF(T) \times CF(P)$$

where

$CF(P)$ = pressure correction factor

and

$CF(T)$ = atmospheric temperature correction factor

The correction factors were obtained from the Fisher - Porter instruction manual.

Next the average velocity in the power jet was calculated from

$$U_o = Q/A_c$$

Where A_c is cross sectional area of the power jet. As predicted by Schlichting [12] these calculated values were found to be 0.82 of the

velocity measured at the center of the power jet exit.

Using the average velocity in the power jet, the corresponding stagnation pressure was calculated.

$$P_o = P_a + \tfrac{1}{2} \rho U_o^2$$

The static wall pressures were put in dimensionless form as

$$\frac{(P_a - P_s)\, r}{(P_o - P_a)\, w}$$

and graphically presented as a function of the convex wall position θ.

Velocities were calculated as

$$U = \frac{2}{\rho}(P_t - P_a)^{\frac{1}{2}}$$

These velocities were then divided by U_o and plotted as functions of the normalized coordinate y/r. Reynolds numbers were calculated as

$$Rew = U_o\, w/\nu$$

All fluid properties were evaluated at 14.7 psia and 70 degrees F.

Experimental Uncertainty. Uncertainty in the velocity parameters was estimated using standard techniques. The following equation

$$\frac{\Delta\left(U/U_o\right)}{U/U_o} = \left[\frac{1}{4}\left(\frac{\Delta P_t}{P_t}\right)^2 + \left(\frac{\Delta Q}{Q}\right)^2 + \frac{1}{4}\left(\frac{\Delta \rho}{\rho}\right)^2 \right]^{\frac{1}{2}}$$

and the following approximate individual uncertainties (calculated for the worst possible conditions),

$$\frac{\Delta P_t}{P_t} \approx 0.030$$

$$\frac{\Delta Q}{Q} \approx 0.020$$

$$\frac{\Delta \rho}{\rho} \approx 0.016$$

yielded a maximum uncertainty interval of

$$U/U_o \ (1 \pm 0.026)$$

Up to this point, the assumption has been made that the static pressure in the jet was atmospheric. Comparing velocity profiles calculated using pressures from the impact tube and those from the Pitot tube, at 16 degrees on the convex wall of test section #3, showed velocities slightly greater in the latter case, particularly near the wall. These differences were of the same order of magnitude as the uncertainty calculated above.

An identical procedure gave a maximum uncertainty interval for the wall pressure parameter of

$$\frac{\left(P_a - P_s\right)_r}{\left(P_o - P_a\right)_w} \ (1 \pm 0.02)$$

3. Discussion of Results and Conclusions.

First the various pressure and velocity profiles obtained from flow over the 90 degree convex wall, varying setback and control port conditions, will be discussed. Next, the somewhat unstabalizing influence of combining the 90 degree convex wall and a straight-walled, cusped, splitter plate will be discussed. Finally, the flow over a convex wall coupled with a splitter plate and straight-walled load port, at different control port conditions and one value of setback, will be examined.

Figures 9 through 50 represent the dimensionless velocity parameter, U/U_m, as a function of the radial distance above the wall. Positions range from 6 degrees to 78 degrees in 12 degree increments. In Figs. 9 through 29 the control port was open and three values of setback were present for each flow rate. In Figs. 30 through 50 the control port was closed and again three values of setback were used. Each plot includes points for three different Reynolds numbers. Investigation of these plots at any angular position shows that all three flow rates coincide convincingly for any value of y/r. This indicates, at least for the range of subsonic flow rates considered, that the flow spread parameters, $y_{m/2}$ and y_m, are independent of the Reynolds number.

Figures 51 through 58 compare the mean velocity profiles described above as the setback is varied. When the control port is open, the velocity profiles are displaced further from the wall as the setback is increased. At the 6 degree position this offset is approximately 0.9 of the relative change in setback. By the time the flow has reached 18 degrees the offset of the profiles have been attenuated and by 30 degrees the outer-half-jets coincide very closely, with some difference in the profiles of the region between the maximum velocity and the wall. For positions corresponding to 42 degrees and greater, the three profiles are

essentially the same. In the case of the closed control port it is evident that there is no discernable difference at any angular position in the velocity profiles measured at different setbacks. This is undoubtably due to a low pressure region established in the closed control port. This region is created and maintained by the entrainment mechanism and, in effect, imposes a pressure gradient across the jet. This gradient "bends" the jet toward the wall negating to a great extent the effect of setback. Further substantiation of this observation is gained by considering a setback of 0.025 inches and comparing the open control-port mean velocity profiles with those of closed control port, Figs. 59 through 65. At 6 degrees, the closed port profile is offset from the open port profile, toward the wall, by a factor of, again, approximately 0.9 of the setback. It should also be noted that the maximum velocity of the open port profile is greater than that of the closed port. As the flow progresses along the wall, the maximum velocities and the radial distances above the wall to the location of the maximum velocities draw closer together. At some position in the vicinity of 42 degrees it appears that the maximum velocities and their respective radial distances are equal. Further downstream the open port velocities are greater than those with closed port at any given radial distance above the wall. The locations of the maximum velocities appear to be the same in the regions beyond 42 degrees but it is rather difficult to ascertain this observation due to the broadness of the profiles. Although not included in this report, similiar comparisons at setbacks of 0.050 inches and 0.075 inches illustrated the same trend.

Numerous analyses and experiments (see Schlichting [13]) have shown that in two-dimensional turbulent jets the centerline velocity decreases with distance from the nozzle as $x^{-\frac{1}{2}}$. But it should be noted that x is

measured from the origin or pole of the jet which does not necessarily coincide with the nozzle outlet. Fig. 66 shows a plot of the maximum velocity parameter, U_m/U_o, as a function of (r θ + control port width)$^{\frac{1}{2}}$. Also included on this graph is the relationship found by Newman using low Reynolds numbers and a w/r of 0.028. Since Newman obtained no data for angles of less than 45 degrees, his data was extrapolated to the left.

It is obvious that the maximum velocity parameter is not a linear function of the downstream distance from the power jet exit for values of θ between 0 and 54 degrees and that Newman's extrapolated curve shows no agreement with the authors except, possibly, for values of θ greater than 54 degrees (corresponding to an abcissa value of 2.23).

In order to compare this decrease in maximum, or centerline, velocity with the decrease in an unbounded free turbulent jet, the maximum velocity parameter was plotted as a function of the distance from the power jet exit divided by w (Fig. 67). The latter parameter is normally used as the independent variable when comparing velocity characteristics of rectangular nozzles with different widths (see Abramovich [14], Williams and Smetana [15], and McRee [16]). Figure 67 also contains curves constructed from free jet data gathered by Abramovich and McRee. Abramovich utilized a nozzle of width of 1.18 inches and a Reynolds number of 70,000. McRee's nozzle width was 0.01 inches and a Reynolds number of 6,200 was used. Both free jet curves show similiar shapes. The rate of maximum velocity decrease of the convex wall flow appears less than the free jet rates of decrease for abcissa values less than 10 (corresponding to θ values of less than 28 degrees) and greater than the free jet rates for abcissa values greater than 10. This phenomenon would, in part, explain the greater pressure recovery characteristics of a convex wall amplifier

or a momentum interaction amplifier. The data of Abramovich and McRee was the only free jet information that was available to the author and further investigation should be undertaken before a definite conclusion is reached.

For applications to fluid amplifiers the spread of the jet is of extreme importance. To be commercially feasible, the amplifiers should be as small as possible and the removal of the jet at the load port must take place before the jet begins to rapidly broaden. The mean velocity profiles were utilized to gain information concerning the spread parameters y_m and $y_{m/2}$. These parameters are defined in Fig. 1. As mentioned in the introduction, the $y_{m/2}$ of both a plane turbulent wall jet and a free jet is directly proportional to x. Figure 68 indicates that the increase in $y_{m/2}$ downstream of 18 degrees is roughly proportional to θ and similiar to the growth of $y_{m/2}$ of a free jet. Inspection of Fig. 69 indicates that y_m is approximately proportional to θ for angles greater than 30 degrees. This includes both open and closed control port conditions.

Figures 70 through 78 illustrate the dimensionless wall pressure as a function of the angular position. Each plot contains points for both the open and closed control port conditions at one value of setback and one Reynolds number. It is immediately apparent that in all cases the wall pressure with the closed control port is higher, i.e., closer to the abcissa which represents atmospheric pressure, than that with the open control port. The closed control port has been shown to deflect the jet before it reaches the upstream edge of the convex wall. Therefore, at the leading edge of the wall it is reasonable to assume that this jet requires less deflection to follow the wall curvature than the jet passing over the open control port. Consequently, the pressure gradient required for deflection is less. But the surprising aspect is that this pressure

difference extends the full length of the 90 degree quadrant. This argument emphasizes the nebulous interdependency of cause and effect.

Investigation of the shapes of these curves shows distinct pressure oscillations. These oscillations indicate the inherent attempt of the jet to proceed in a direction tangent to the circular wall. The jet might be thought of as undergoing a series of attachments, separations, and reattachments as it progresses along the wall. But it should be emphasized that none of the velocity profiles indicate actual separation with its resultant backflow.

Comparing all the pressure curves it is seen that their shapes are similiar from 18 to 84 degrees. All have maximum pressures at 18, 30, and 48 degrees. Beyond 66 degrees the pressure increases to accommodate the atmospheric pressure imposed at the end of the wall. The effect of setback, Reynolds number, and the control port conditions predominate between 0 and 12 degrees. As would be expected, at 6 degrees the difference between the open and closed control port conditions becomes greater as the setback is increased.

The value of the average pressure parameter between 18 and 66 degrees is in the vicinity of 1.80. Using Eq. 4 and measured average values of $y_{m/2}$ yields values of approximately 1.95 at 18 degrees decreasing to 1.80 at 66 degrees. Therefore, this equation appears to yield a fair approximation for the average wall pressure. It would thus be natural to conjecture that the measured velocity profiles will show enough similarity to Newman's proposed wall jet profiles. But a closer inspection of the equation reveals that his is an invalid conclusion. Assuming $y_{m/2}/r$ is much less than 1.0, expanding the logarithmic terms in a series, and rewriting gives

$$\frac{\left(P_a - P_s\right)_r}{\left(P_o - P_a\right)_w} \approx \frac{8}{\left(\frac{6\,r + 2\,y_{m/2}}{3\,r - 2\,y_{m/2}}\right) + 2} \approx 1.8 \text{ to } 2.0$$

This range will be maintained as long as r is large and the power jet exit width, w, is small. Newman's reported pressure measurements were made at values of w/r ranging from .040 to .013 and for various Reynolds numbers. The average pressure parameters varied between 1.2 and 1.6, increasing as w/r increased. Equation 4 again predicted values between 1.9 and 1.8 for these cases.

It is obvious by now that the present theoretical analyses are unable to completely explain flow around a convex wall. This is particularly true in the region of interest between 0 and 45 degrees.

Next a cusped straight wall splitter plate was added to the test section. This addition led to an unstable condition. At low Reynolds numbers (control port open) the flow remained attached to the curved wall with occasional small bursts along the straight wall of the splitter plate. The static wall pressure measured at the pressure tap located directly under the leading edge of the splitter plate indicated a much lower pressure than had previously been recorded. This was undoubtably caused by the upper part of the flow attempting to attach to the wall of splitter plate. As the Reynolds numbers increased the entire flow began oscillating between the curved wall and the splitter wall and finally attached fully to the splitter wall. Increasing the Reynolds number further, the sequence was reversed until the flow was again attached to the curved wall. With closed control port, the flow stayed attached to the curved wall until a very high flow rate was reached. At this point it attached to the splitter wall and remained attached through the highest flow rate that could be

achieved with the experimental apparatus. Measured velocity profiles at a position on the convex wall upstream of the splitter plate were identical to those obtained when the splitter was absent.

For the final phase of this investigation a vent and load port were added to the above test section. This, in effect, completed one half of the bistable amplifier described by Sarpkaya and Kirshner [2]. A setback of 0.025 inches and a control port width of 0.125 inches were used in this device. The convex wall extended to 24 degrees where a 0.375 inch wide vent was placed. Downstream of this a straight wall was installed parallel to the lower splitter wall to complete the load port.

Figure 79 shows the normalized velocity versus the normalized distance above the wall at 21 degrees with the control port open. Five flow rates, corresponding to Reynolds numbers ranging from 10,100 to 63,000, were used. All points fall convincingly on a single curve except those corresponding to a Reynolds number of 32,700. It was noted that for Reynolds numbers in the interval between 28,000 and 40,000 the vortex created by the cusp of the splitter ceased circulation and vented upwards. The vortex remained intact for flow rates outside this Reynolds number range. No mention is made of this phenomenon in the previous studies of convex-walled bistable amplifiers. This projects the possibility that the addition of the second convex wall in a complete amplifier affects conditions such that the vortex is not lost. Obviously further investigation is indicated.

Figure 80 is the velocity profile for the closed control port case. All points lay on a common curve and the vortex remained intact for all Reynolds numbers. Comparing the mean velocity profiles for open and closed control port conditions, Fig. 81,it is seen that the latter is closest to the wall and has a somewhat smaller maximum velocity. This

follows the trend observed with the 90 degree quadrant.

To ascertain the effect of the splitter plate and the vent on the flow along the convex wall upstream of the vent, the velocity profiles measured at 21 degrees on the 24 degree circular segment and those measured at 18 degrees on the 90 degree quadrant (without the splitter plate installed), were compared. As the control port width of the latter test section was 0.25 inches and that of the former was 0.125 inches, the 21 and 18 degree positions were approximately the same distance from the power jet exit. Figures 82 and 83 show that these profiles are virtually identical. It is also seen from Fig. 66 that the maximum velocity parameters measured at the 16 and 21 degree positions on the 24 degree segment lie very close to the locus of maximum velocities measured along the 90 degree quadrant. These observations indicate that the splitter plate and vent had a negligible influence on the velocity profiles upstream of the vent.

The load port captures the jet after it leaves the trailing edge of the convex wall and passes over the vent. In an attempt to estimate the amount of mass and momentum recovery at the load port, the following assumptions were made:

1) The velocity profile measured at 30 degrees on the 90 degree quadrant of the first test section would give a conservative approximation of the profile that enters the load port (See Fig. 84);
2) The velocity profile measured at 21 degrees on the 24 degree circular segment of the third test section would give a slightly high estimation of the profile that enters the load port;
3) The flow was two dimensional. It is known that the flow was

uniform across 3/4 of the width of the convex wall therefore this assumption appears valid.

The two profiles were projected on a tangent to the convex wall at the 24 degree position until they reached the load port. The captured portions of the profiles were manually integrated to ascertain the mass rate of flow and the momentum flux entering the load port. The first velocity profile (at the 30 degree position) yielded a mass rate of flow at the load port of 1.2 times that leaving the power jet exit and a momentum flux per unit mass of 1.05 times that at the power jet exit. The second velocity profile (at the 21 degree position) yielded a mass rate of flow of 1.26 times that at the power jet exit and a momentum flux per unit mass of 1.07 times that at the power jet exit. This relatively large increase in the mass rate of flow from the power jet exit to the load port is apparently caused by the entrainment of surrounding air as the jet progresses along the convex wall. If this entrainment is of the magnitude indicated by the above calculations, it is apparent that a steady flow analysis must include this entrainment effect in order to accurately describe the flow conditions at the load port. This reasoning would explain why the previously mentioned pressure recoveries in a vented convex-walled amplifier exceed those predicted by one-dimensional isentropic flow analysis.

The five static wall pressures measured on the 24 degree circular segment at Reynolds numbers of 21,700 and 51,500 (Figs. 85 and 86) again show the pressures with the control port open to be less than those with the closed control port except at the tap 2 degrees downstream of the leading edge of the wall. The pressures decrease downstream to a minimum value measured 1.5 degrees from the end of the segment. This seems in disagreement with the trend observed using only the 90 degree wall. But, since

the tangent to the 24 degree segment where the flow leaves is not parallel to the splitter wall, it can again be surmised that this pressure decrease is required to offset the tendency of the flow to leave the curved wall and attach to the straight wall of the splitter. Figure 87 illustrates the effect caused by the loss of the vortex on the wall pressure. The pressures obtained with the control port open at a Reynolds number of 32,700 are much higher than all other pressures measured.

In conclusion it can be seen that the observation of a two dimensional air jet, attached to a convex wall on one side and open to the atmosphere on the other, has implicitly delineated flow characteristics which would optimize the performance of a fluid logic device. These characteristics include:

1) Relatively small decrease in the maximum velocity up to the 40 degree position on the convex wall;
2) Velocity distributions such that high energy flow is maintained near the centerline of the jet and this centerline remains approximately the same radial distance above the convex wall for positions between 0 and 30 degrees;
3) Increased mass rate of flow due to entrainment of surrounding air;
4) Minimial effect on the flow due to various values of setback and different control port conditions.

The final phase of this investigation has shown that the addition of a splitter plate and a vent did not alter these convex wall flow characteristics.

4. Recommendations for Further Work.

The investigation described herein should be extended to:

1) the study of optimizing recovery pressures and flow rates by varying the relative positions of the load port panel and the splitter plate;
2) the effect of adding another convex wall and load port panel to complete the geometry of a bistable amplifier;
3) the effect of increasing the Mach number.

BIBLIOGRAPHY

1. Kesler, K., "Turbulent Jet Attachment to Convex Walls," Thesis submitted to the Naval Postgraduate School, Monterey, Calif.

2. Sarpkaya, T. and Kirshner, J., "The Comparative Performance Characteristics of Vented and Unvented, Cusped, and Straight and Curved-Wall Bistable Amplifiers," Proceedings of the Third Cranfield Fluidics Conference, Turin, Paper F3, May 1968.

3. Kadosch, M., "Attachment of a Jet to a Curved Wall," Proceedings of the 2nd Fluid Amplification Symposium, Vol. IV, May 1964.

4. Newman, B. G., "The Deflection of Plane Jets by Adjacent Boundaries - Coanda Effect," Boundary Layer and Flow Control - Its Principles and Application, ed. G. V. Lachmon, Vol. 1, Pergamon Press, 1961.

5. McGlaughlin, D. W. and Greber, I., "Experiments on the Separation of a Fluid Jet from a Curved Surface," Advances in Fluidics, ASME, 1967, pp: 14-30.

6. Liepmann, H. W. and Laufer, J., "Investigations of Free Turbulent Mixing," NACA TN 1947.

7. Gortler, H., "Berechnung von Aufgaben der frein Turbuleny auf Grund enies neuen Naherungsansatyes," Z. Angew. Math. Mech., 22, 244, 1942.

8. Glauert, M. B., "The Wall Jet," J. Fluid Mech., 1, 625, 1956.

9. Lamb, J. P., "An Approximate Theory for Developing Turbulent Free Shear Layers," J. Basic Eng., ASME, pp: 633-639, Sept. 1967.

10. Reichardt, H., "On a New Theory of Free Turbulence," J. Roy. Aero. Soc., 47, pp. 167, 1943.

11. Forthamann, E., "Uberturbulente Strahlausbreitung," Eng. - Arch., 5, 42, 1943: NACA TM 789, 1936.

12. Sigalla, A., "Measurements of Skin Friction in a Plane Turbulent Wall Jet," J. Roy. Aero. Soc., 62, 873, 1958.

13. Schlichting, H., Boundary - Layer Theory, Pergamon Press, 1955.

14. Abramovich, G. N., Theory of Turbulent Jets, M.I.T. Press, 1963.

15. Williams, J. C. and Smetana, F., "Theoretical Study of a Convergent Nozzle and Free Jet Flow," Proceedings of the Fluid Amplification Symposium, Vol. I, Oct. 1965.

16. McRee, D., "Experimental Study of a Convergent Nozzle and Free Jet Flow," Proceedings of the Fluid Amplification Symposium, Vol. I, Oct. 1965.

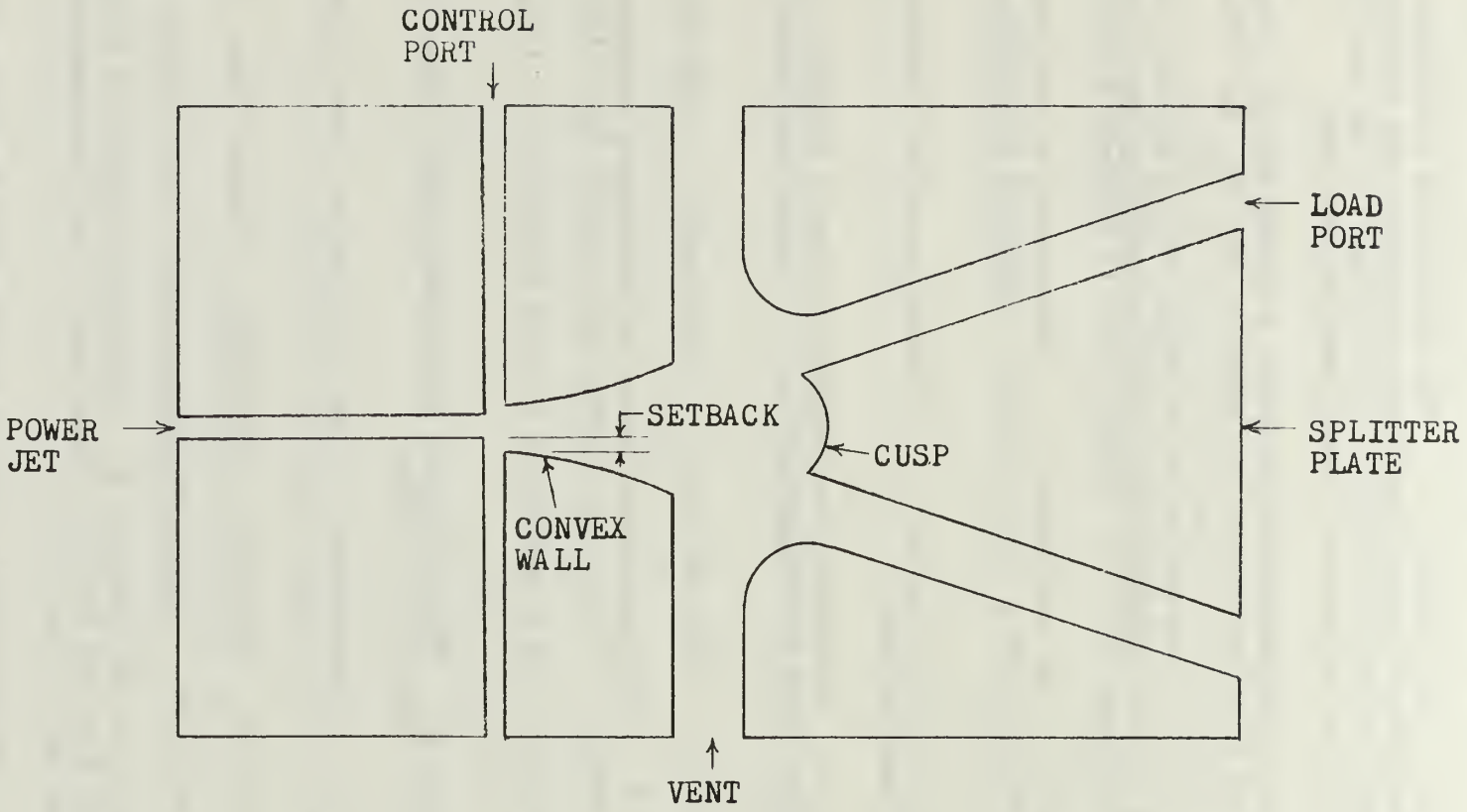

FIGURE 1. CONVEX-WALLED VENTED BISTABLE AMPLIFIER

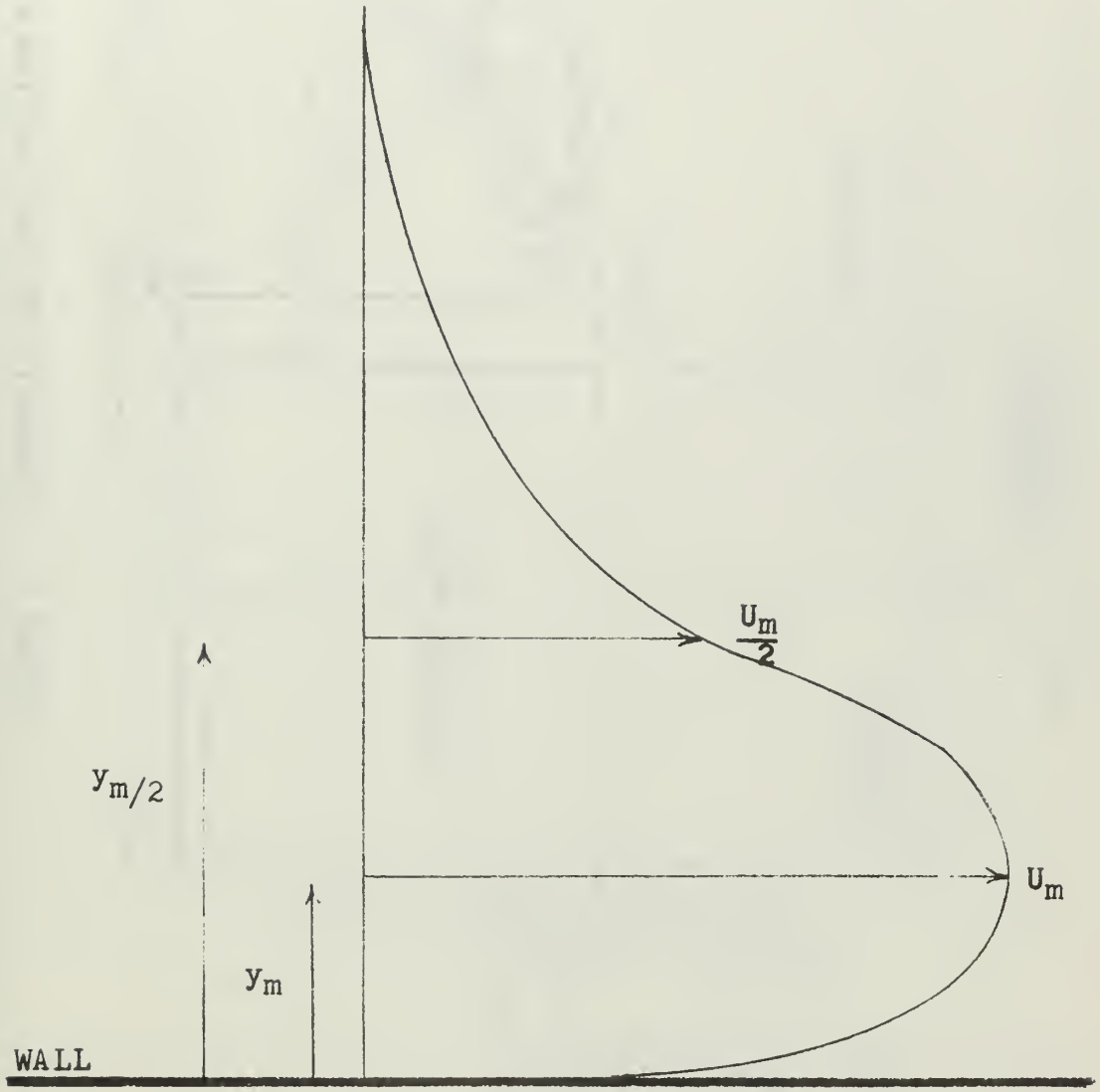

FIGURE 2. WALL JET

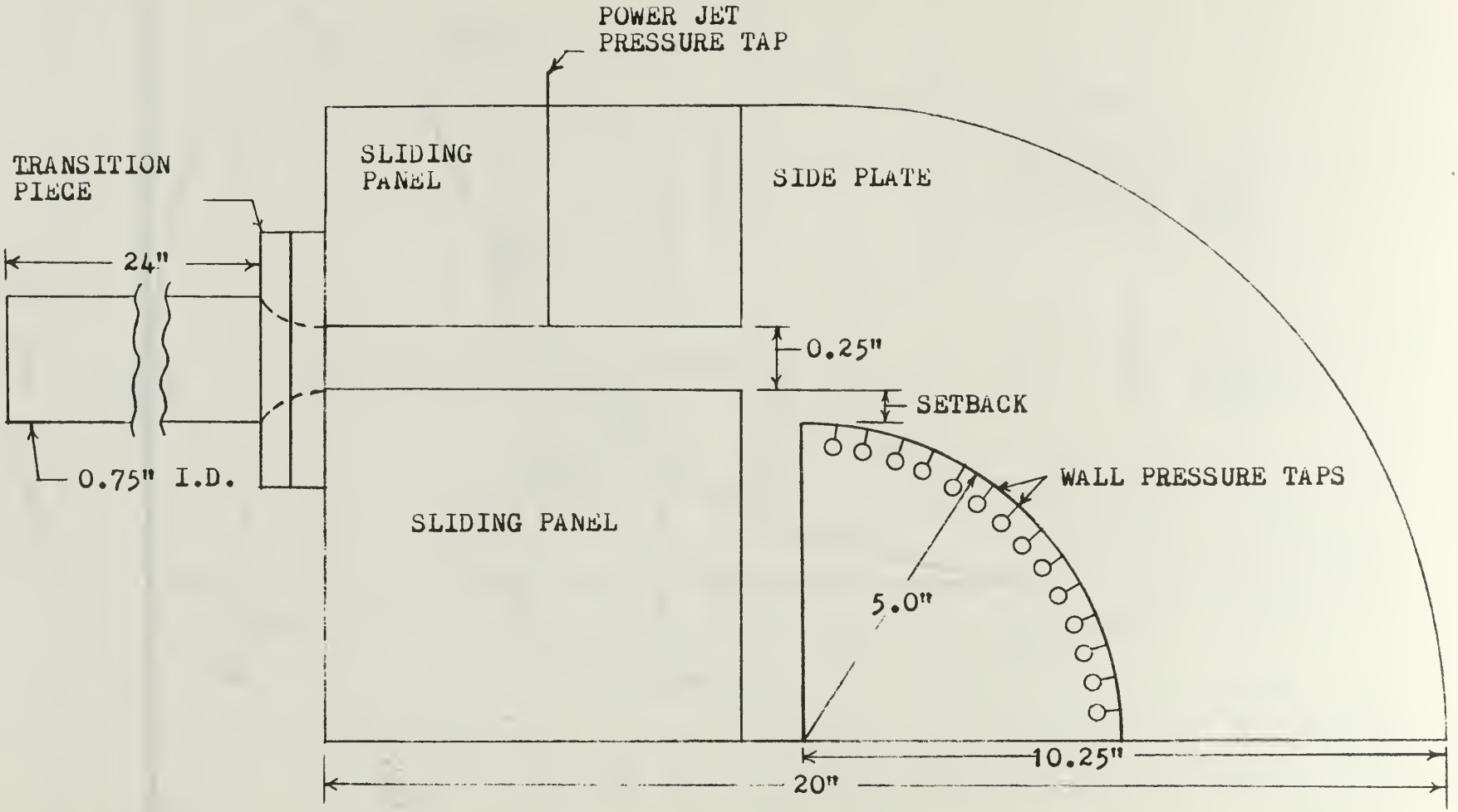

FIGURE 3. SCHEMATIC OF TEST SECTION #1

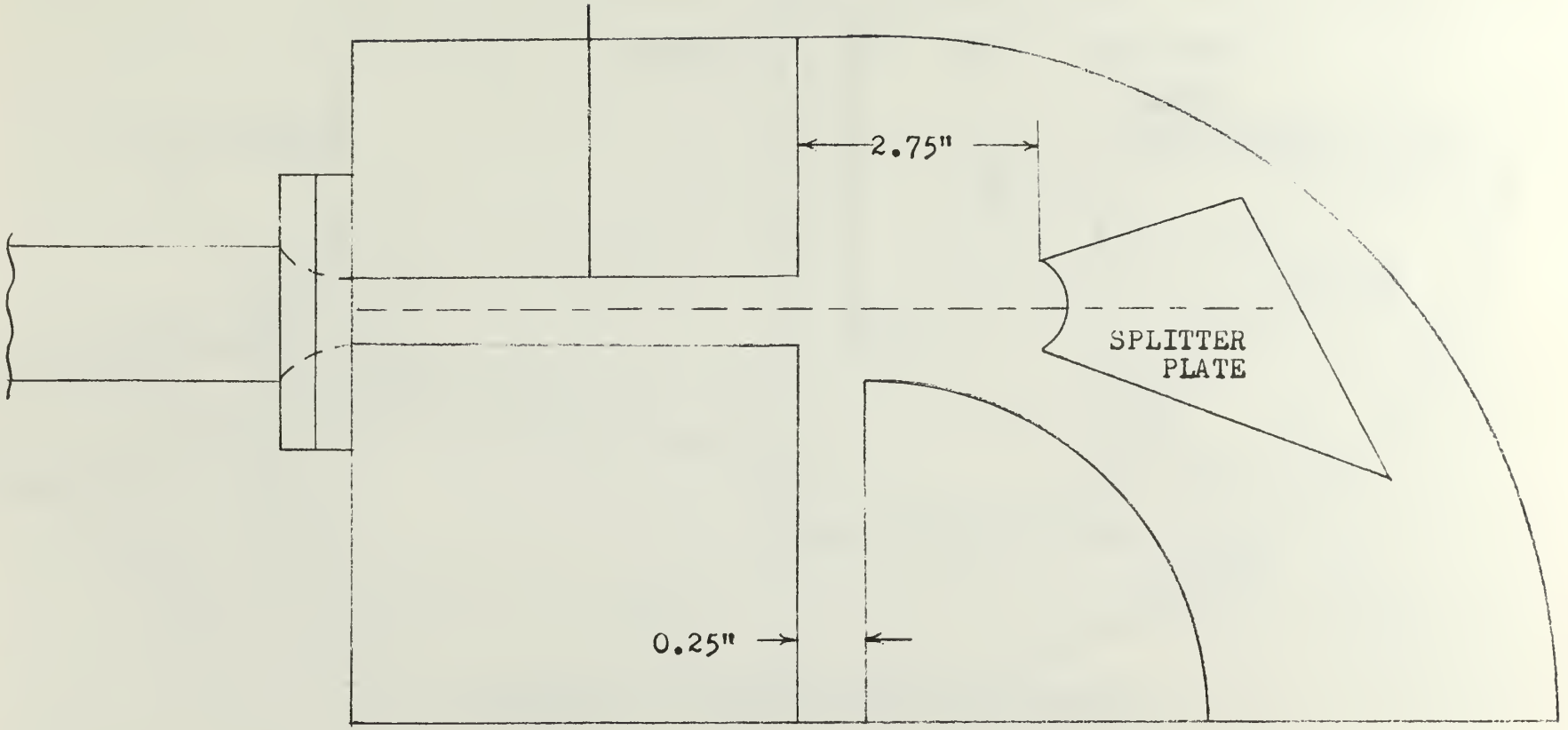

FIGURE 4. SCHEMATIC OF TEST SECTION #2

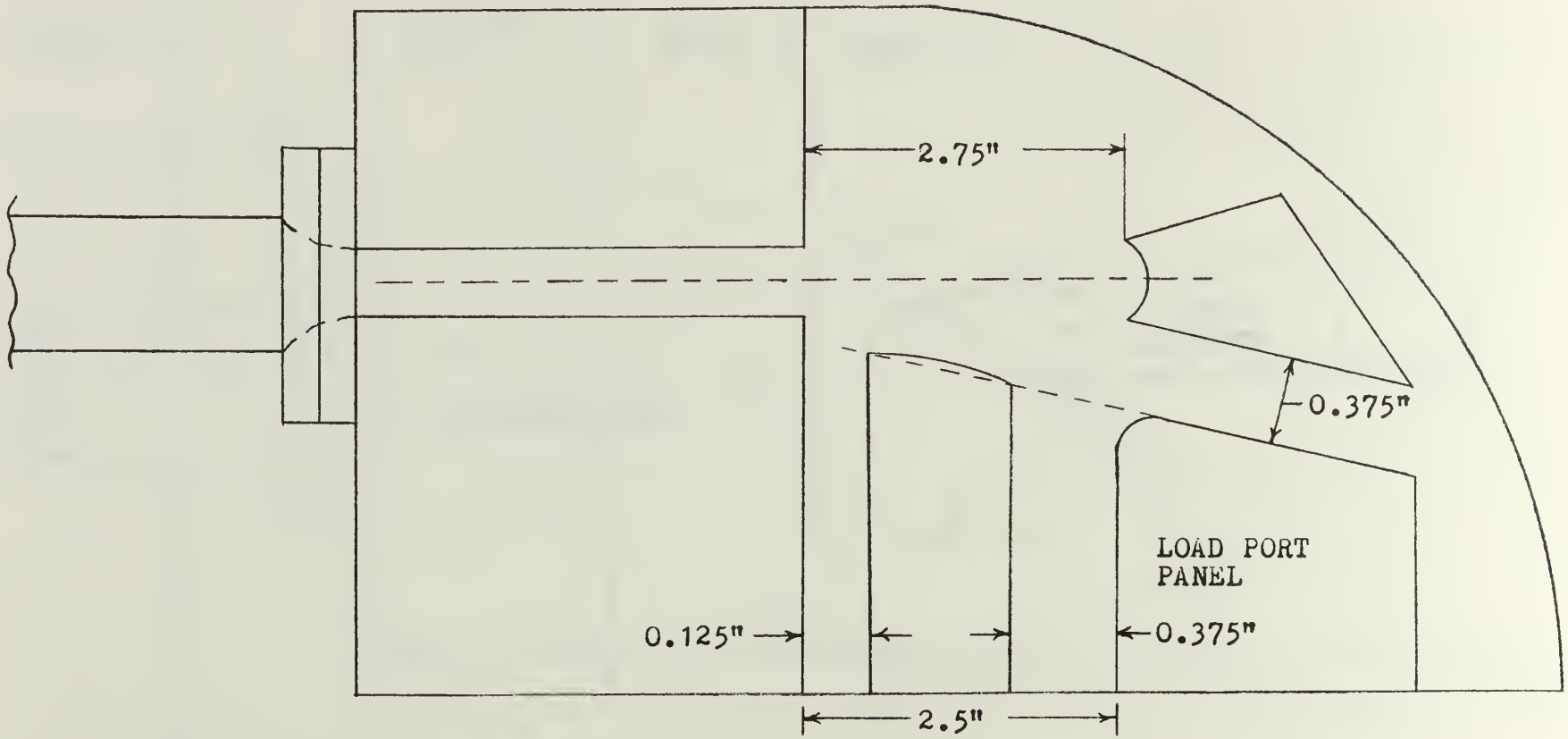

FIGURE 5. SCHEMATIC OF TEST SECTION #3

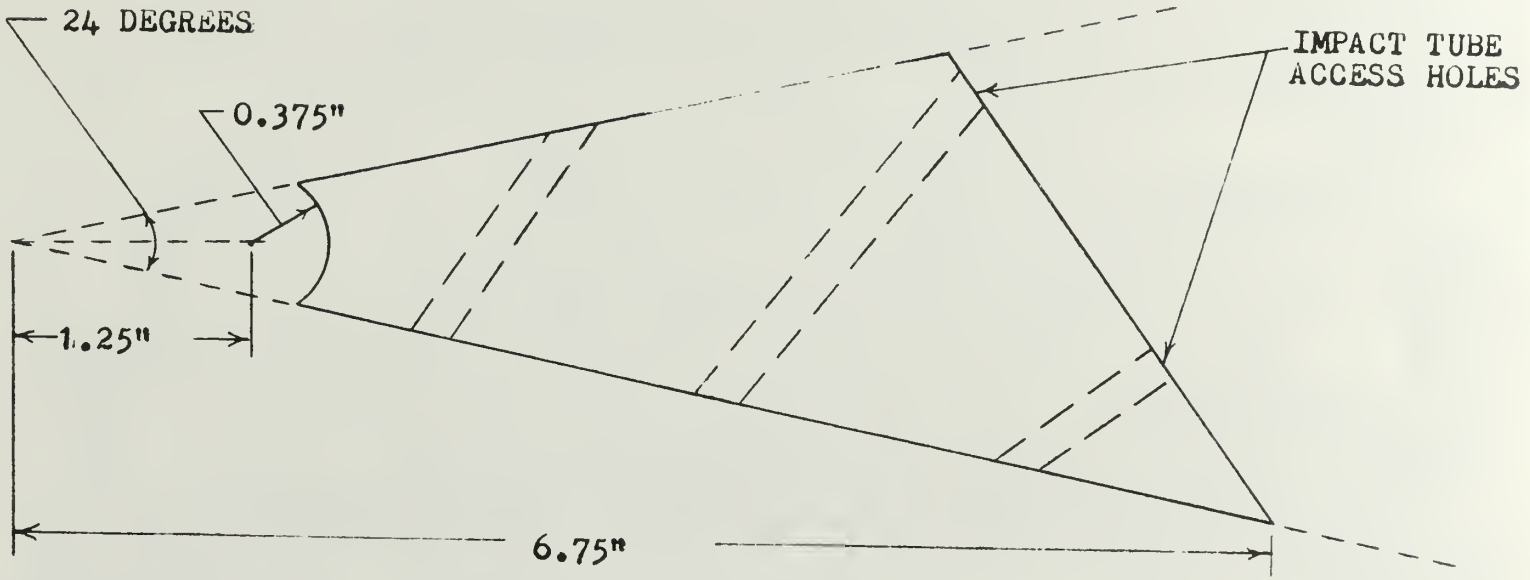

FIGURE 6. SCHEMATIC OF SPLITTER PLATE

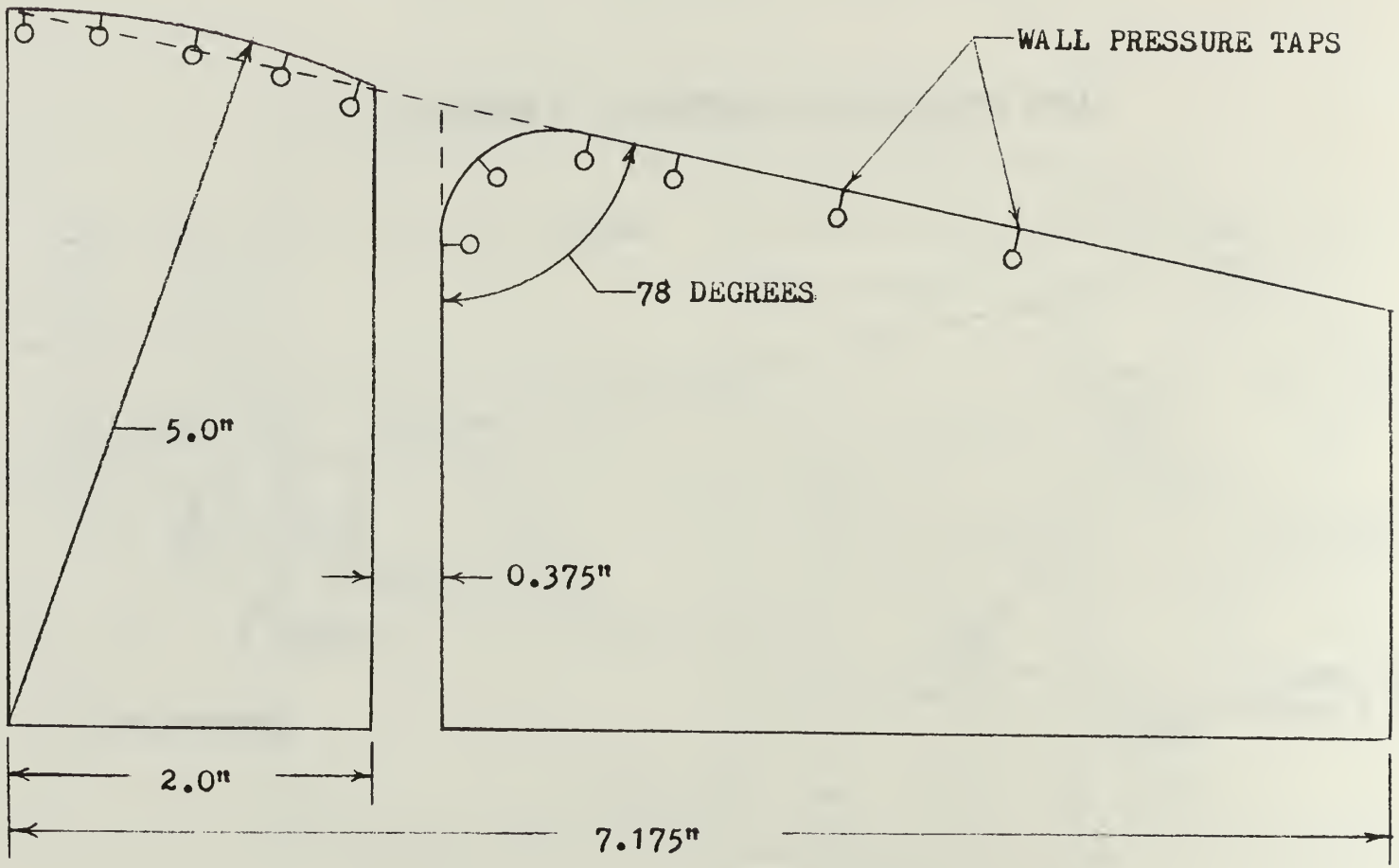

FIGURE 7. SCHEMATIC OF 24 DEGREE CIRCULAR SEGMENT AND LOAD PORT PANEL

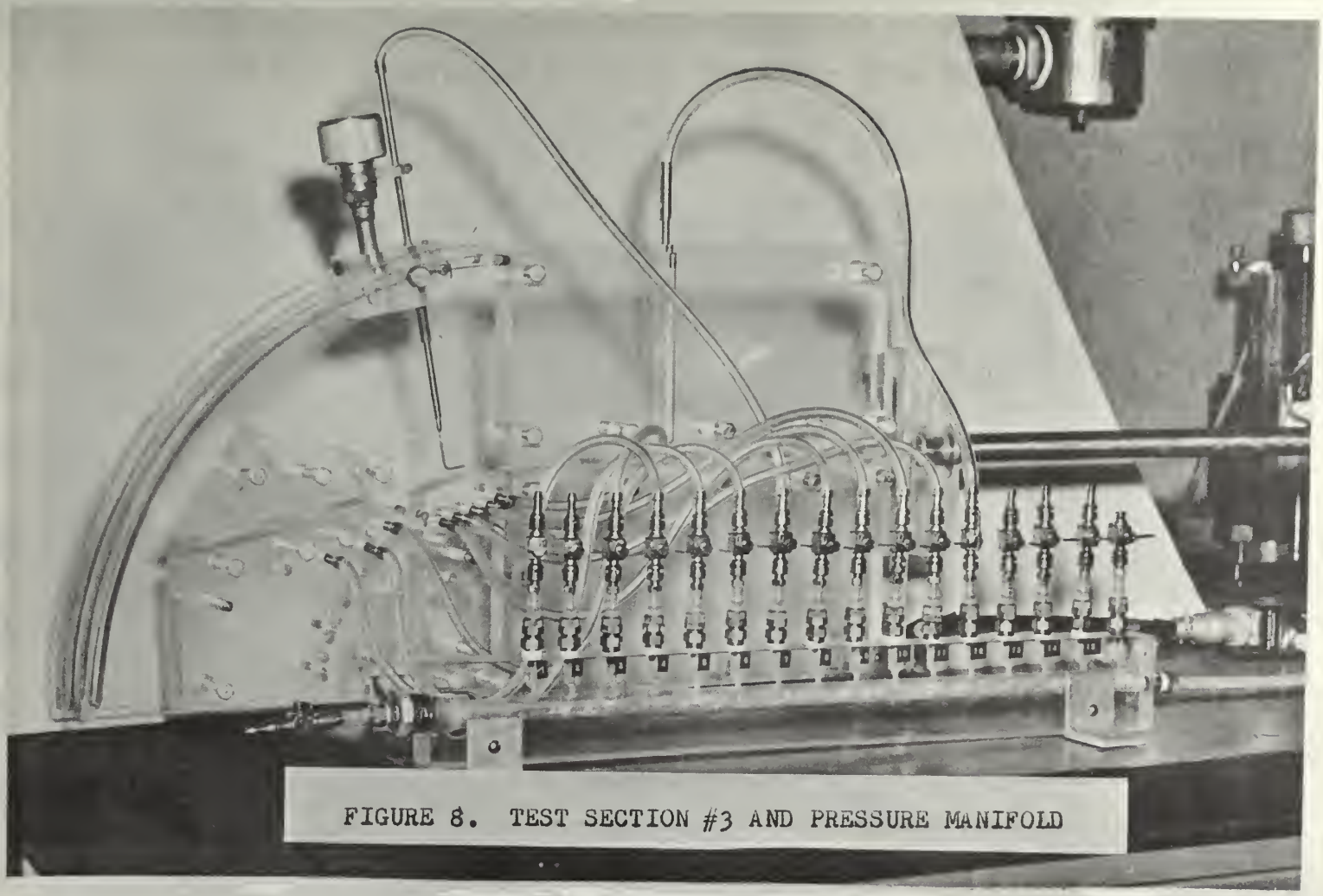

FIGURE 8. TEST SECTION #3 AND PRESSURE MANIFOLD

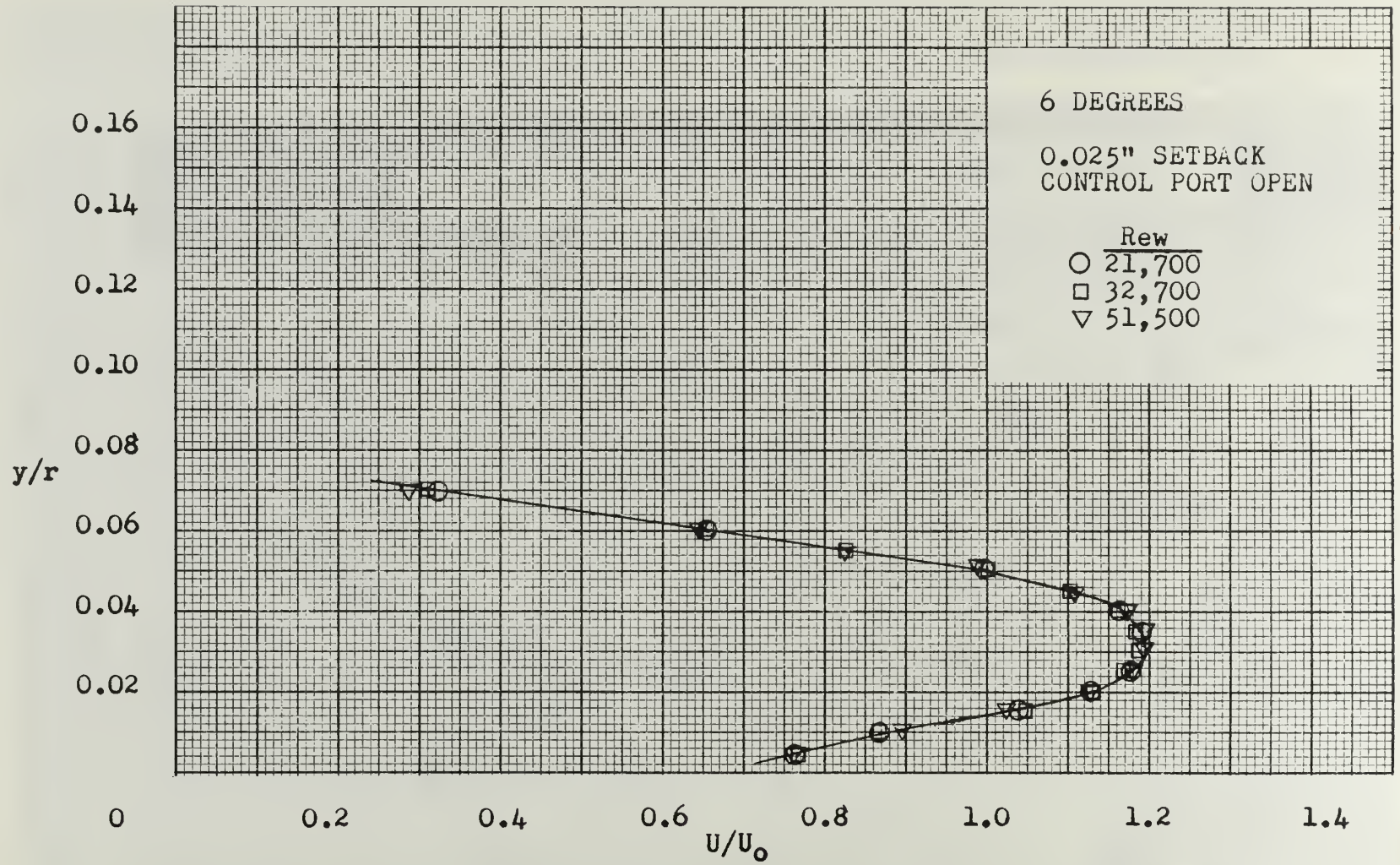

FIGURE 9. NORMALIZED VELOCITY PROFILE - TEST SECTION #1

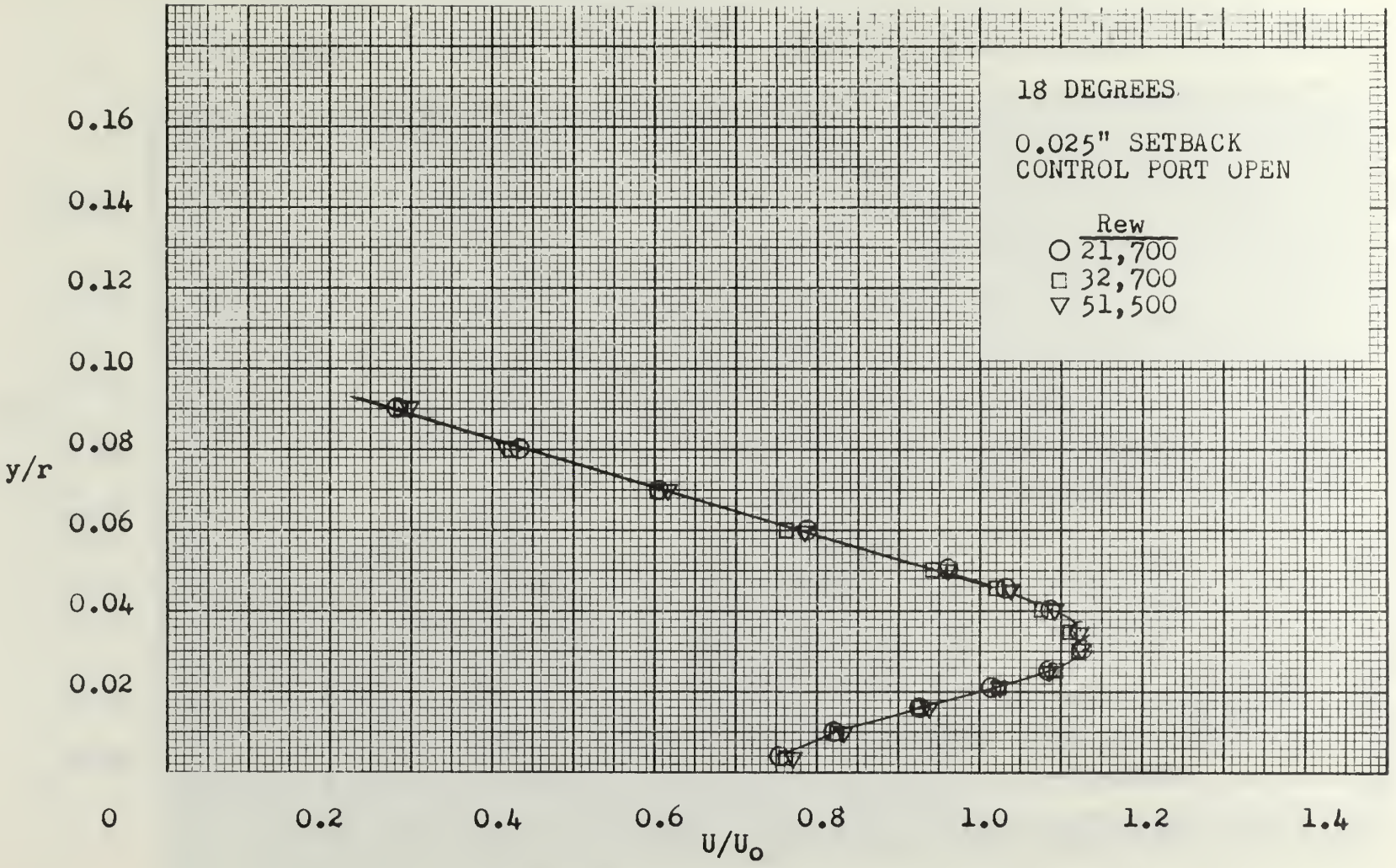

FIGURE 10. NORMALIZED VELOCITY PROFILE - TEST SECTION #1

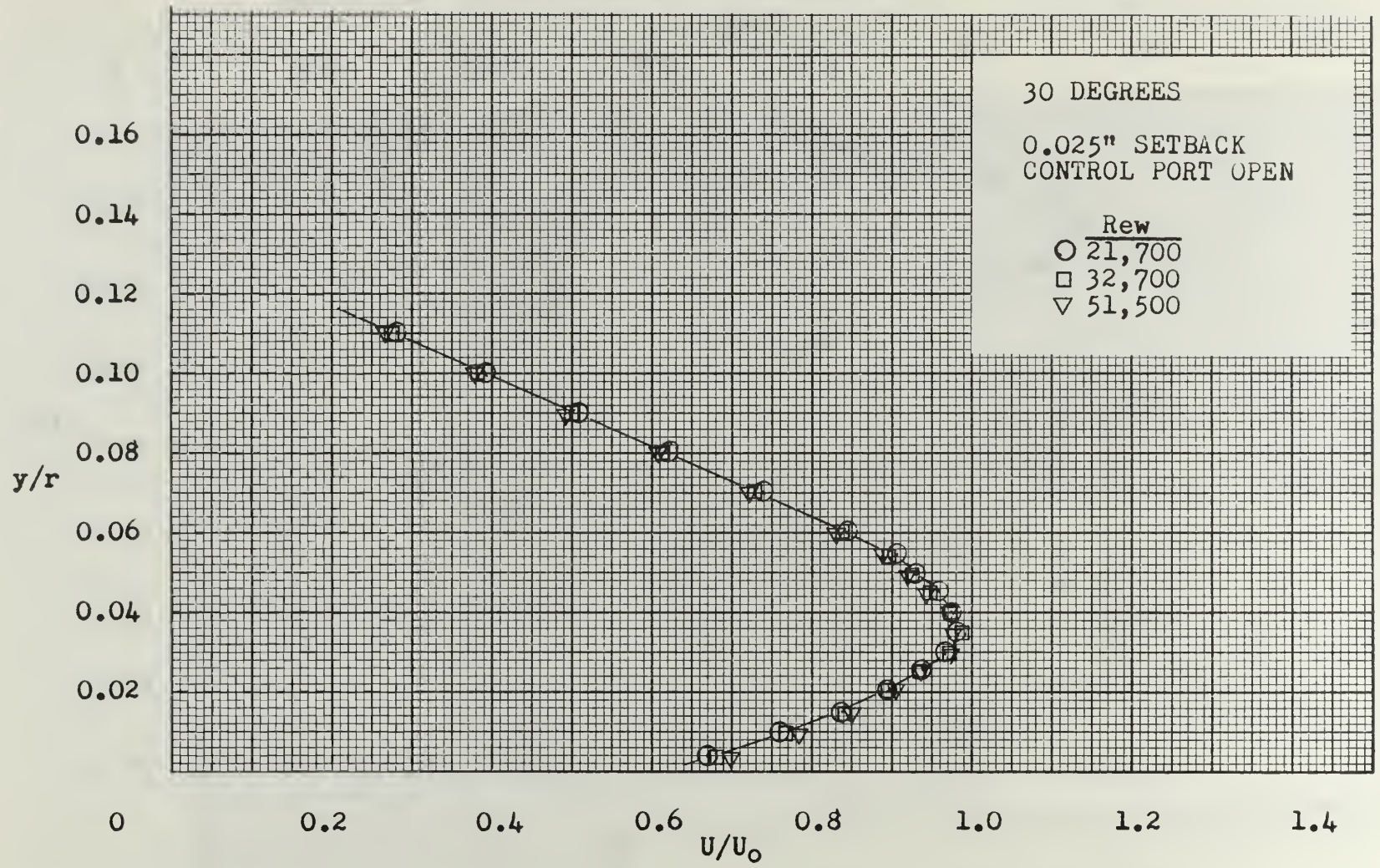

FIGURE 11. NORMALIZED VELOCITY PROFILE - TEST SECTION #1

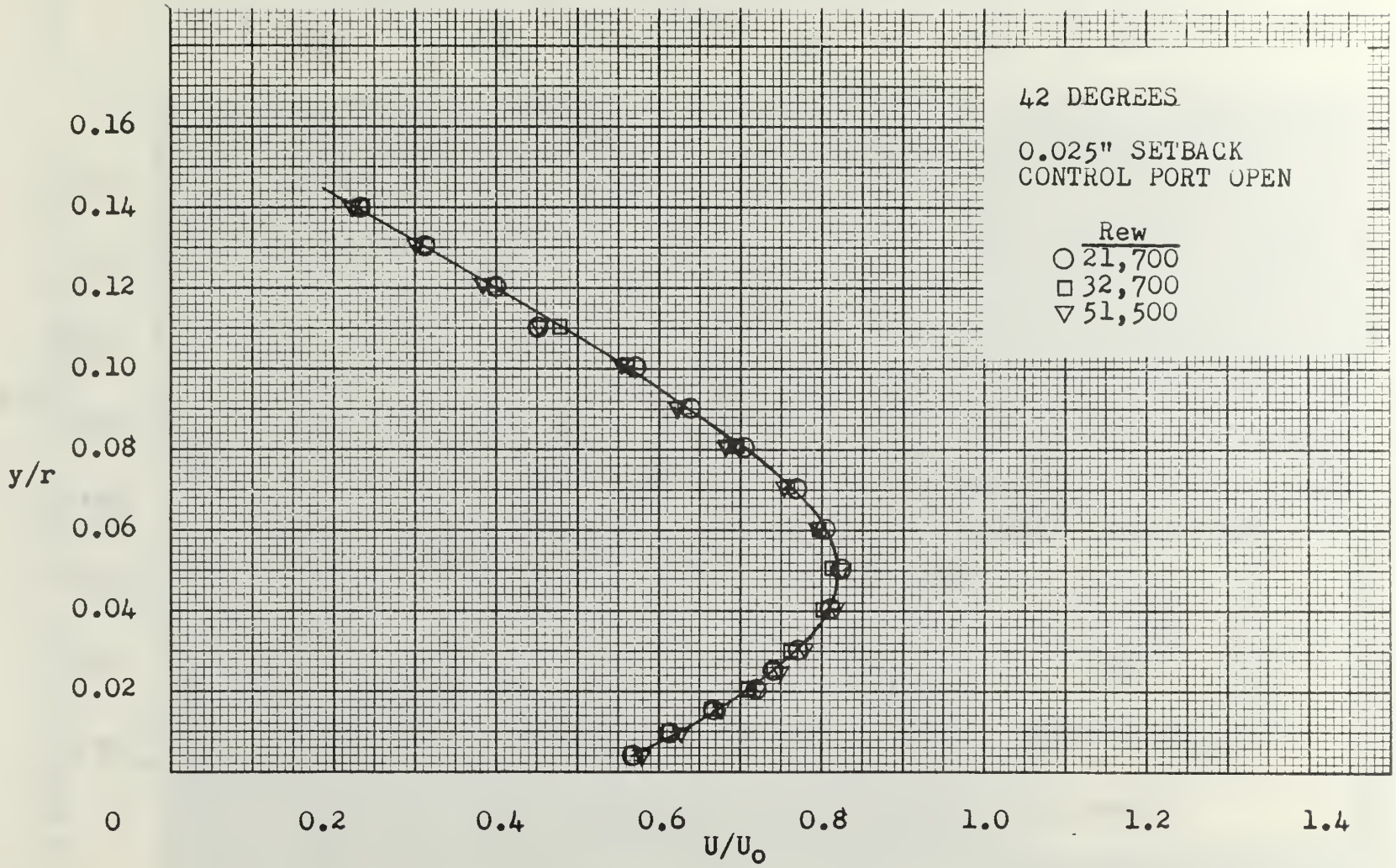

FIGURE 12. NORMALIZED VELOCITY PROFILE - TEST SECTION #1

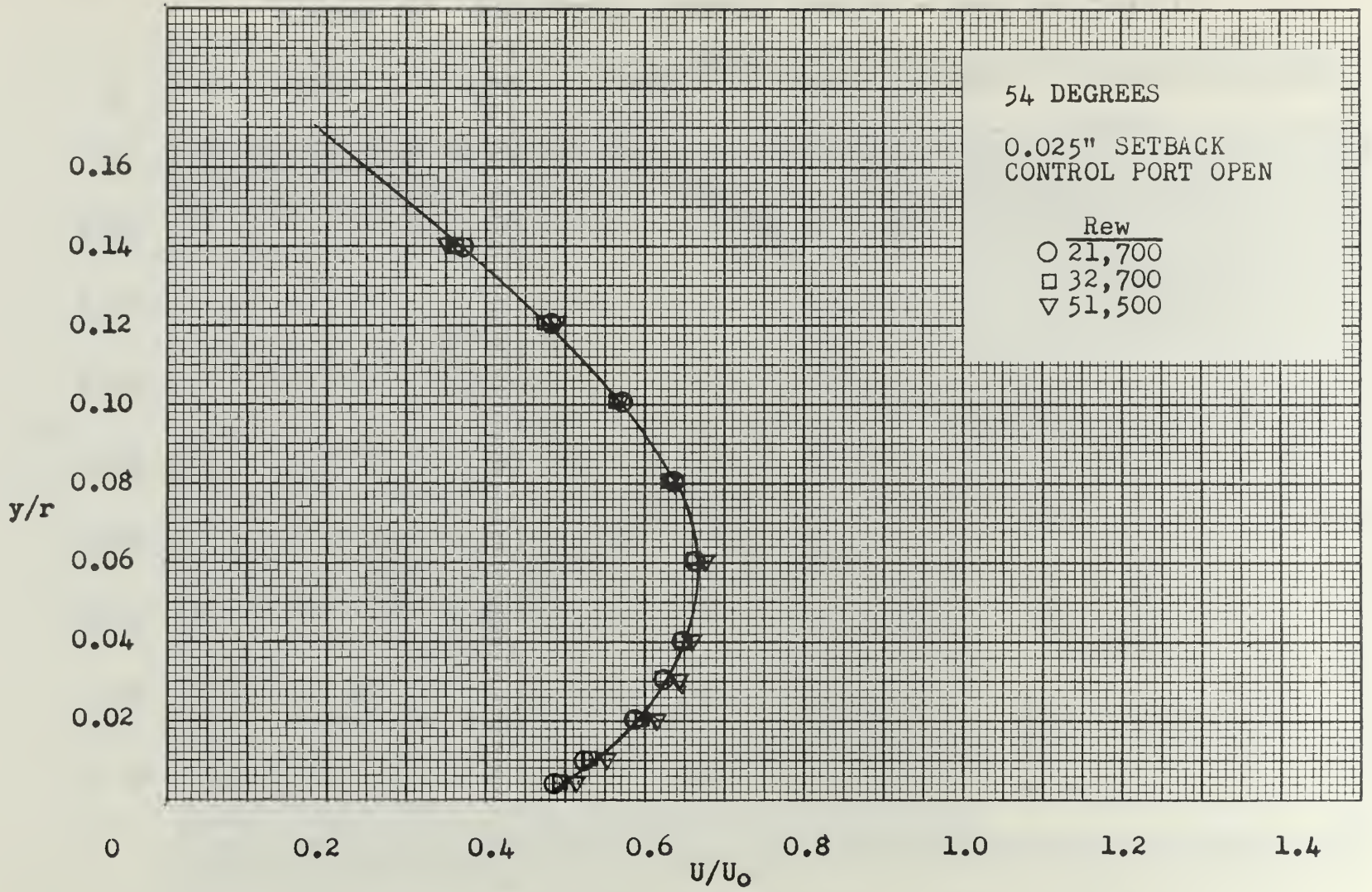

FIGURE 13. NORMALIZED VELOCITY PROFILE - TEST SECTION #1

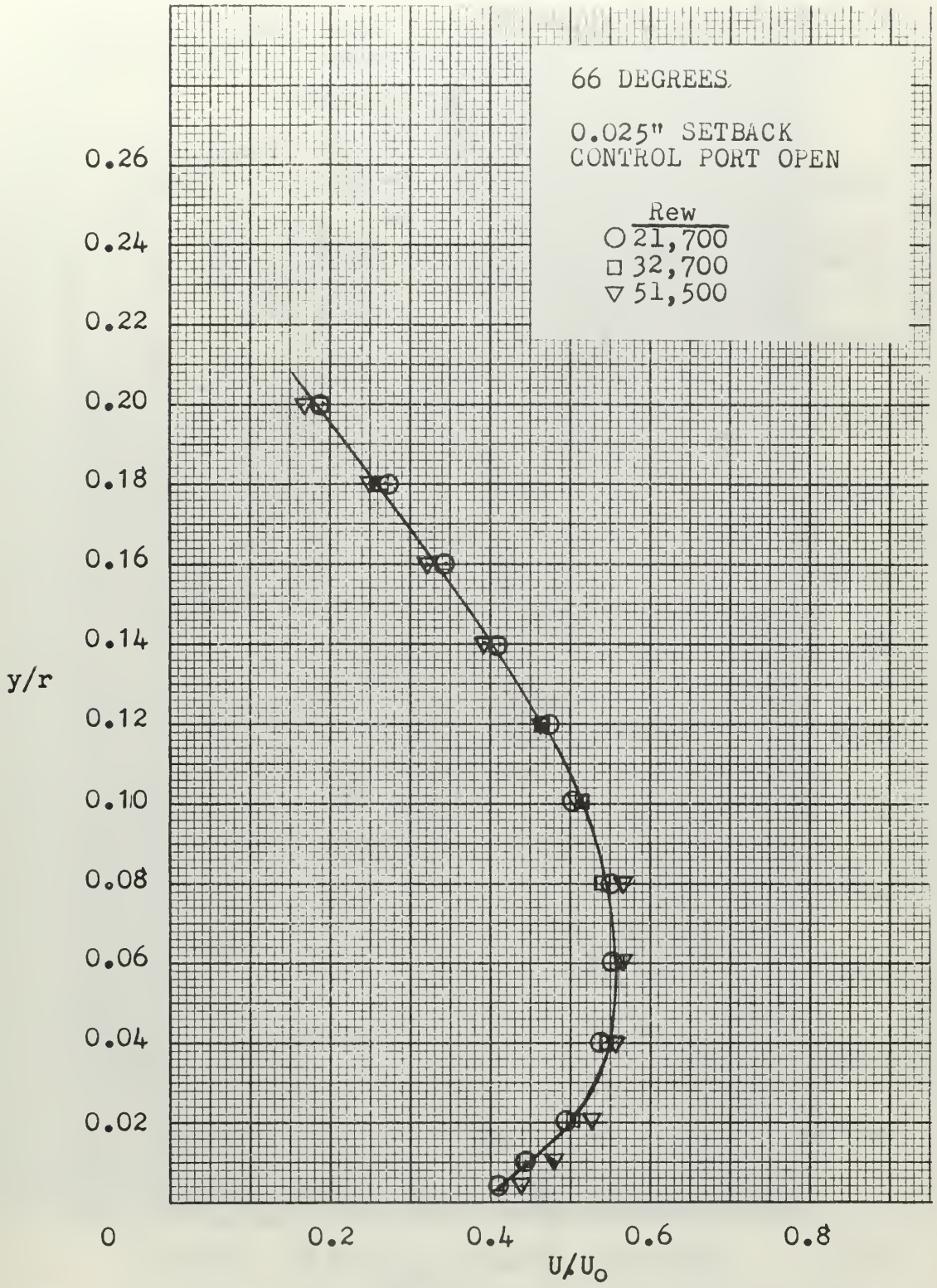

FIGURE 14. NORMALIZED VELOCITY PROFILE - TEST SECTION #1

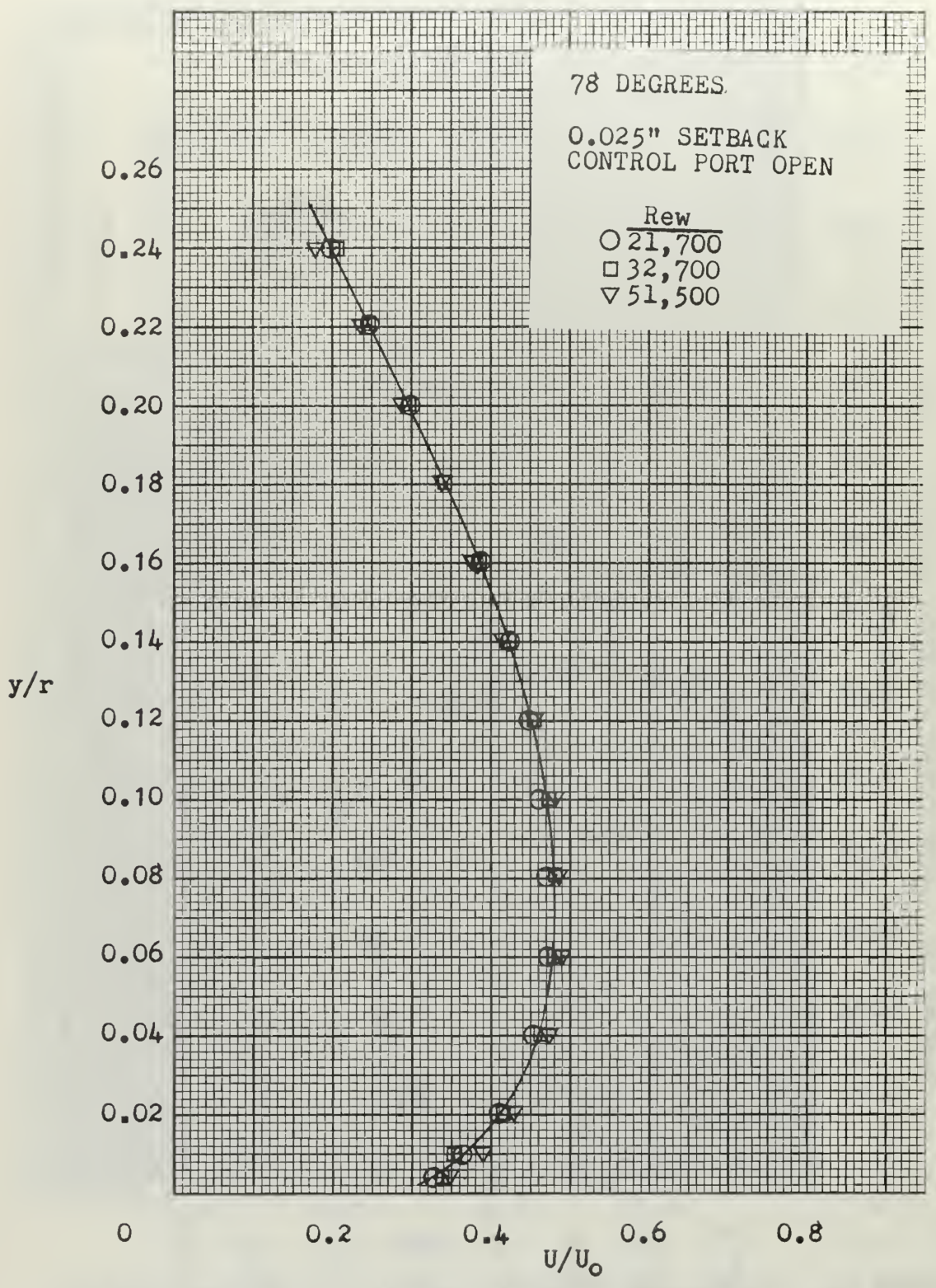

FIGURE 15. NORMALIZED VELOCITY PROFILE - TEST SECTION #1

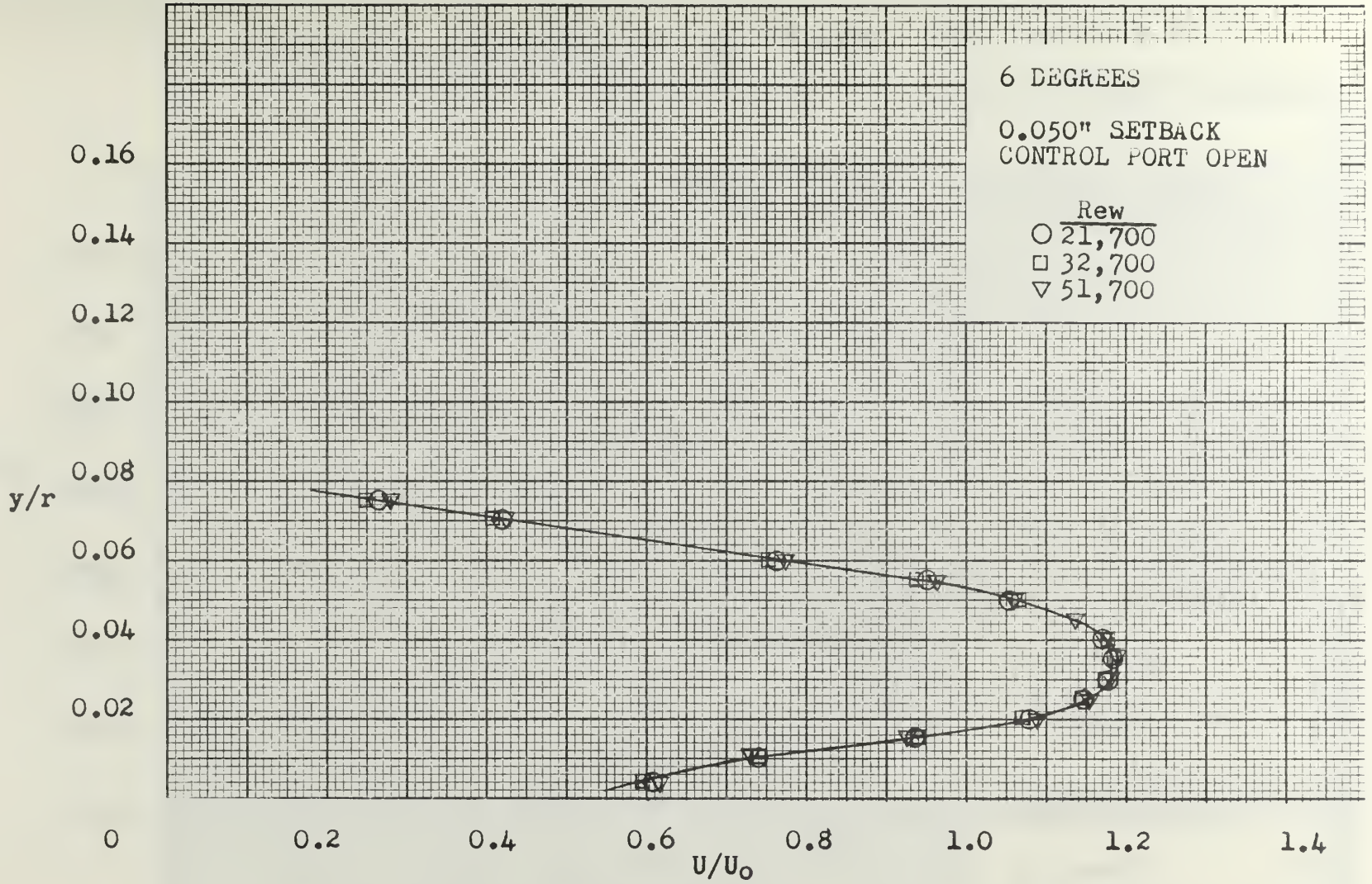

FIGURE 16. NORMALIZED VELOCITY PROFILE - TEST SECTION #1

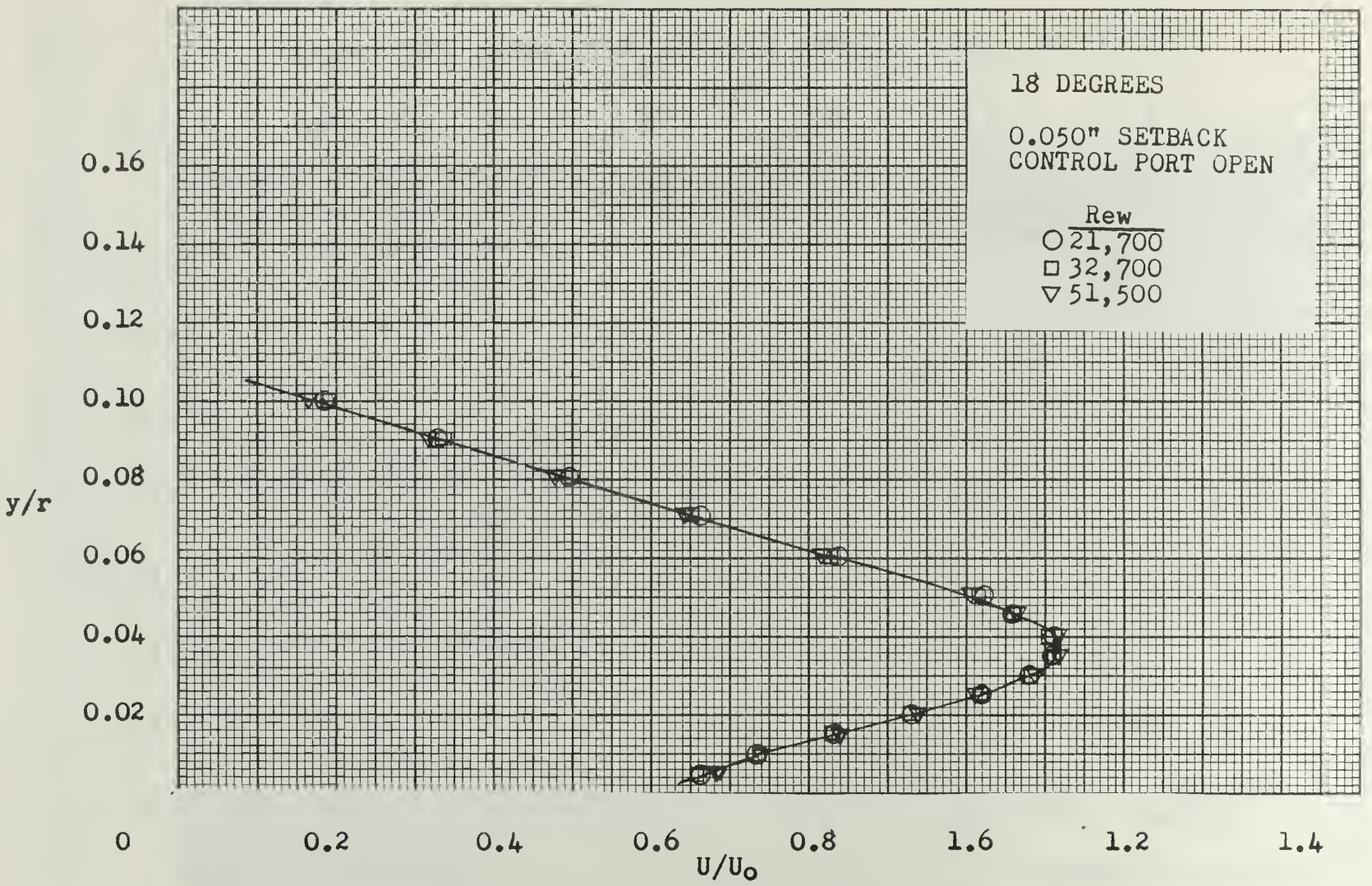

FIGURE 17. NORMALIZED VELOCITY PROFILE - TEST SECTION # 1

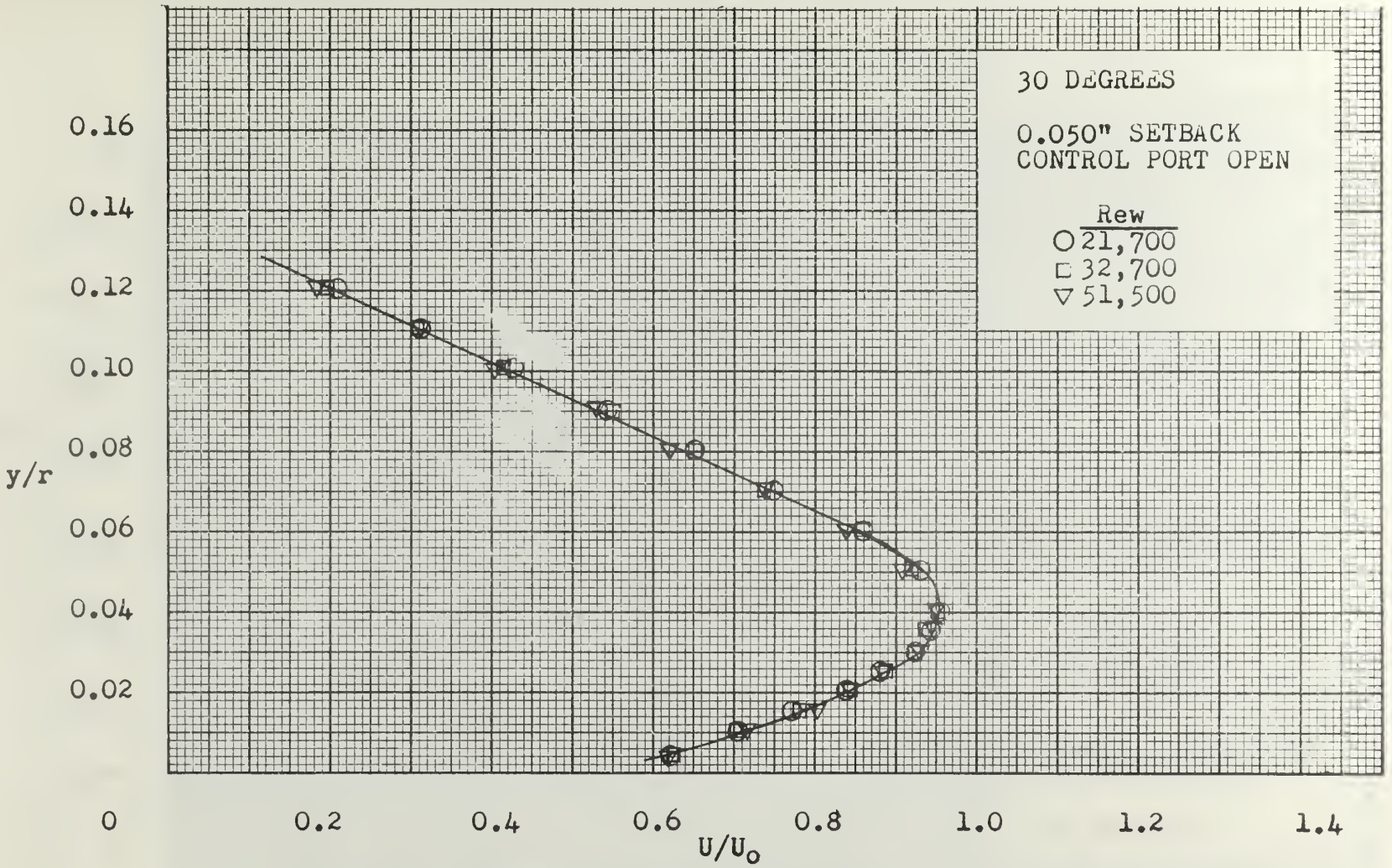

FIGURE 18. NORMALIZED VELOCITY PROFILE - TEST SECTION #1

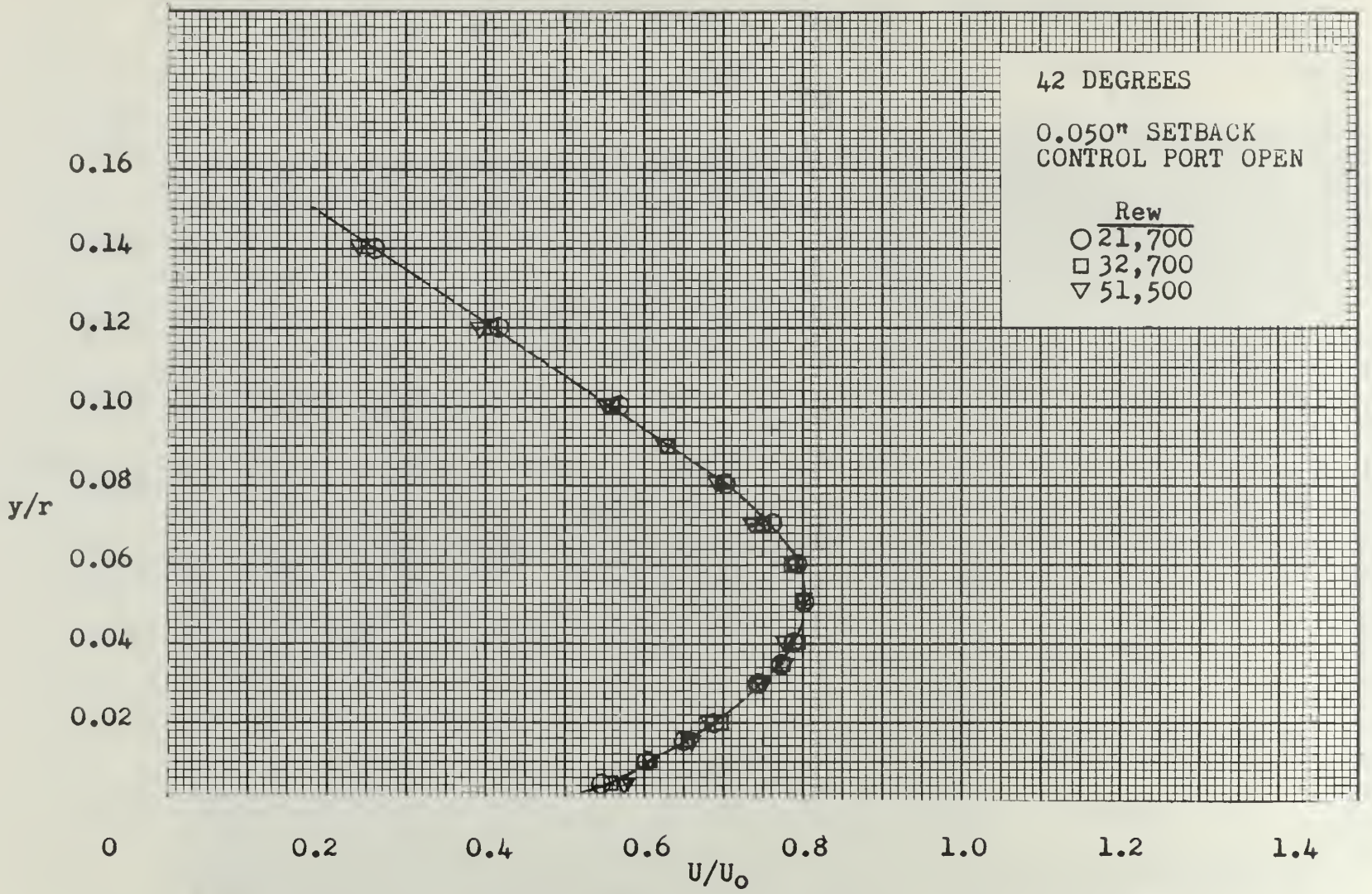

FIGURE 19. NORMALIZED VELOCITY PROFILE - TEST SECTION #1

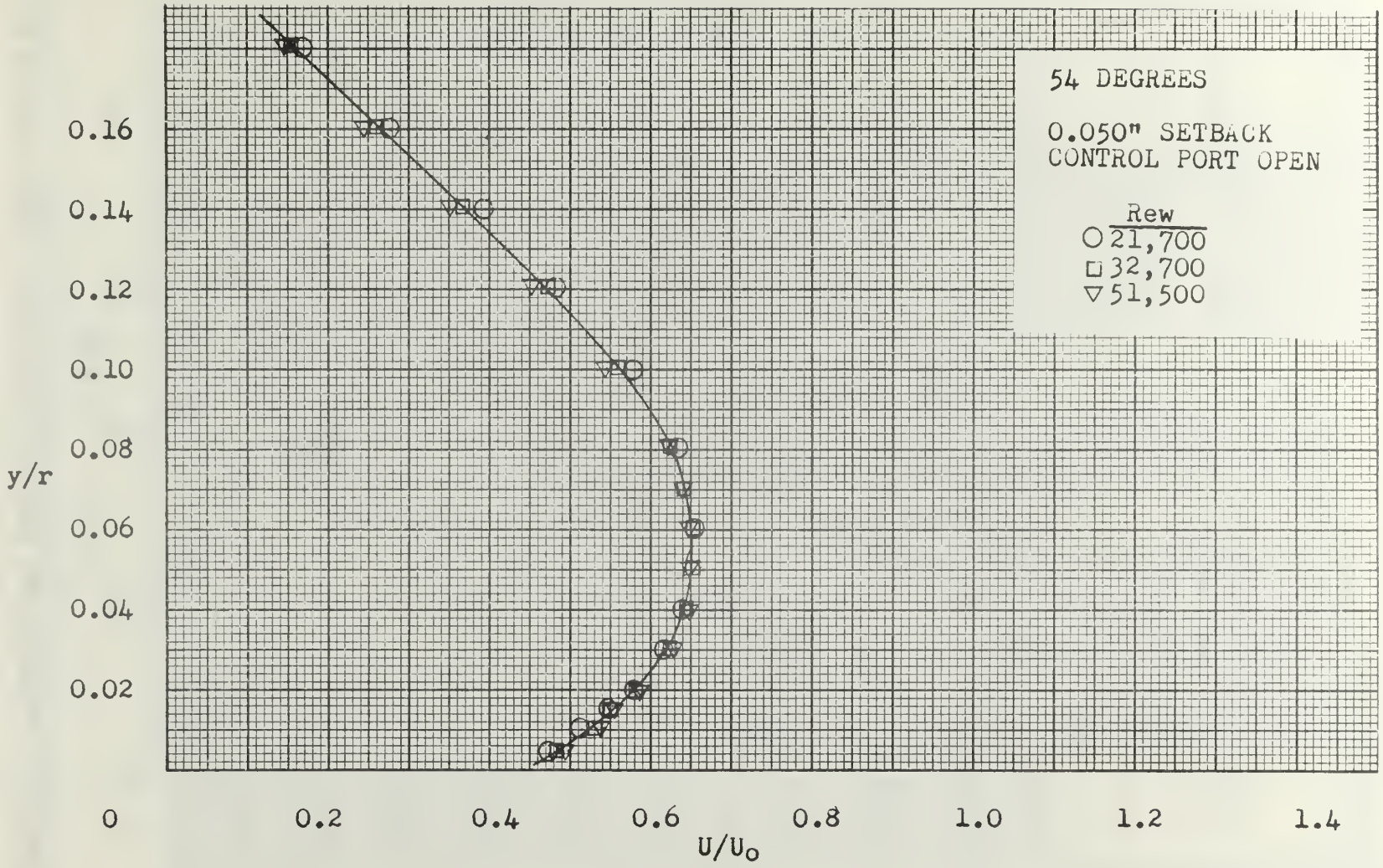

FIGURE 20. NORMALIZED VELOCITY PROFILE - TEST SECTION #1

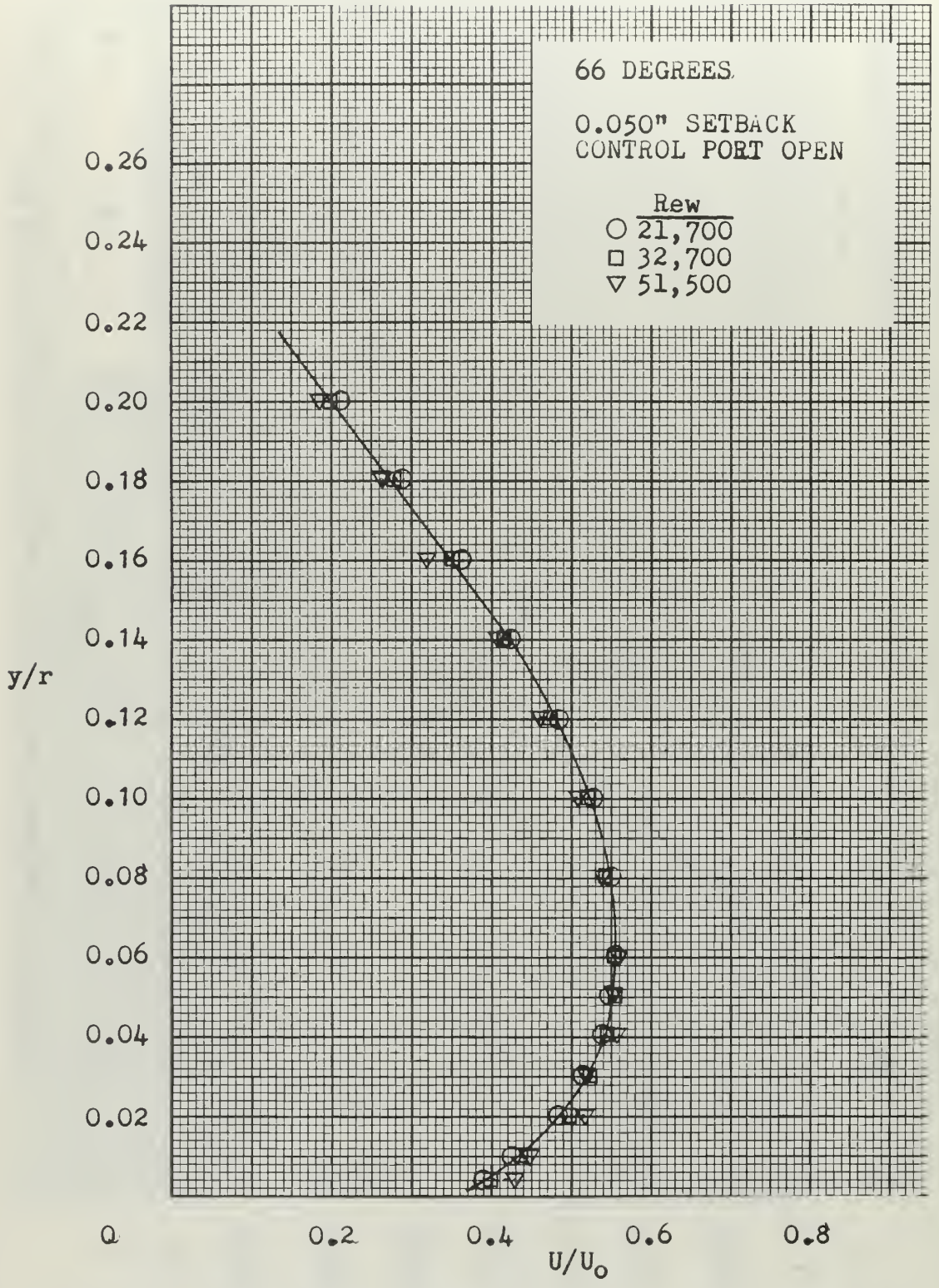

FIGURE 21. NORMALIZED VELOCITY PROFILE - TEST SECTION #1

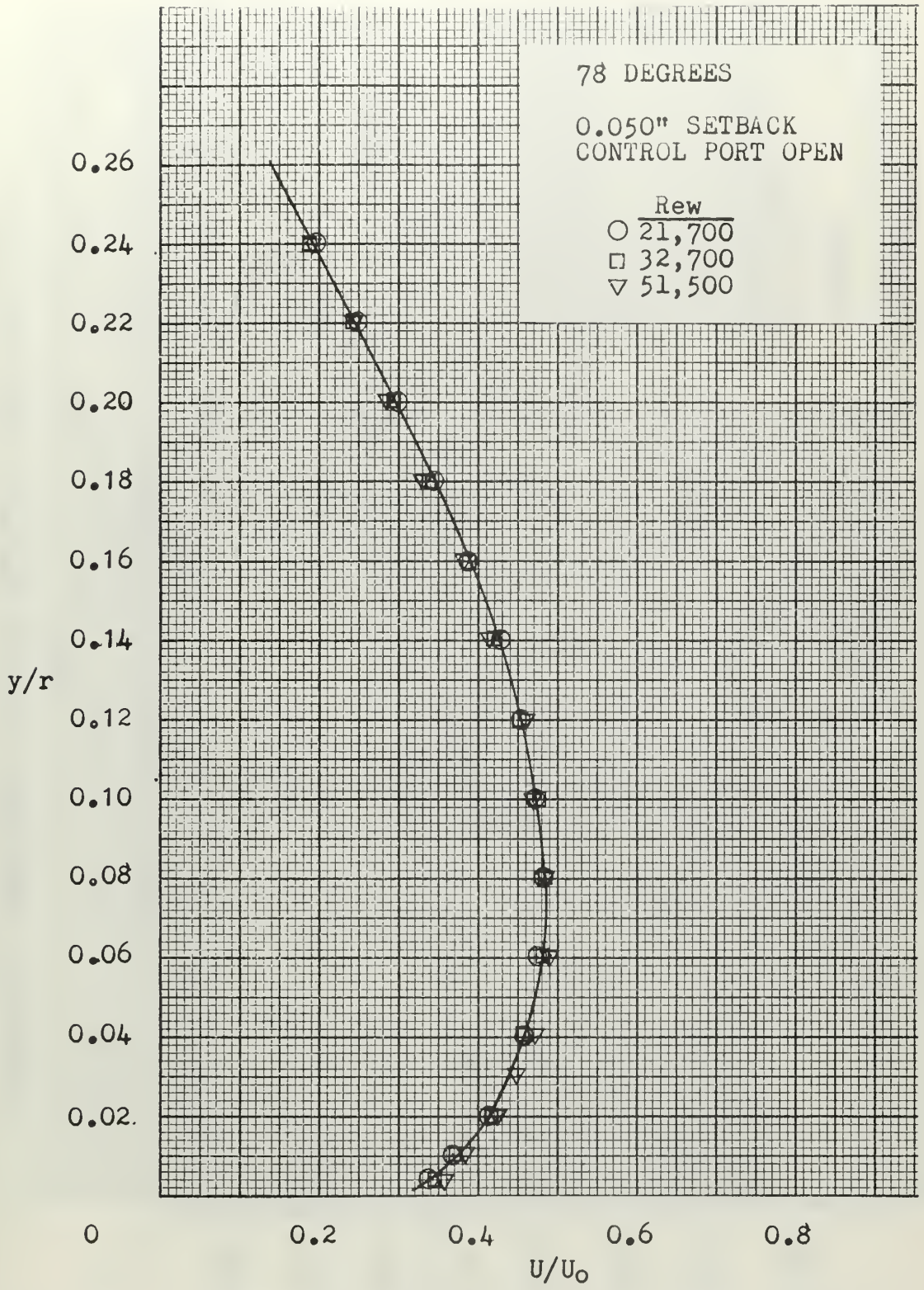

FIGURE 22. NORMALIZED VELOCITY PROFILE - TEST SECTION #1

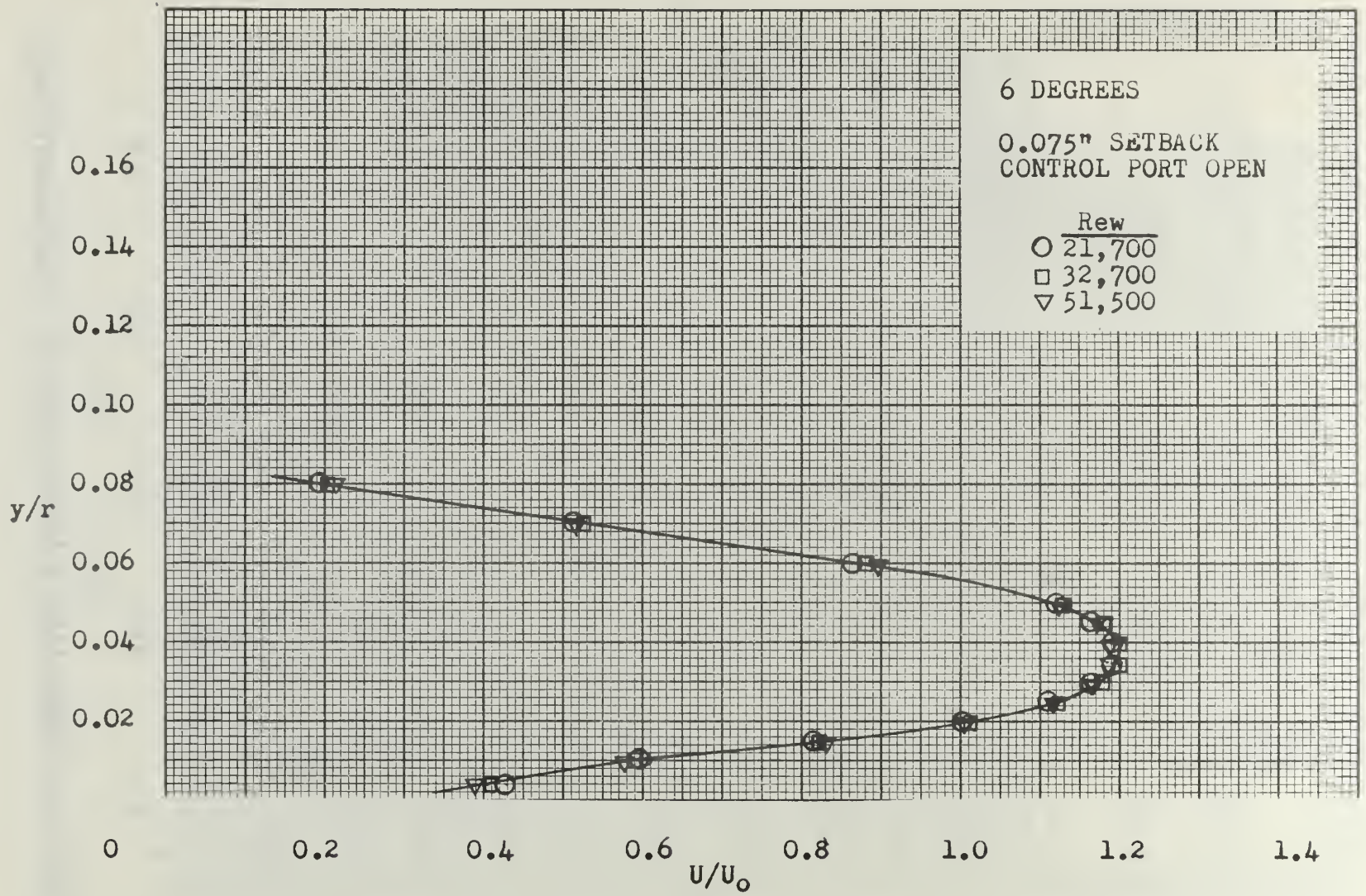

FIGURE 23. NORMALIZED VELOCITY PROFILE - TEST SECTION #1

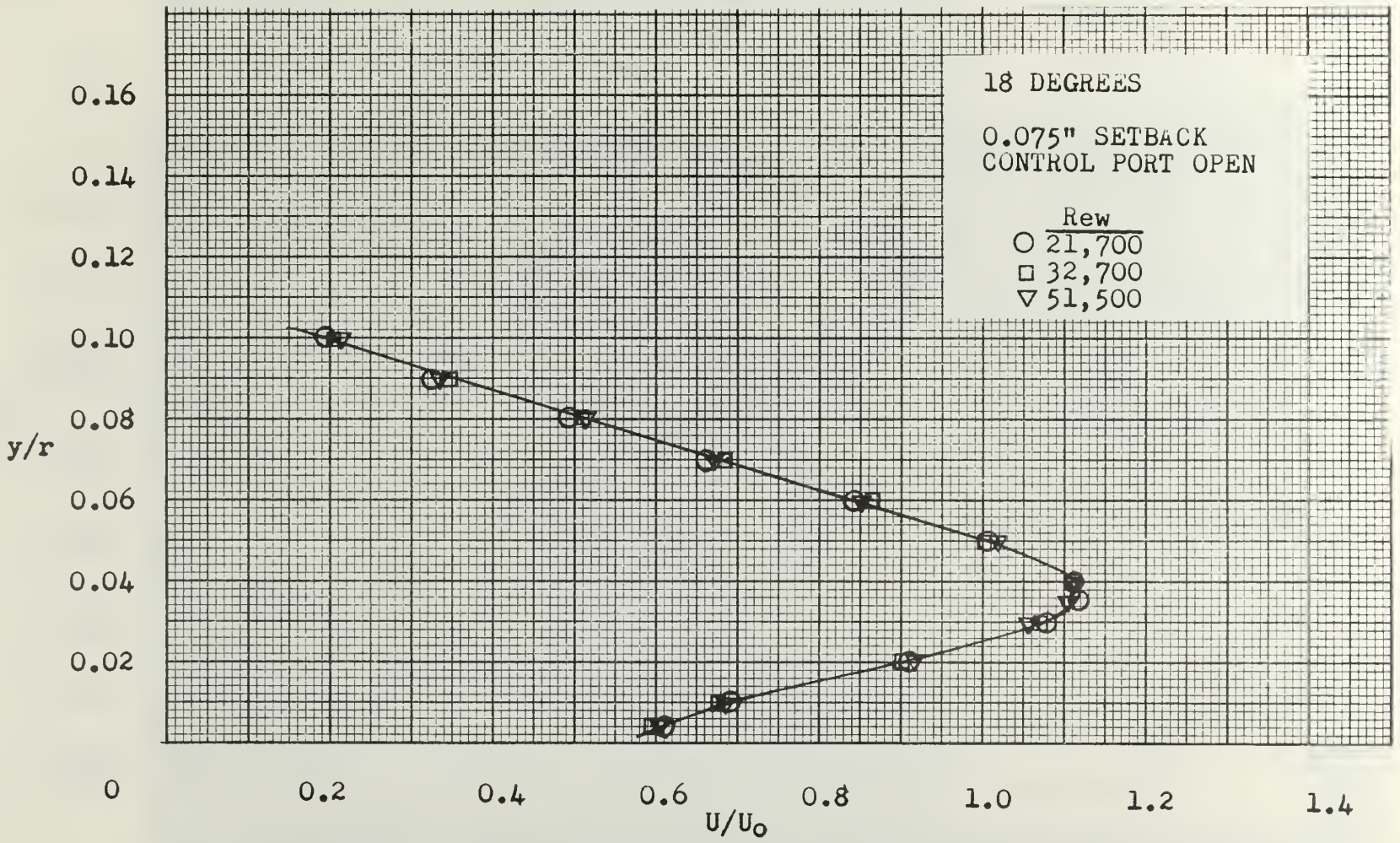

FIGURE 24. NORMALIZED VELOCITY PROFILE - TEST SECTION #1

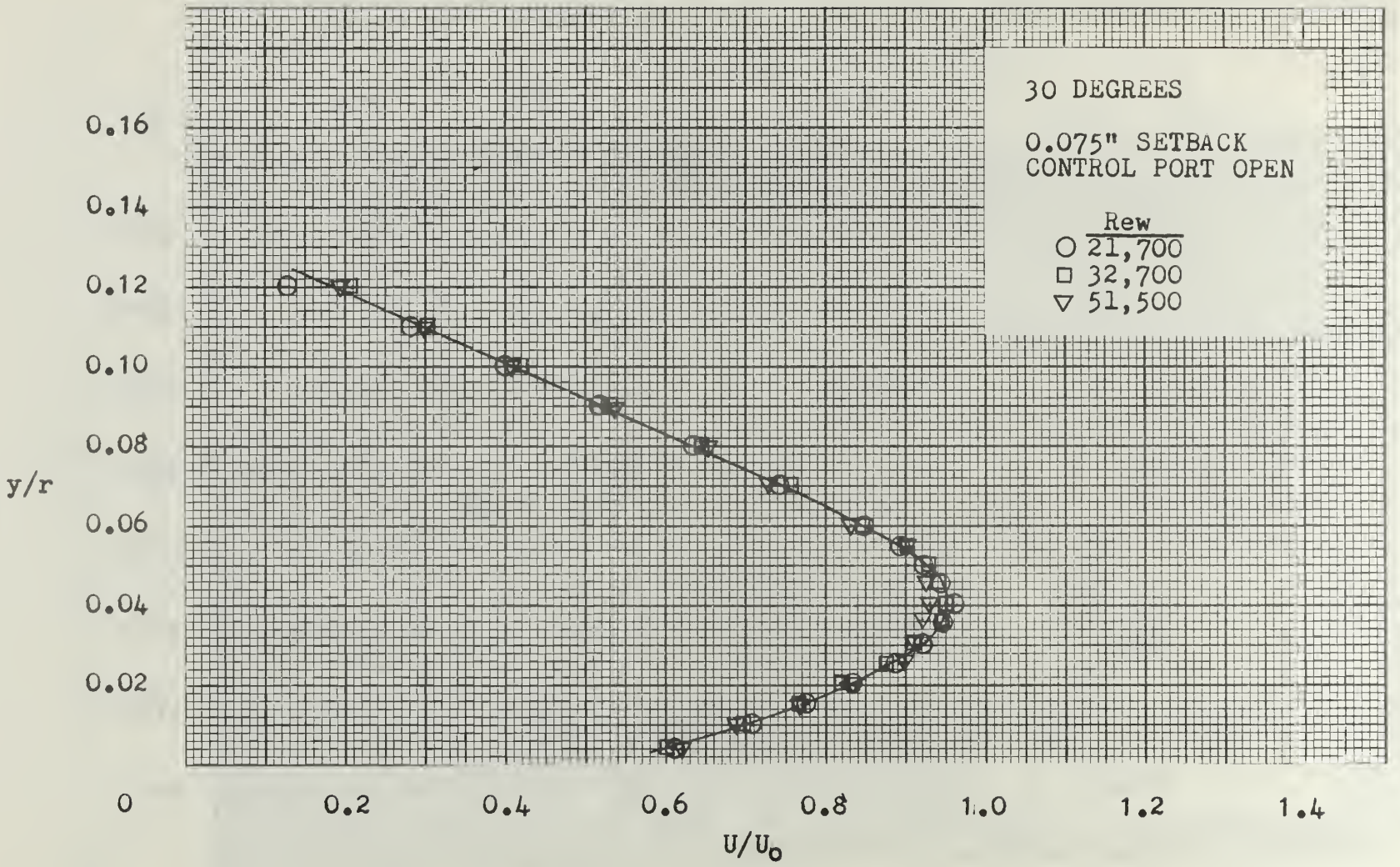

FIGURE 25. NORMALIZED VELOCITY PROFILE - TEST SECTION #1

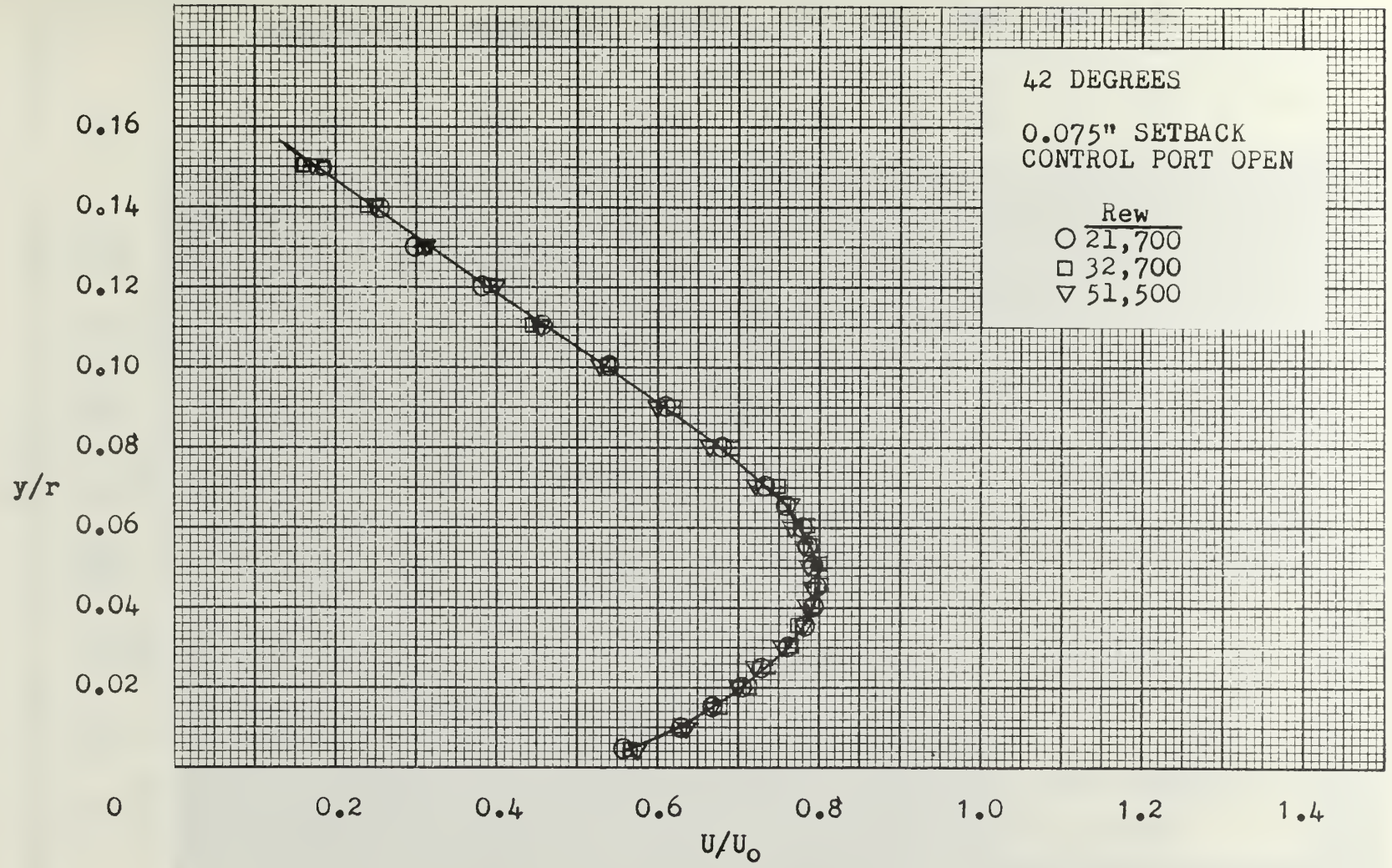

FIGURE 26. NORMALIZED VELOCITY PROFILE - TEST SECTION #1

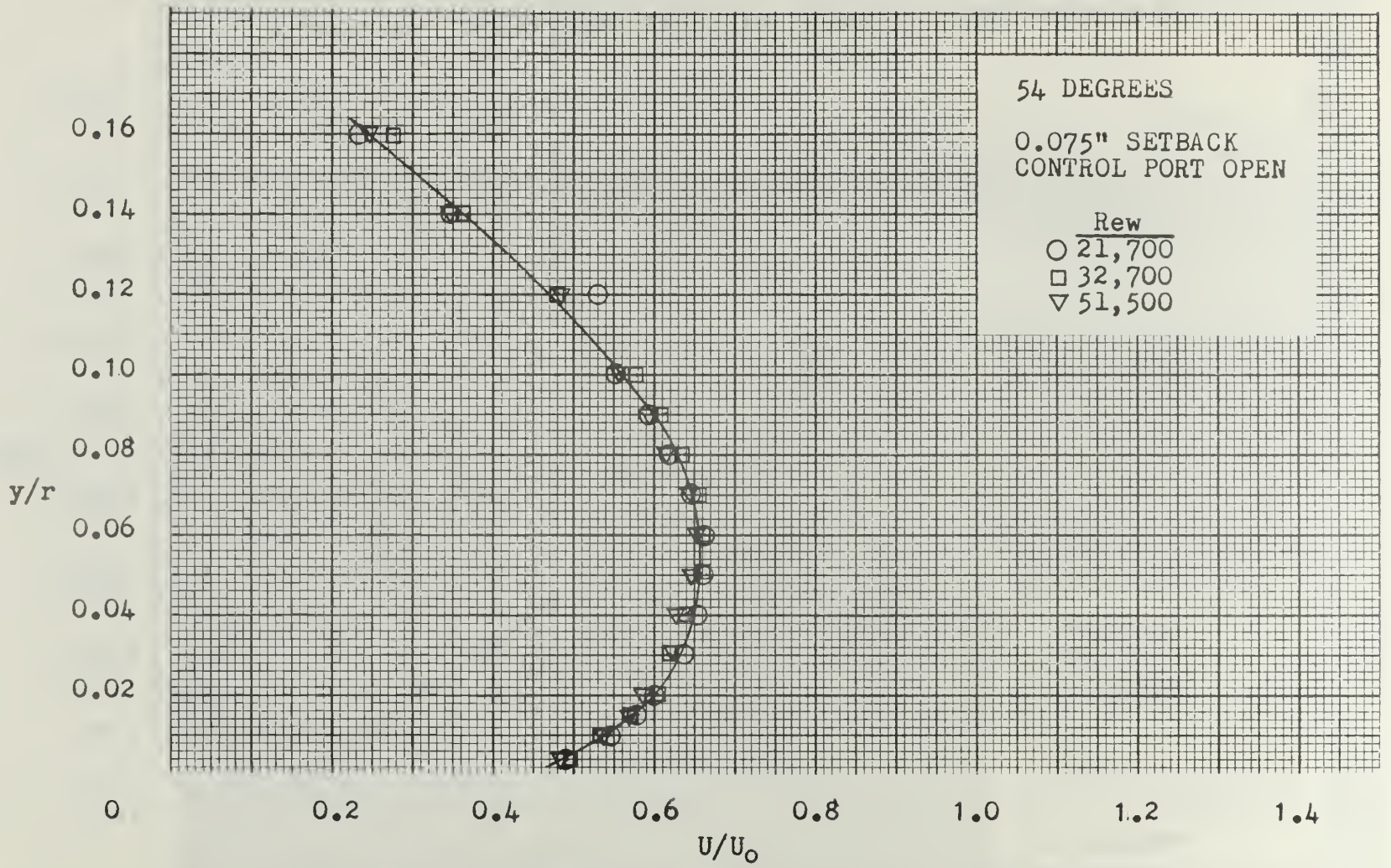

FIGURE 27. NORMALIZED VELOCITY PROFILE - TEST SECTION #1

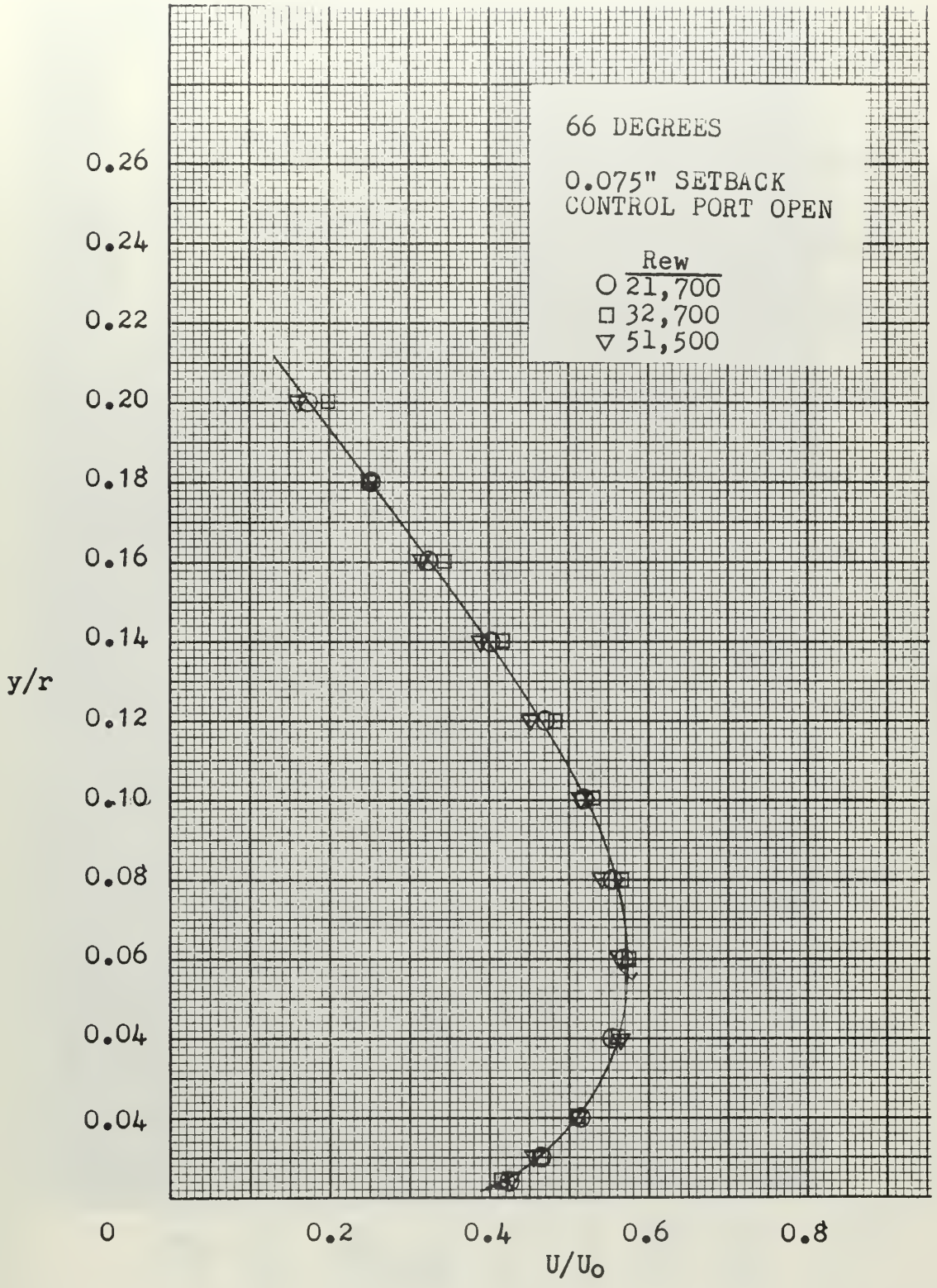

FIGURE 28. NORMALIZED VELOCITY PROFILE - TEST SECTION #1

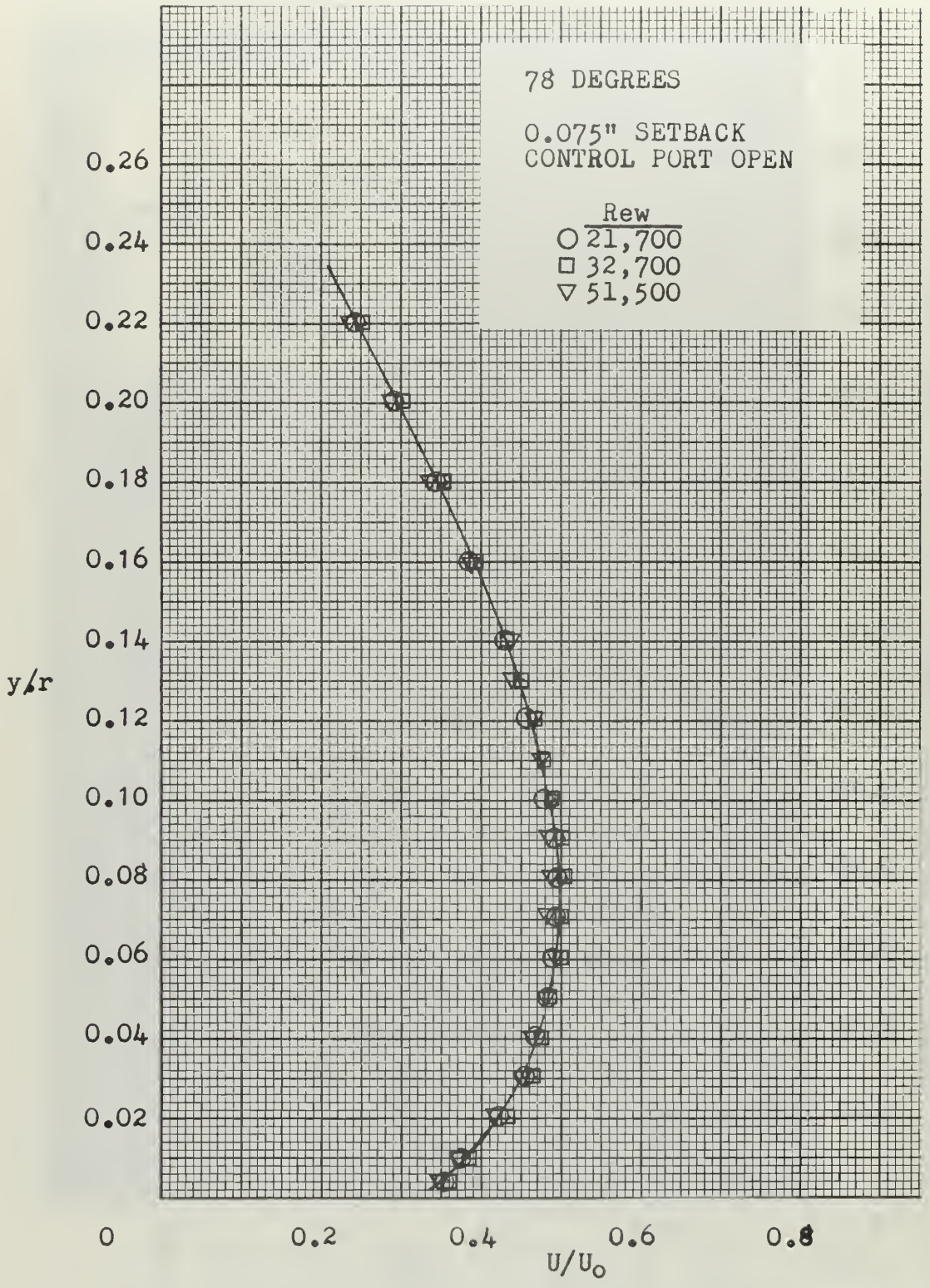

FIGURE 29. NORMALIZED VELOCITY PROFILE - TEST SECTION #1

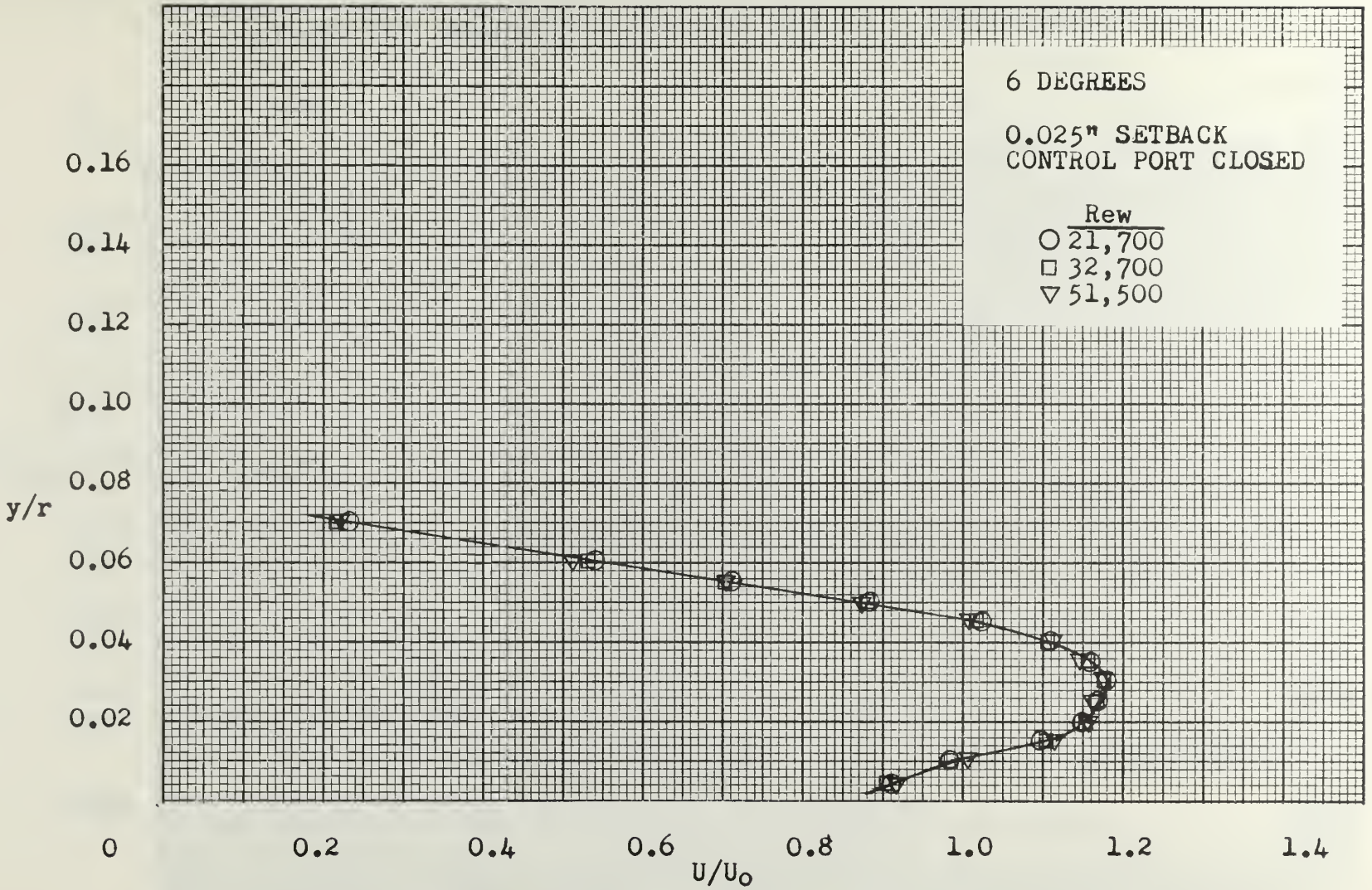

FIGURE 30. NORMALIZED VELOCITY PROFILE - TEST SECTION #1

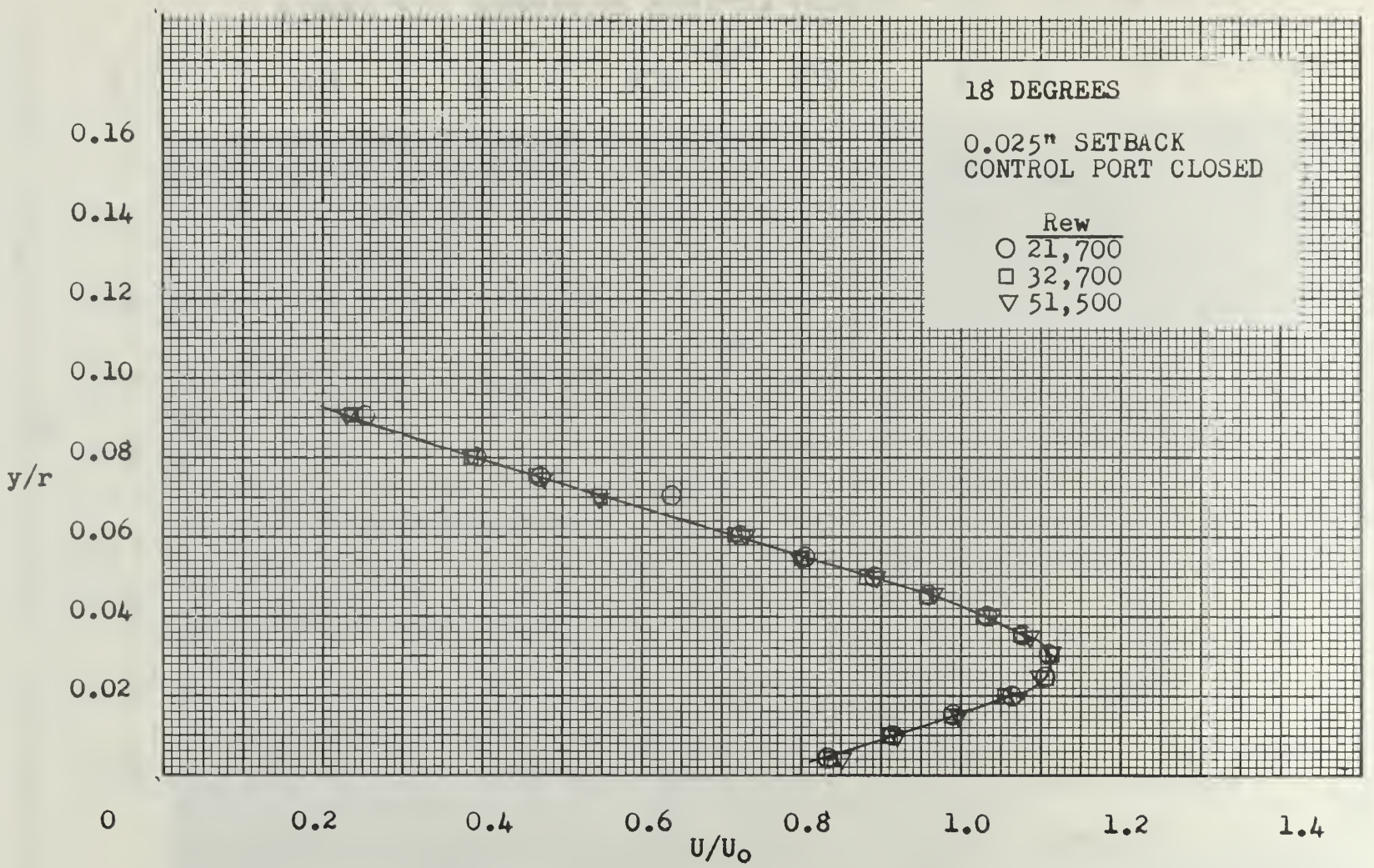

FIGURE 31. NORMALIZED VELOCITY PROFILE - TEST SECTION #1

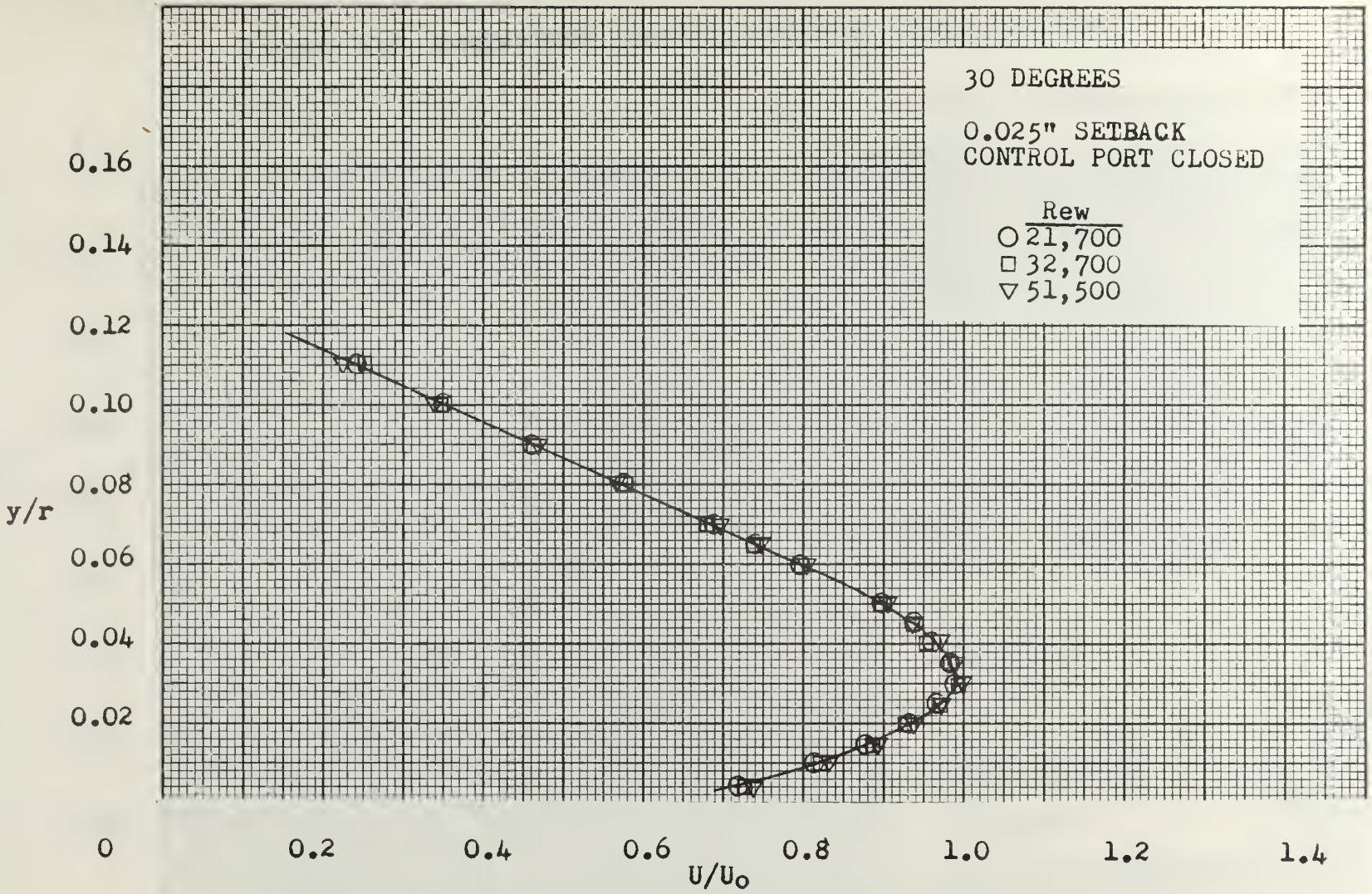

FIGURE 32. NORMALIZED VELOCITY PROFILE - TEST SECTION #1

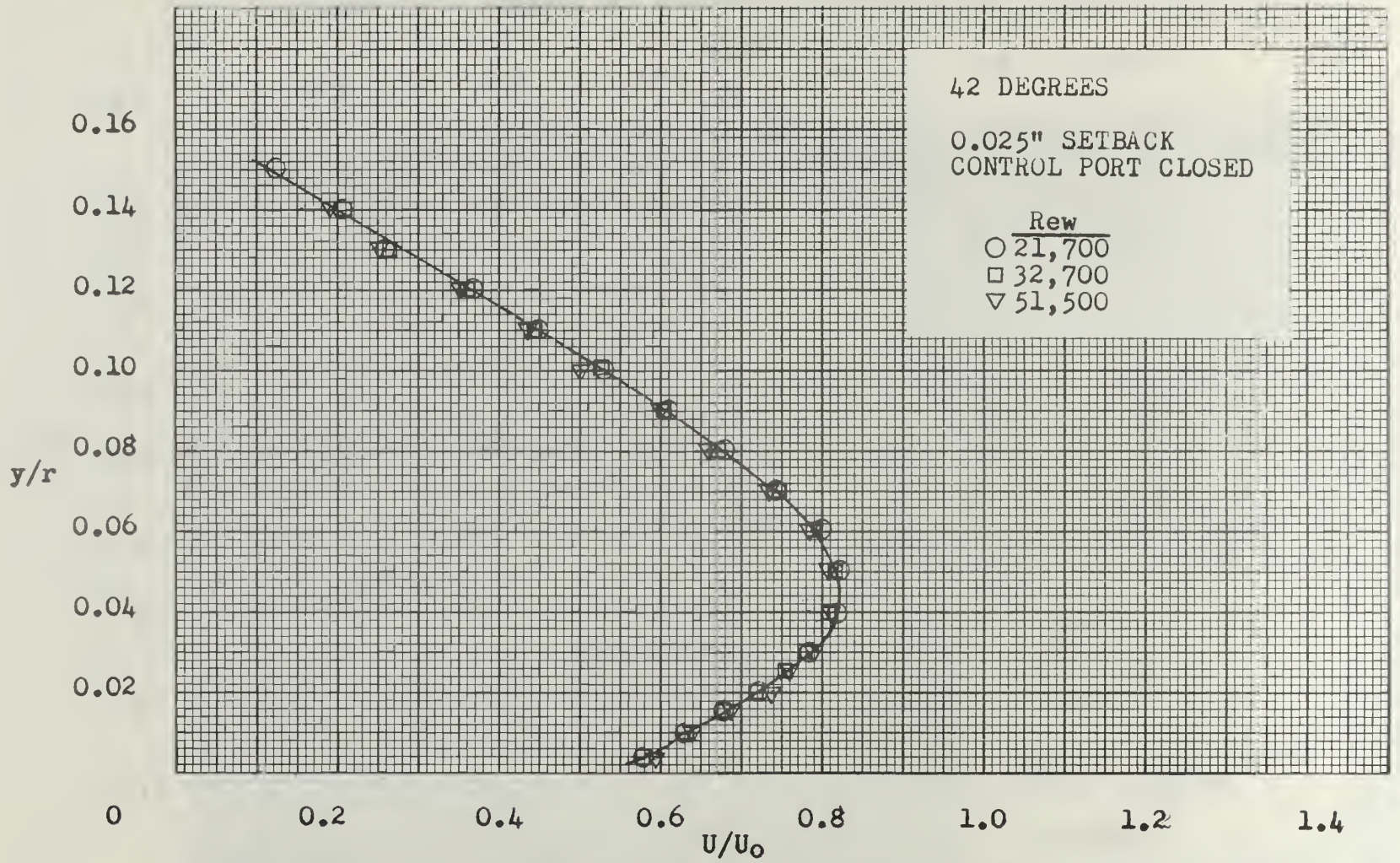

FIGURE 33. NORMALIZED VELOCITY PROFILE - TEST SECTION #1

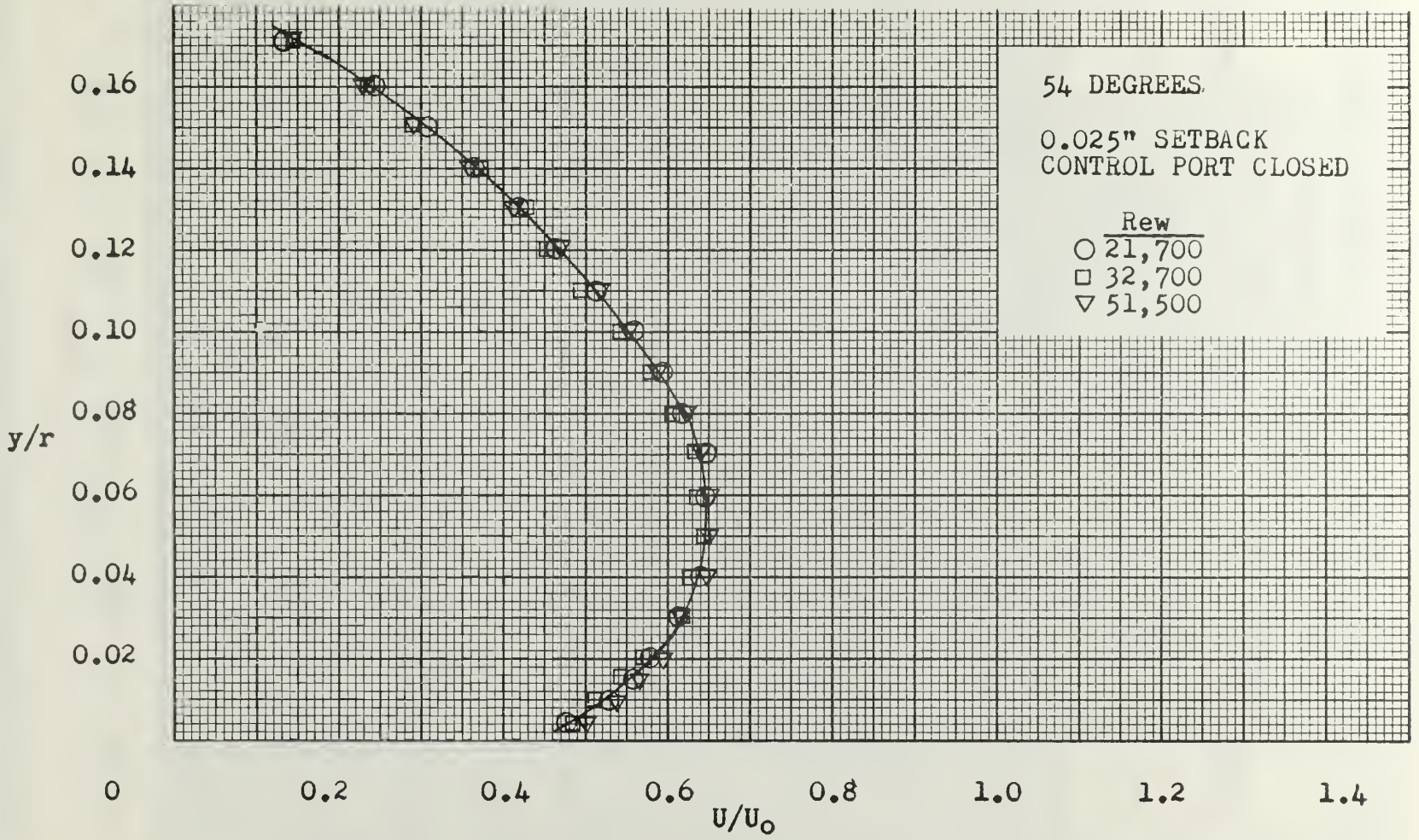

FIGURE 34. NORMALIZED VELOCITY PROFILE - TEST SECTION #1

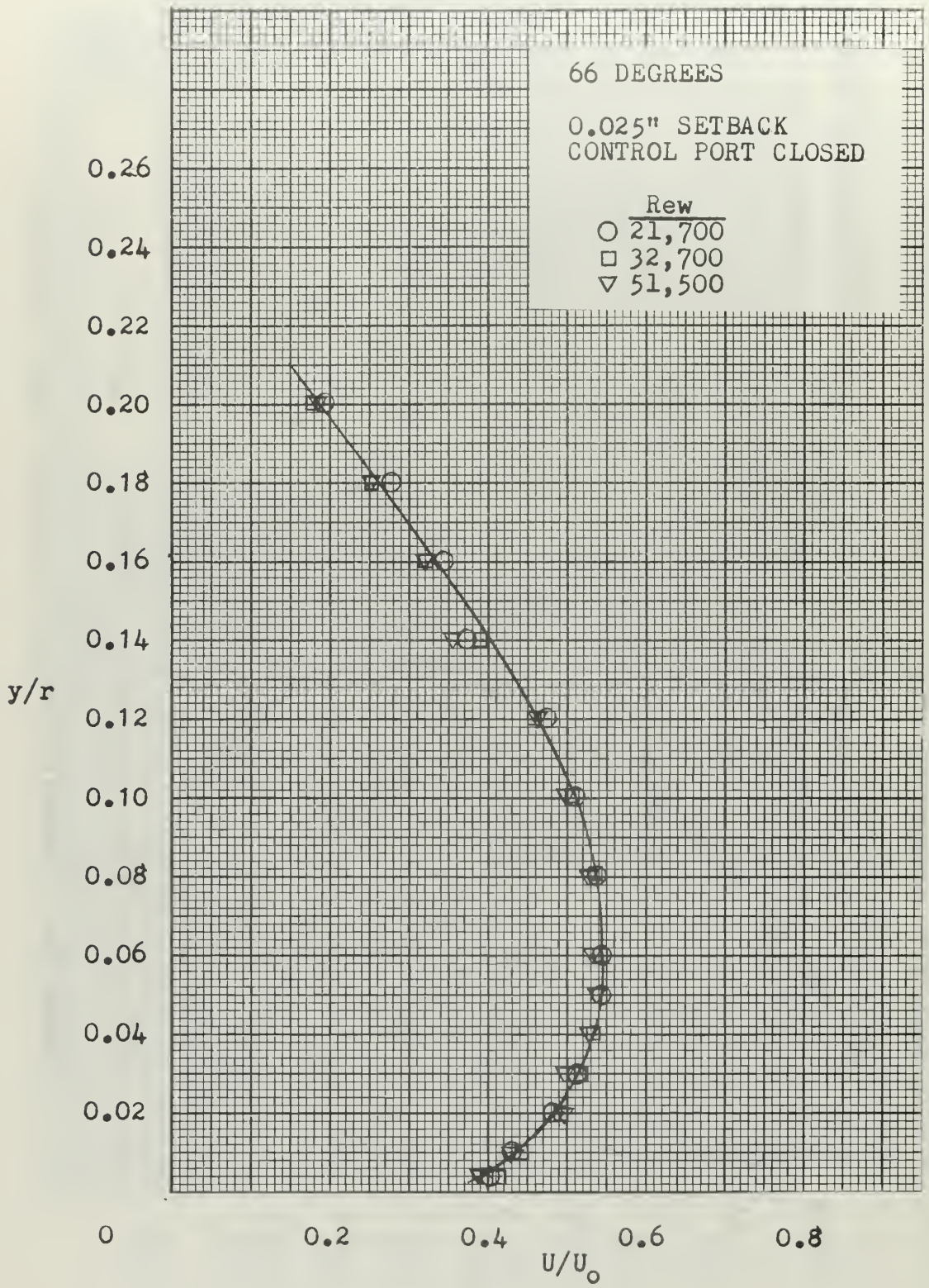

FIGURE 35. NORMALIZED VELOCITY PROFILE - TEST SECTION #1

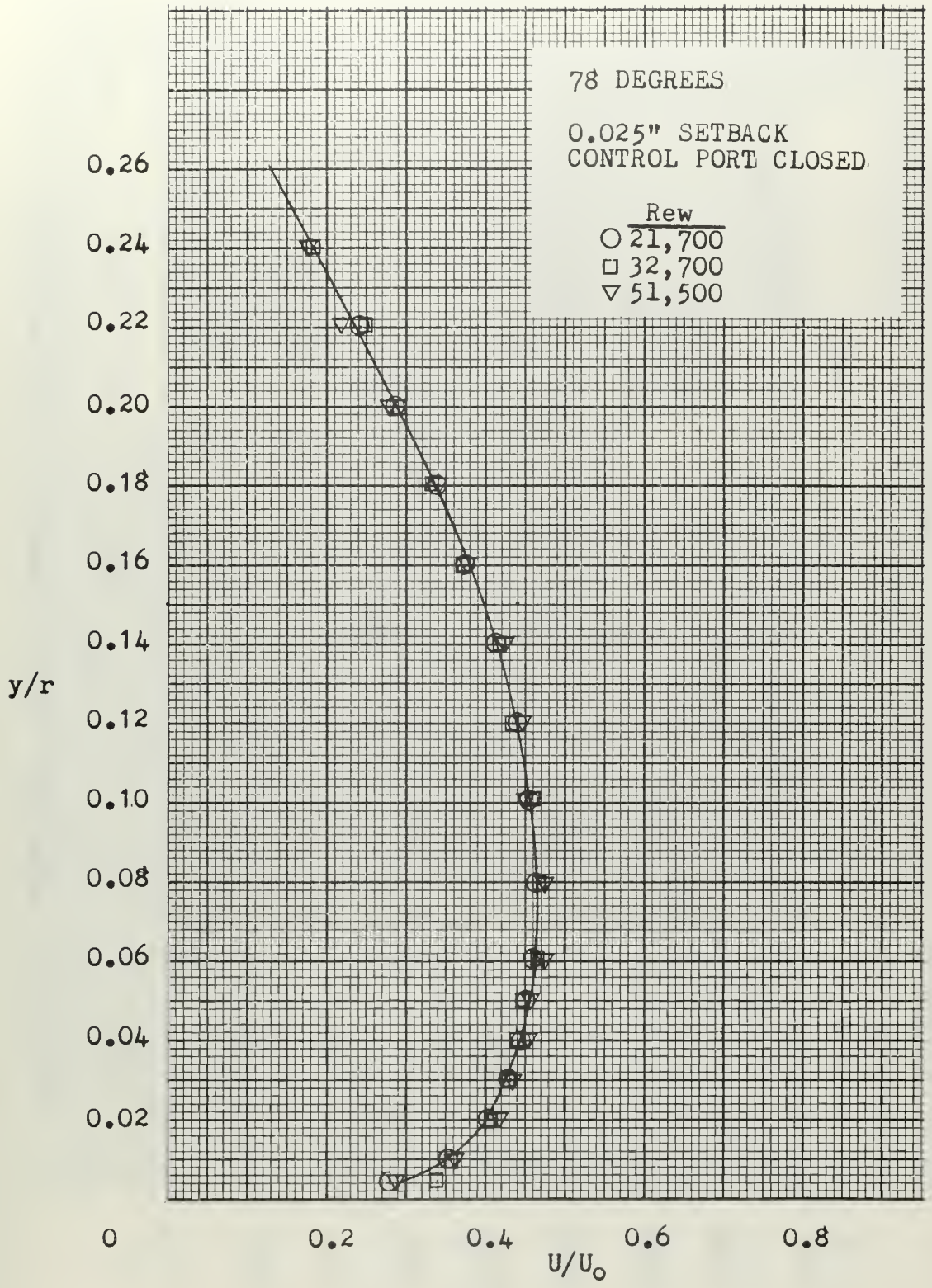

FIGURE 36. NORMALIZED VELOCITY PROFILE - TEST SECTION #1

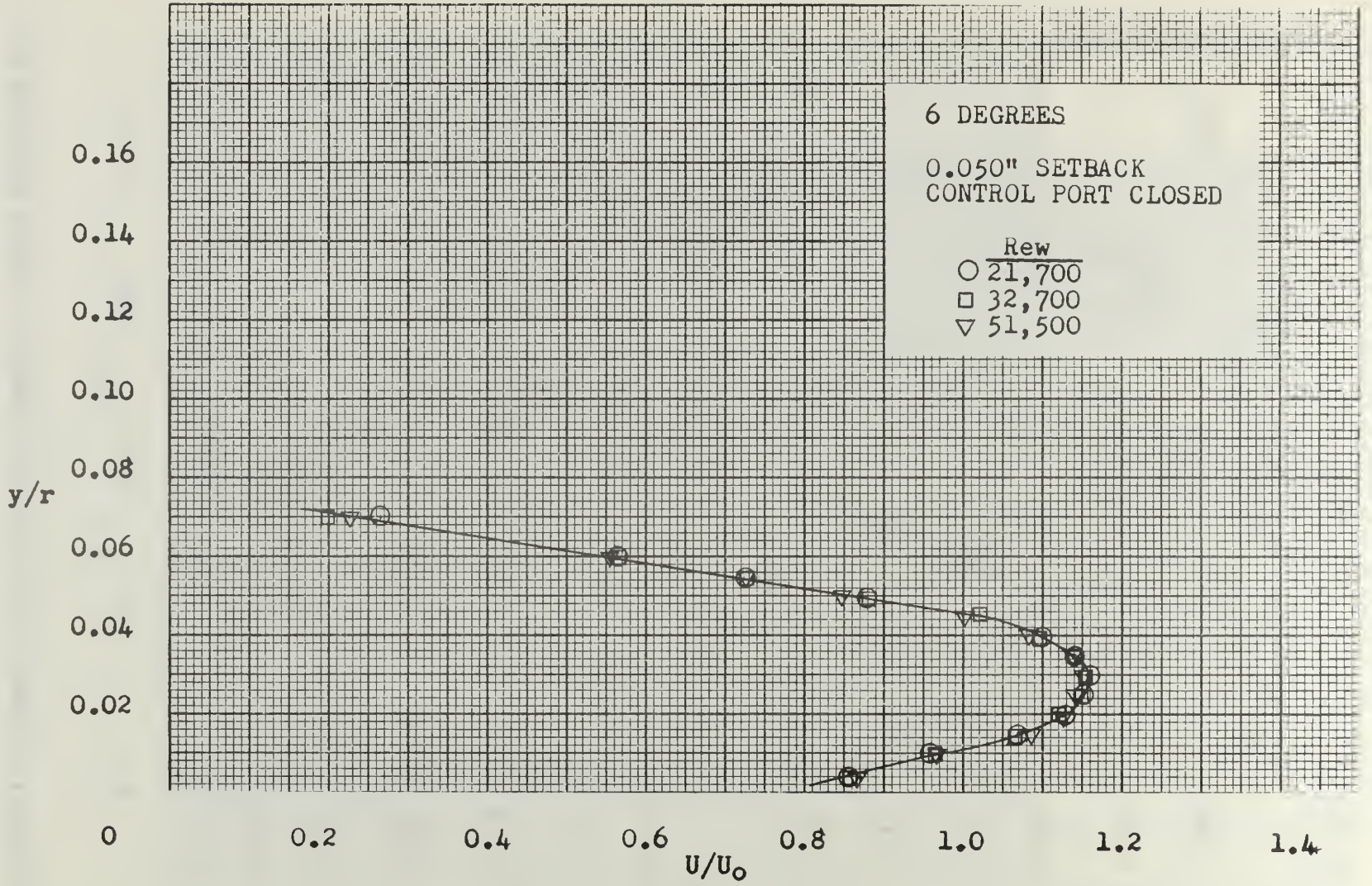

FIGURE 37. NORMALIZED VELOCITY PROFILE - TEST SECTION #1

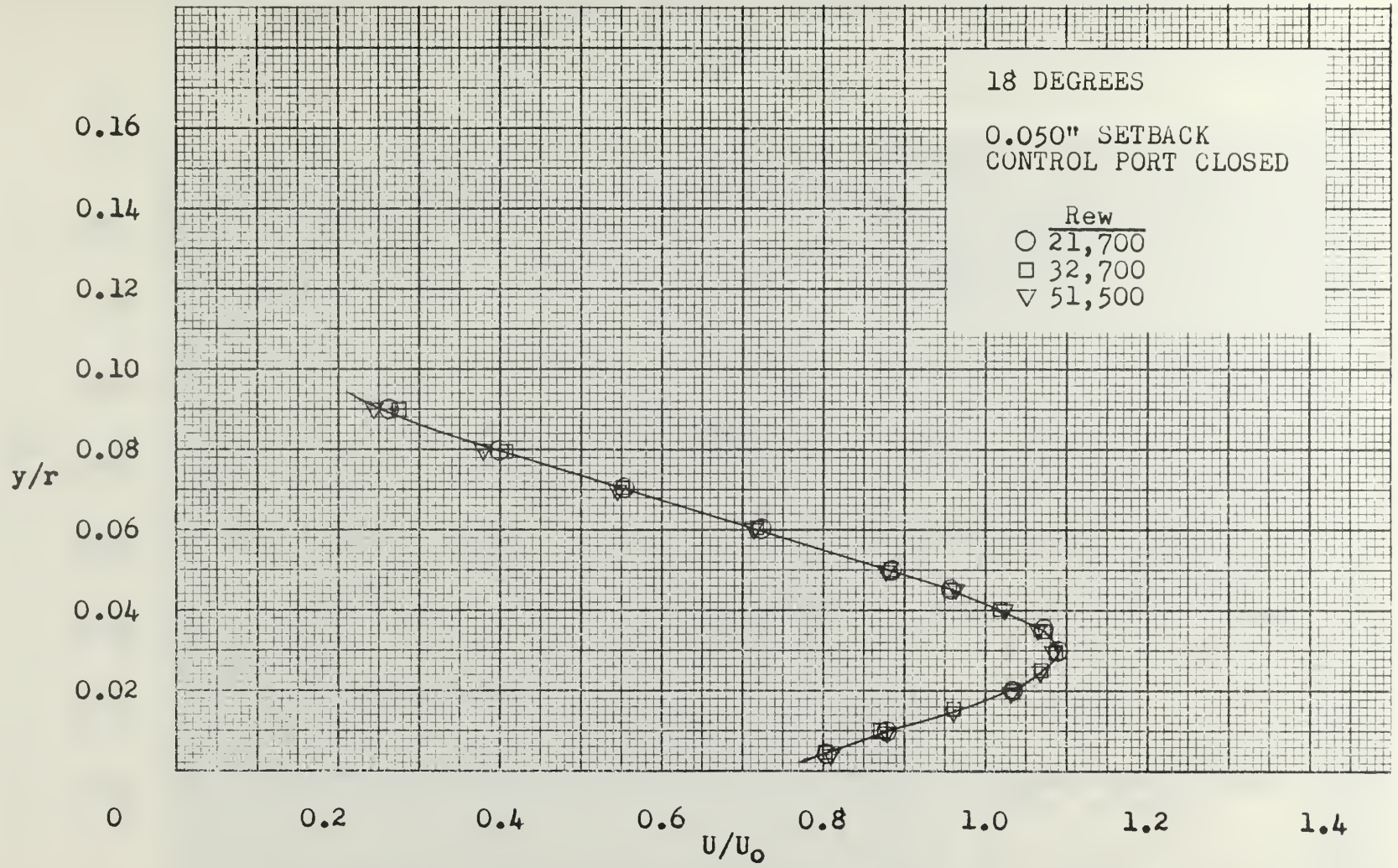

FIGURE 38. NORMALIZED VELOCITY PROFILE - TEST SECTION #1

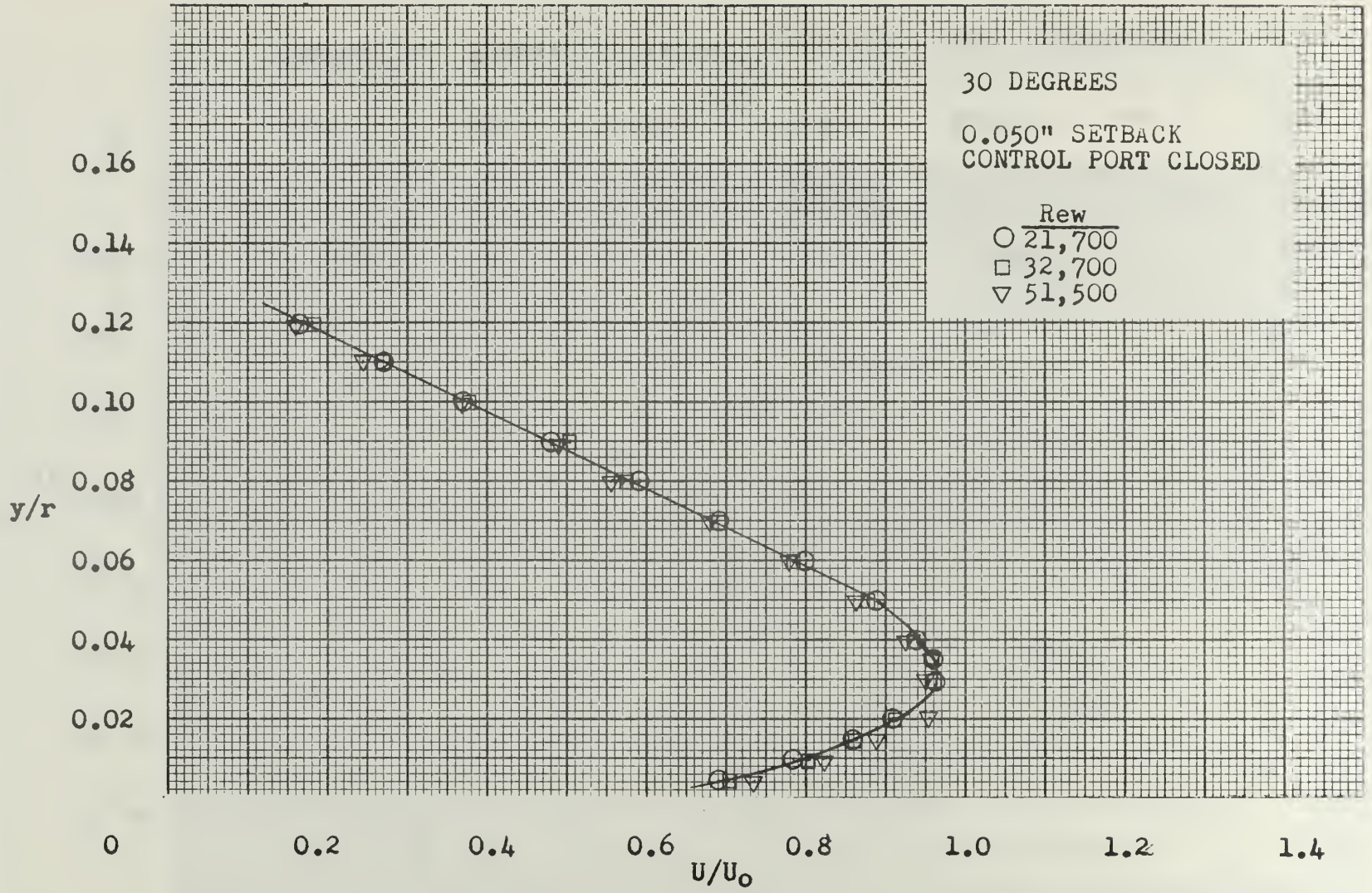

FIGURE 39. NORMALIZED VELOCITY PROFILE - TEST SECTION #1

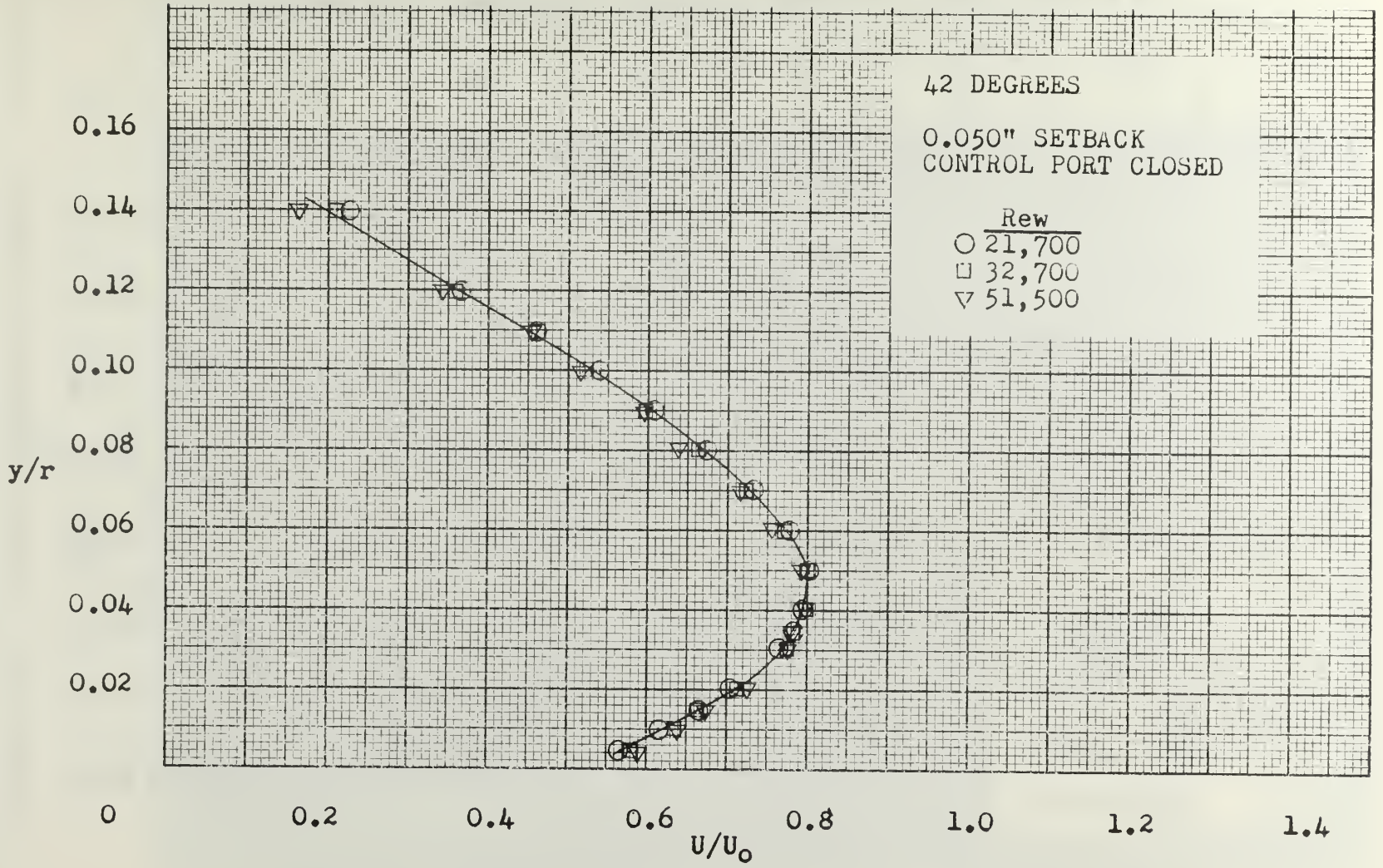

FIGURE 40. NORMALIZED VELOCITY PROFILE - TEST SECTION #1

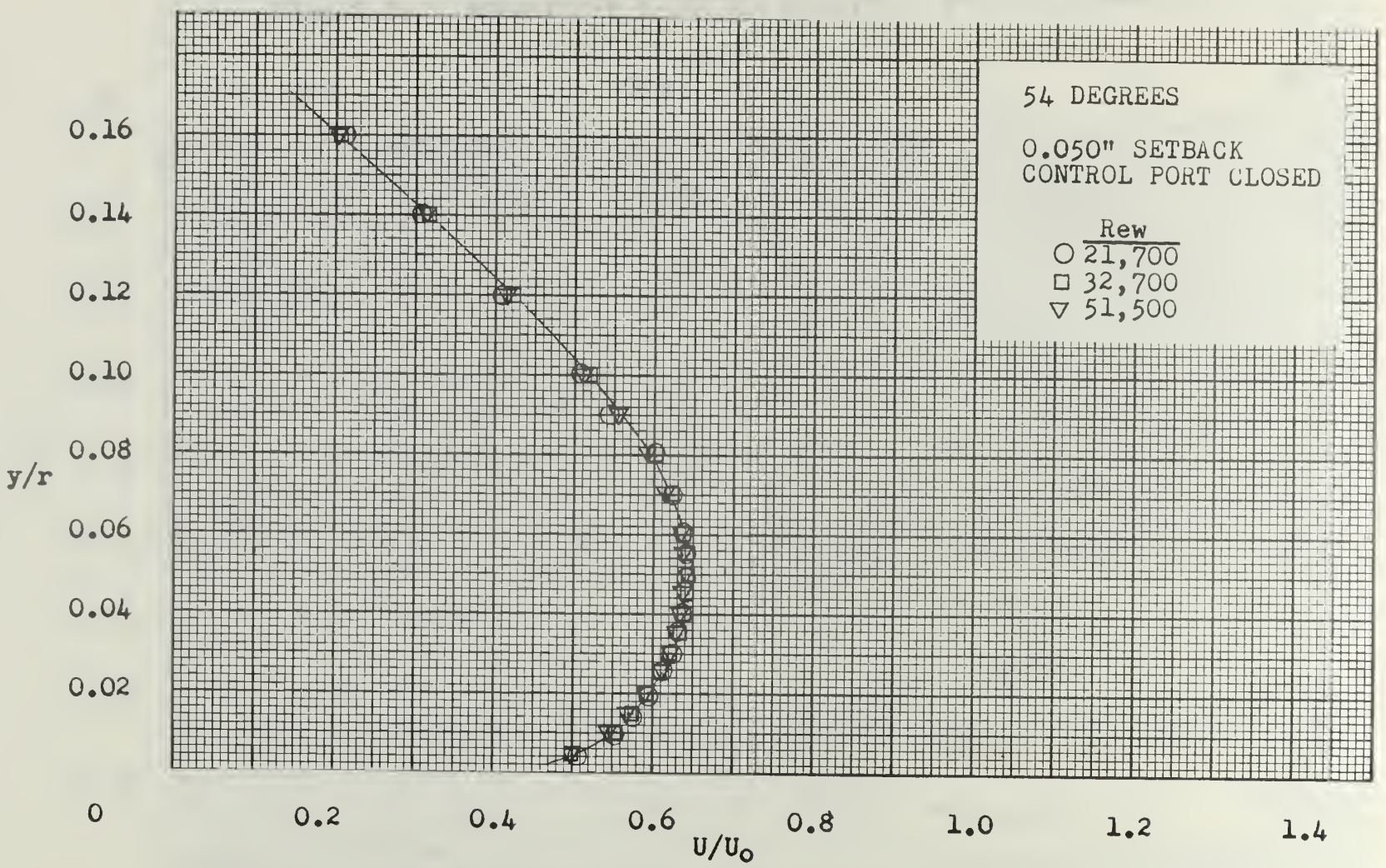

FIGURE 41. NORMALIZED VELOCITY PROFILE - TEST SECTION #1

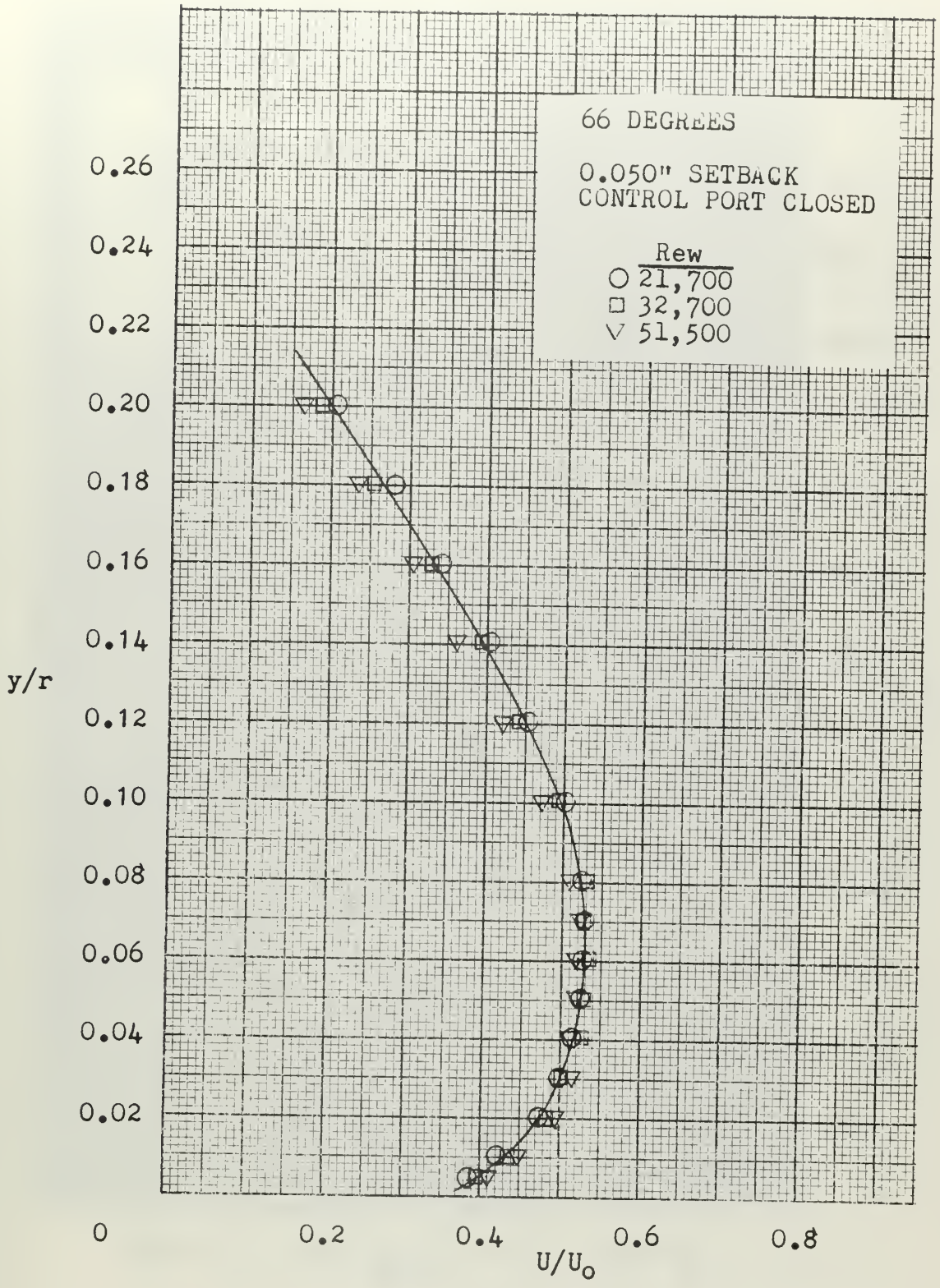

FIGURE 42. NORMALIZED VELOCITY PROFILE - TEST SECTION #1

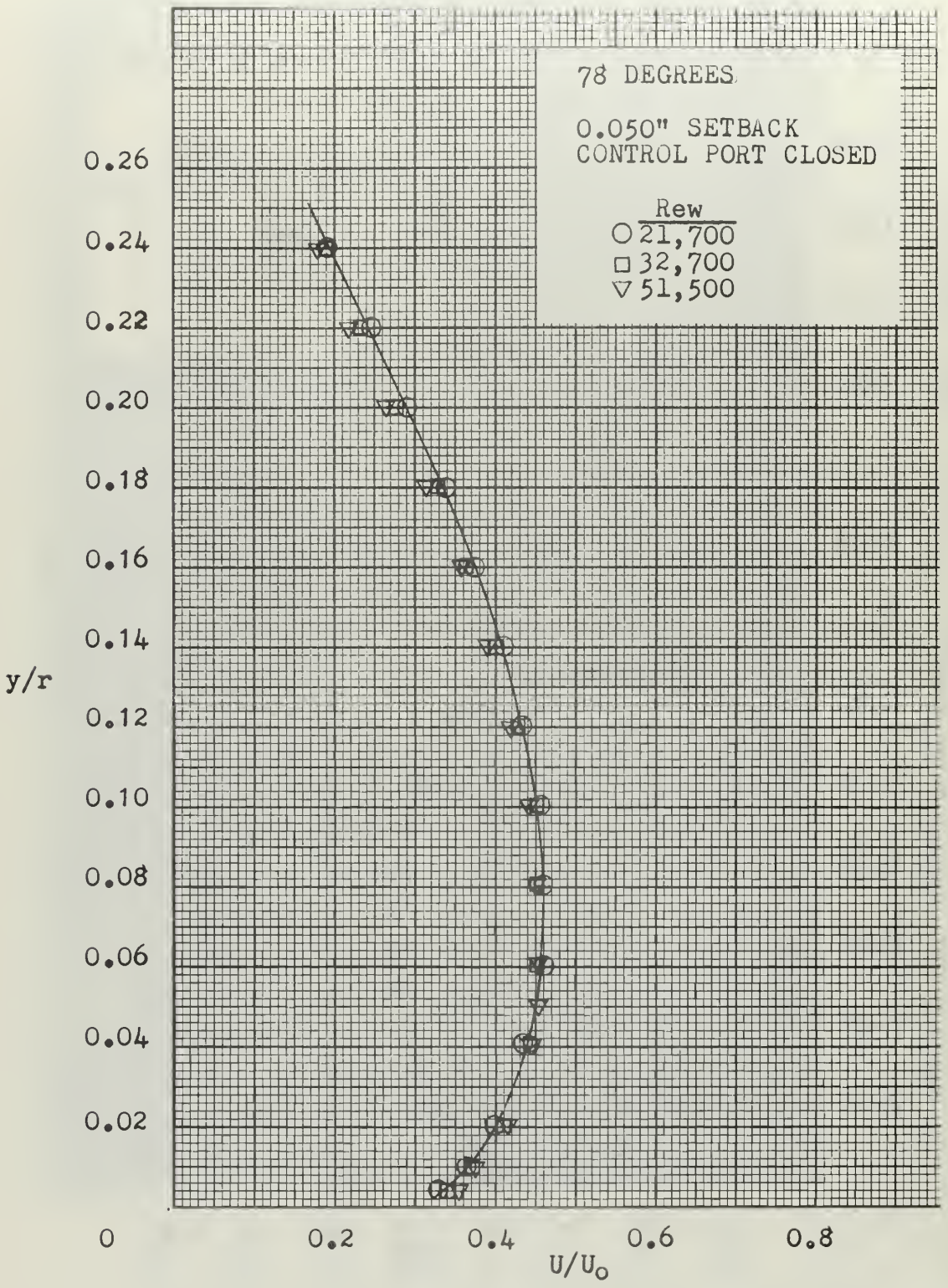

FIGURE 43. NORMALIZED VELOCITY PROFILE - TEST SECTION #1

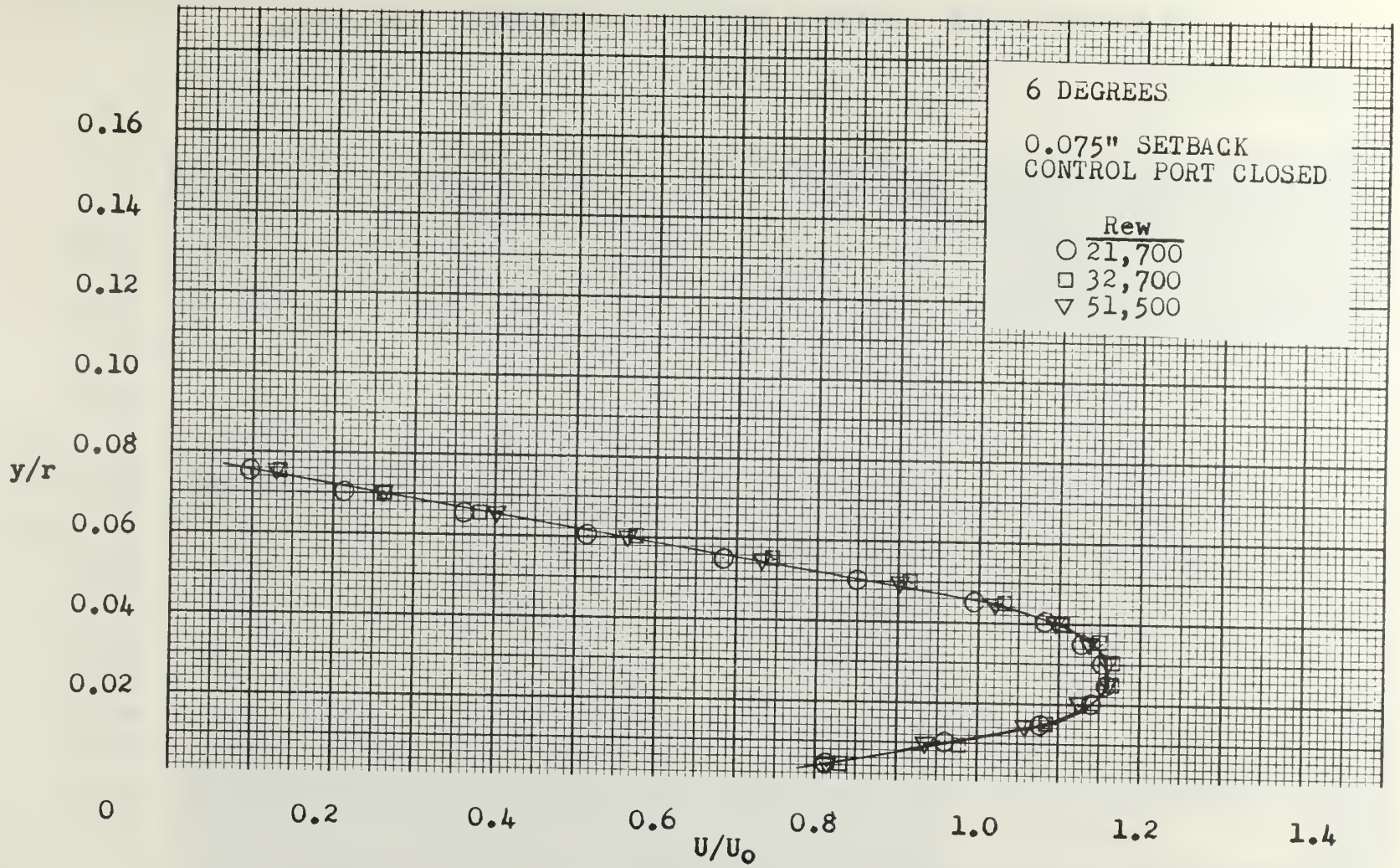

FIGURE 44. NORMALIZED VELOCITY PROFILE - TEST SECTION #1

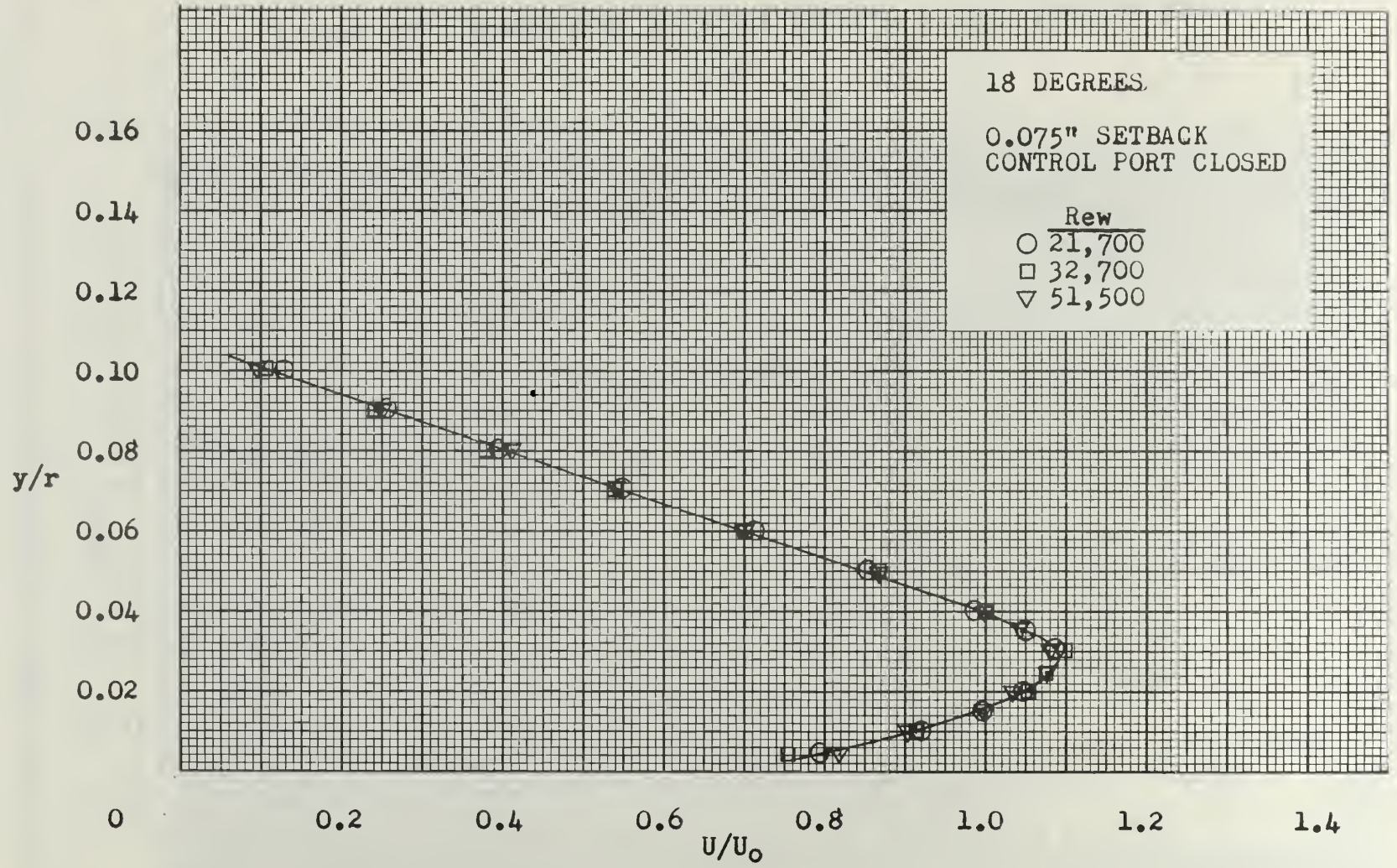

FIGURE 45. NORMALIZED VELOCITY PROFILE - TEST SECTION #1

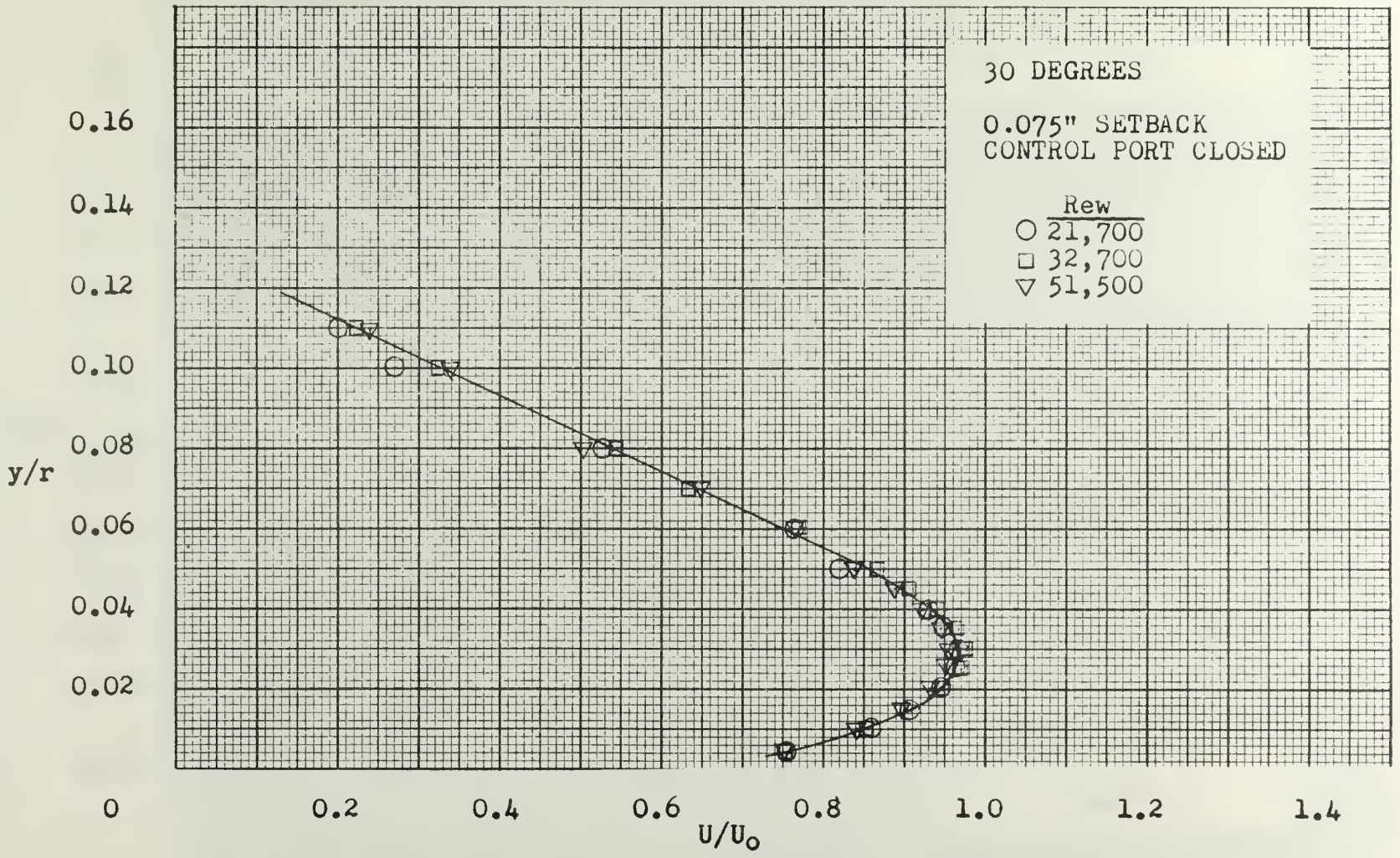

FIGURE 46. NORMALIZED VELOCITY PROFILE - TEST SECTION #1

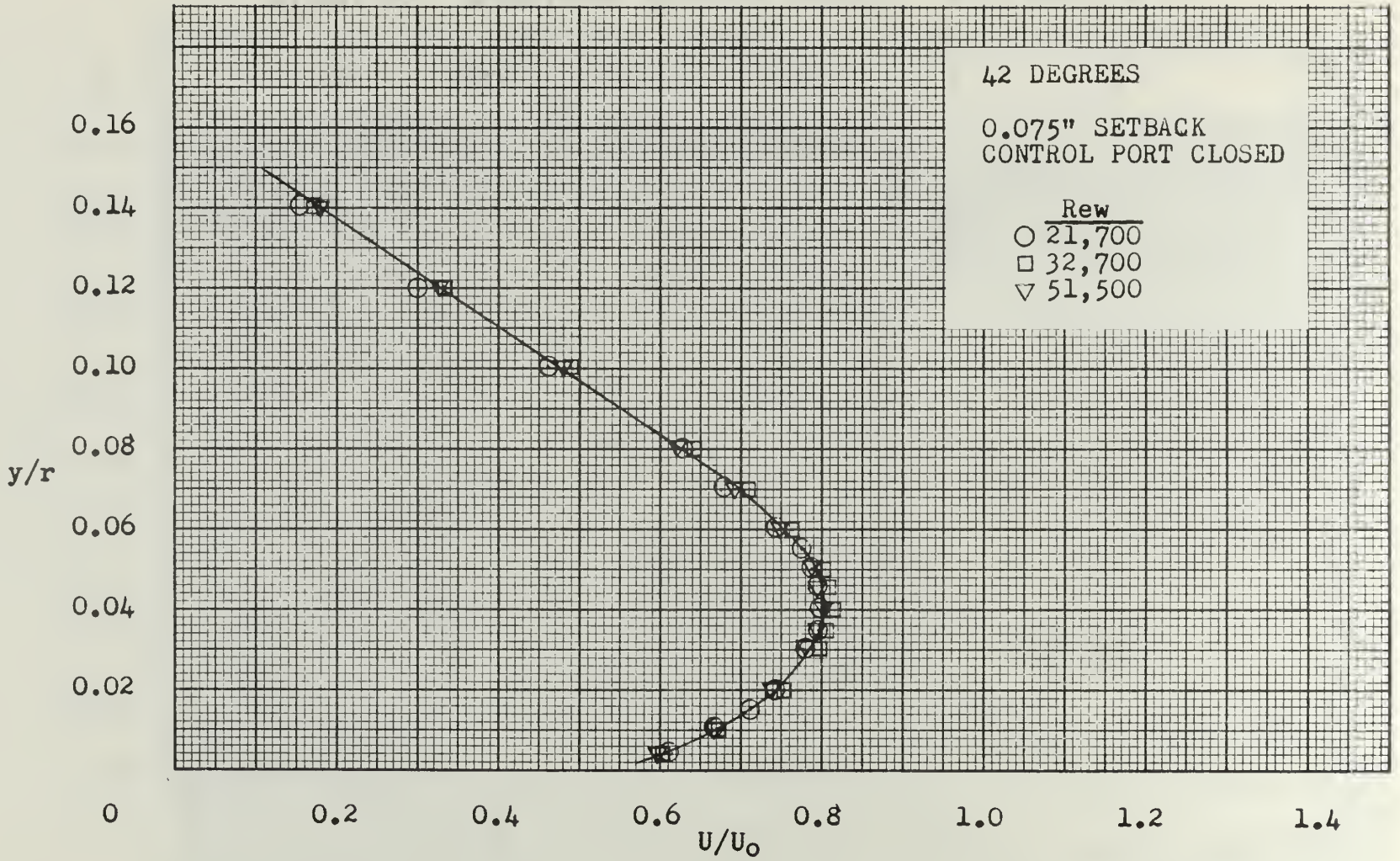

FIGURE 47. NORMALIZED VELOCITY PROFILE - TEST SECTION #1

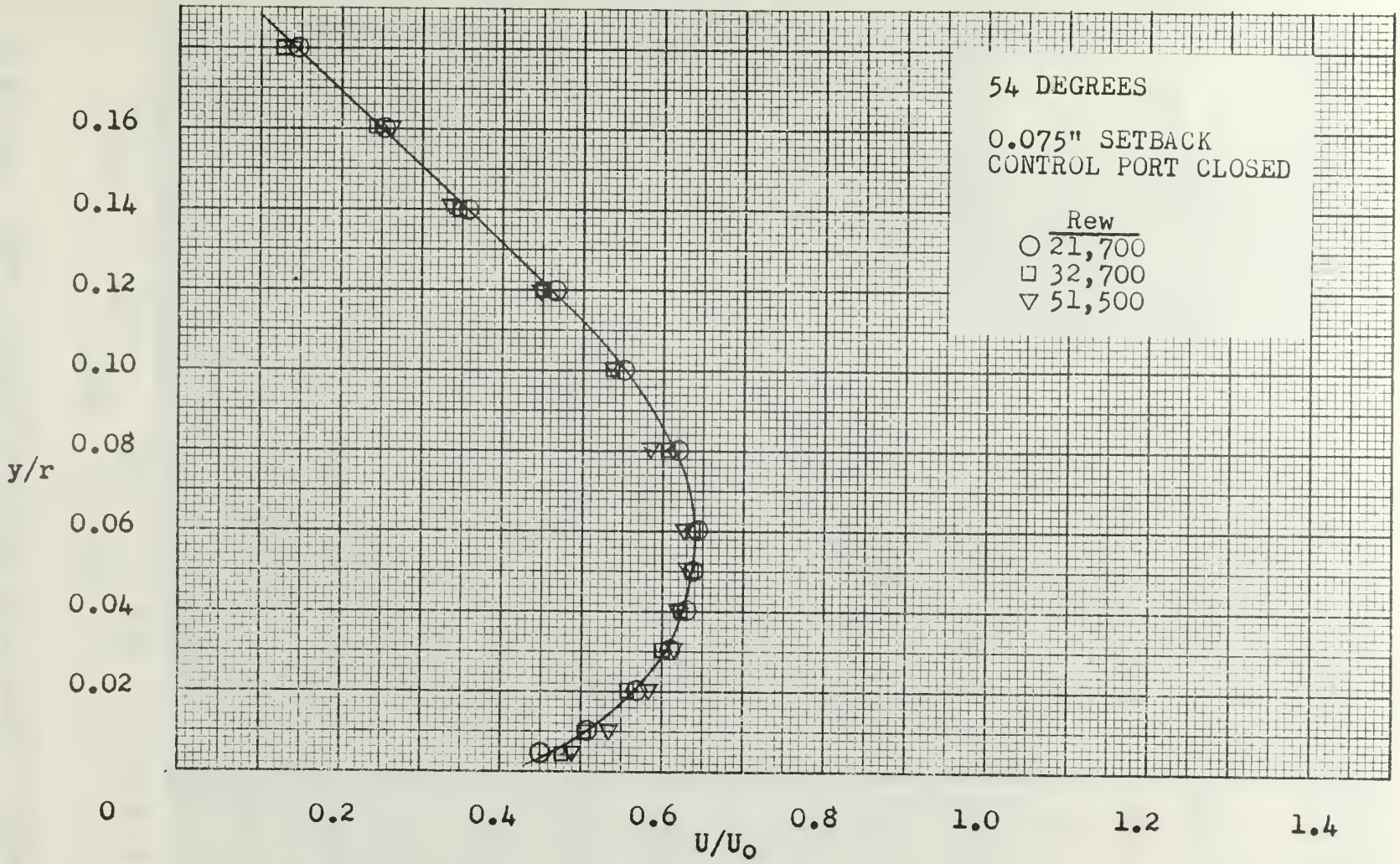

FIGURE 48. NORMALIZED VELOCITY PROFILE - TEST SECTION #1

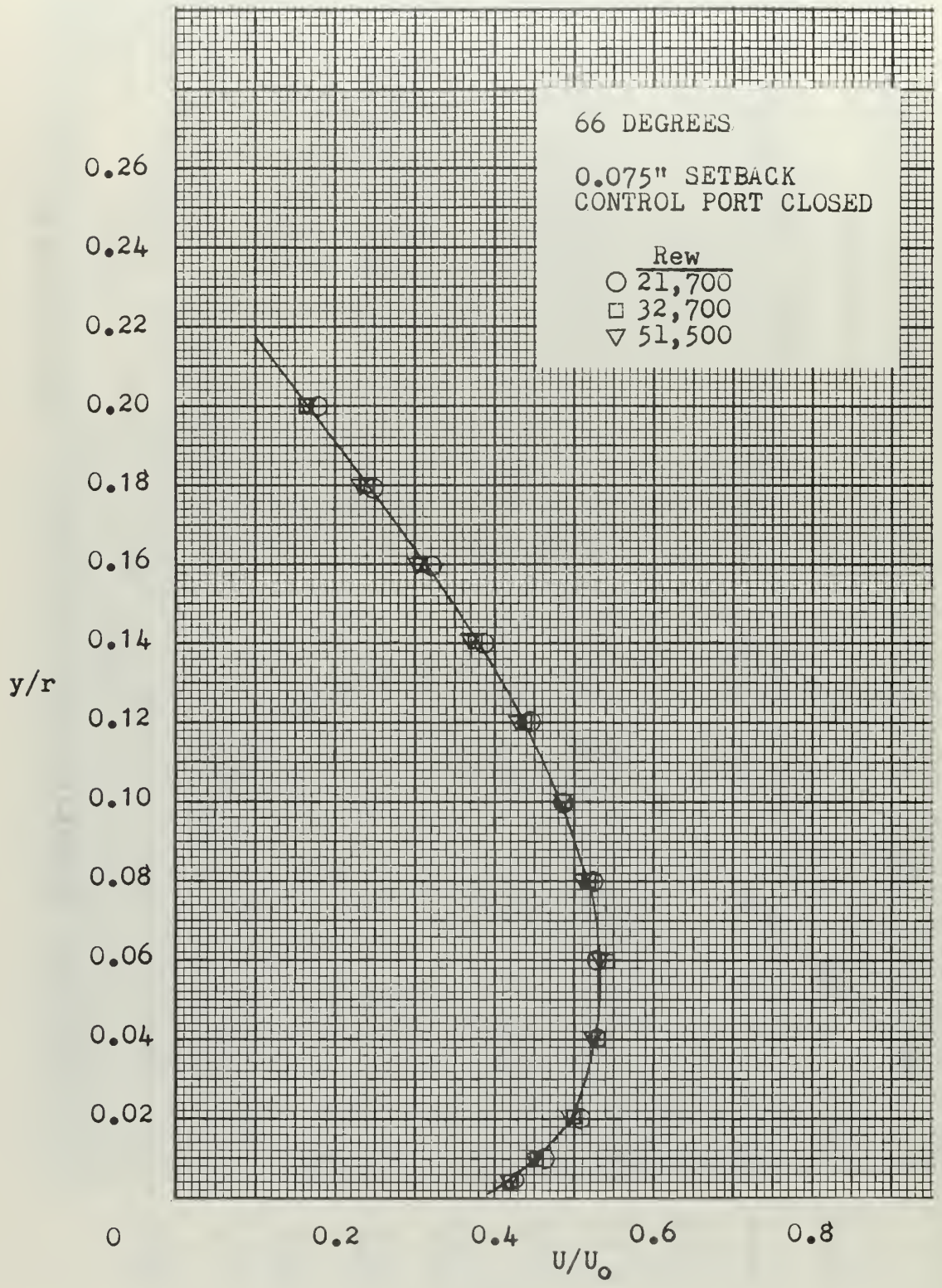

FIGURE 49. NORMALIZED VELOCITY PROFILE - TEST SECTION #1

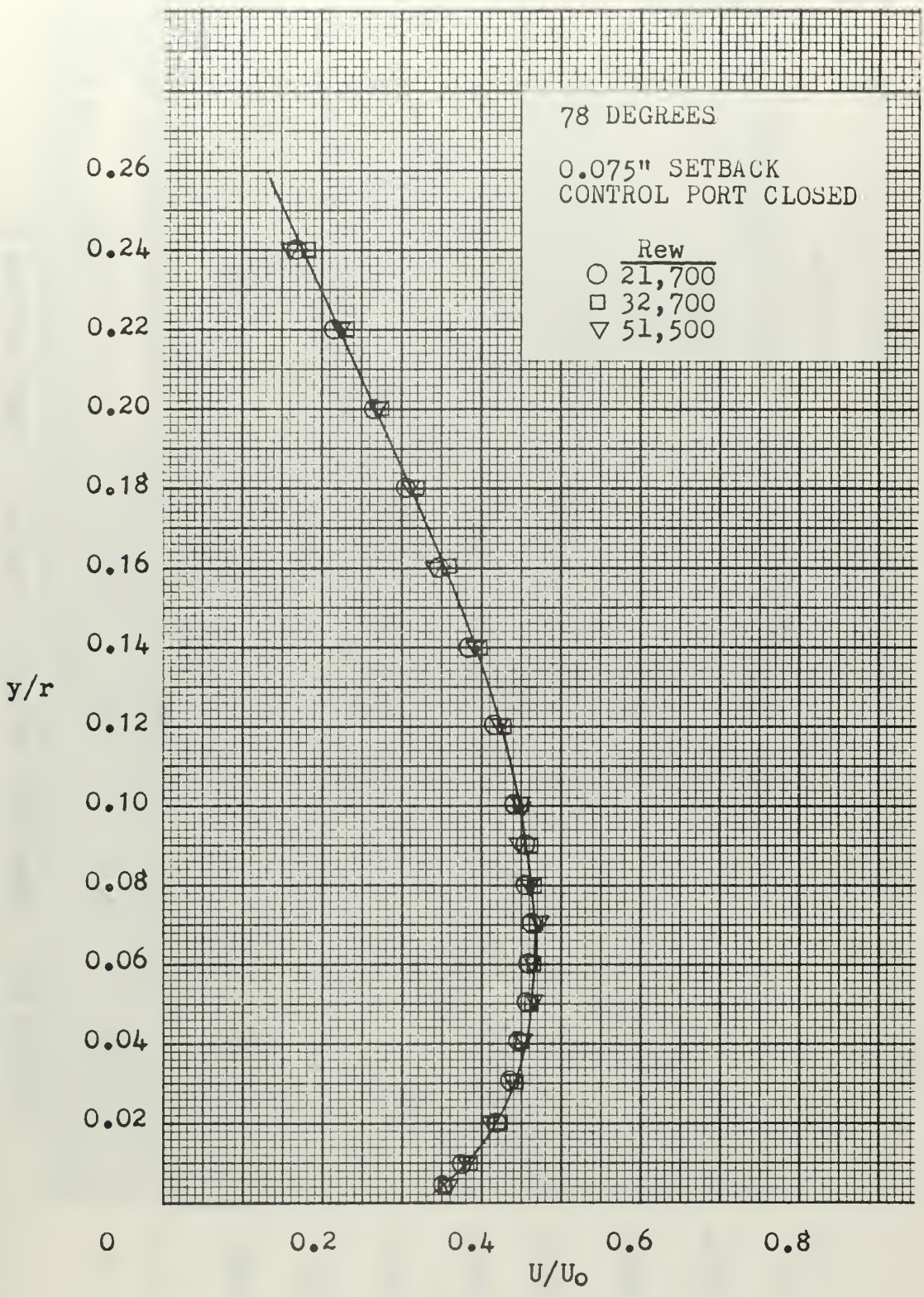

FIGURE 50. NORMALIZED VELOCITY PROFILE - TEST SECTION #1

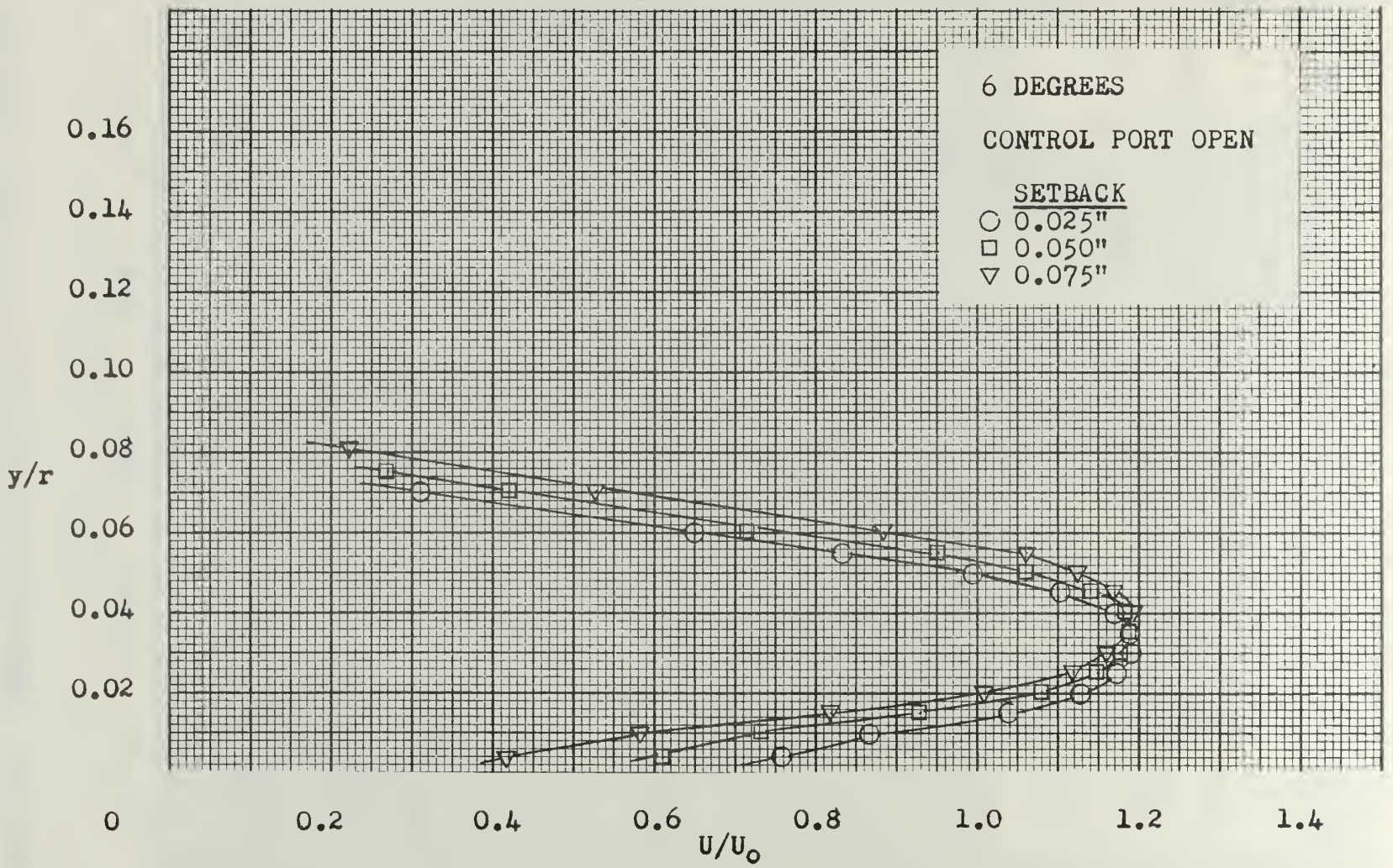

FIGURE 51. NORMALIZED VELOCITY PROFILE - TEST SECTION #1

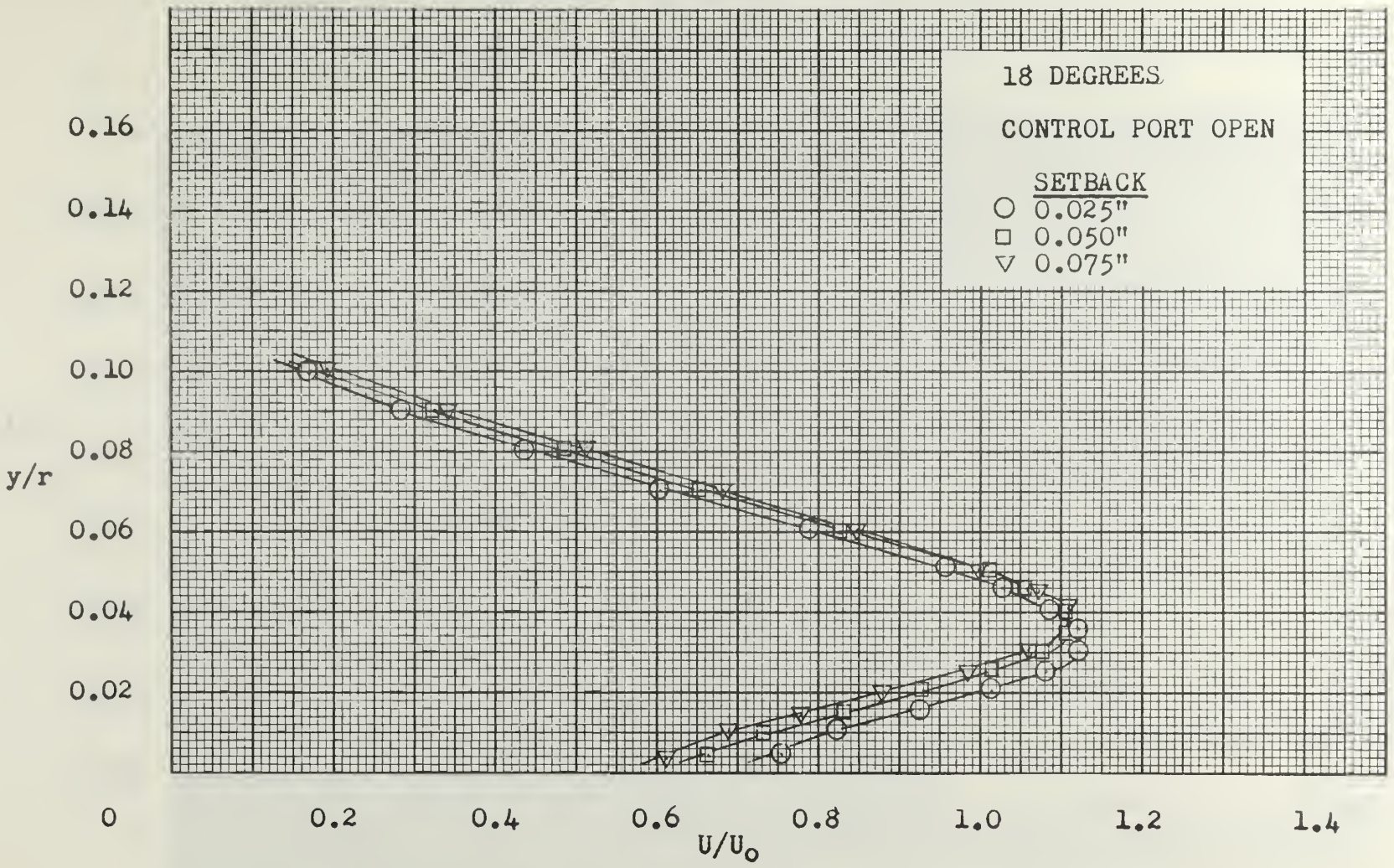

FIGURE 52. NORMALIZED VELOCITY PROFILE - TEST SECTION #1

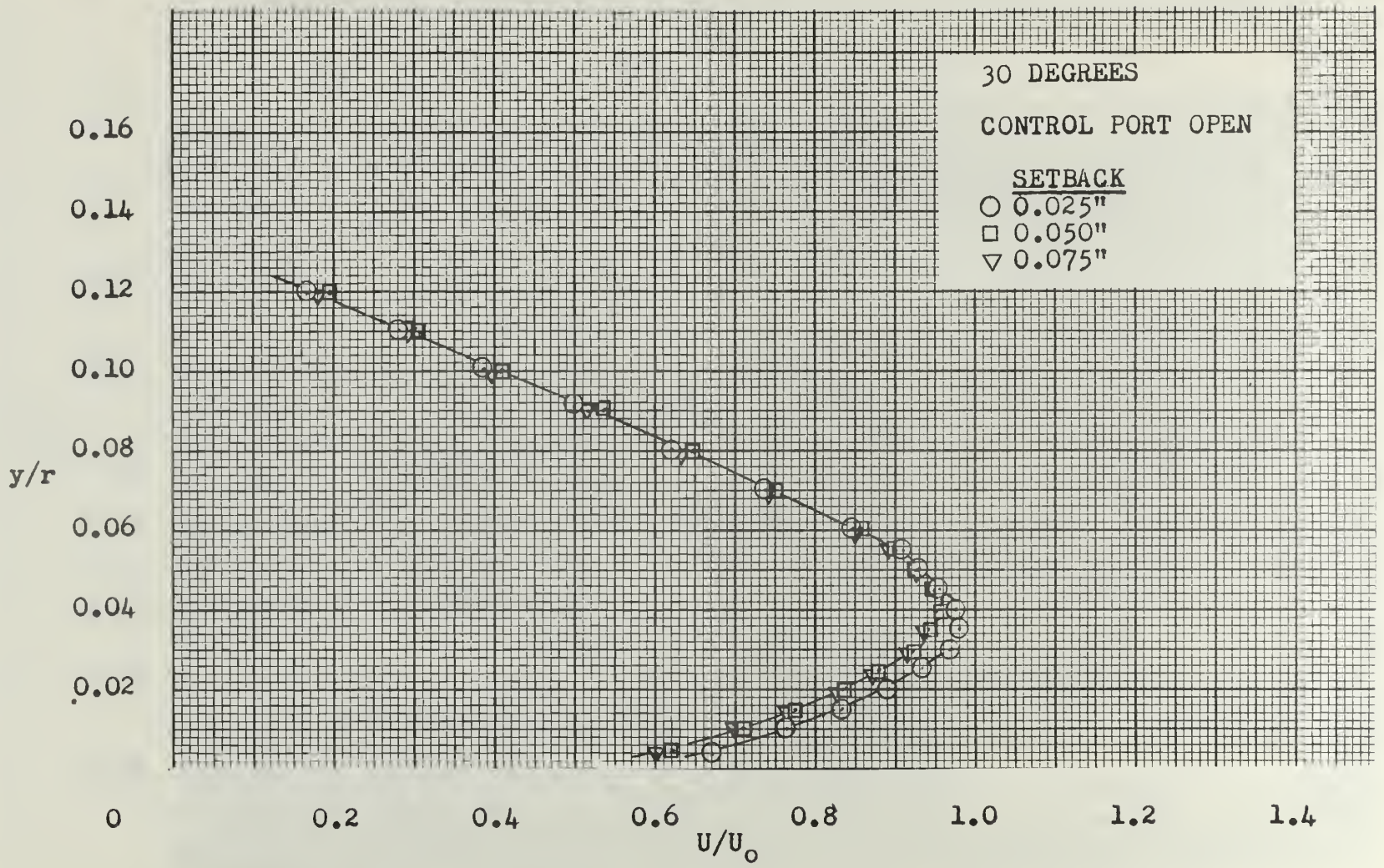

FIGURE 53. NORMALIZED VELOCITY PROFILE - TEST SECTION #1

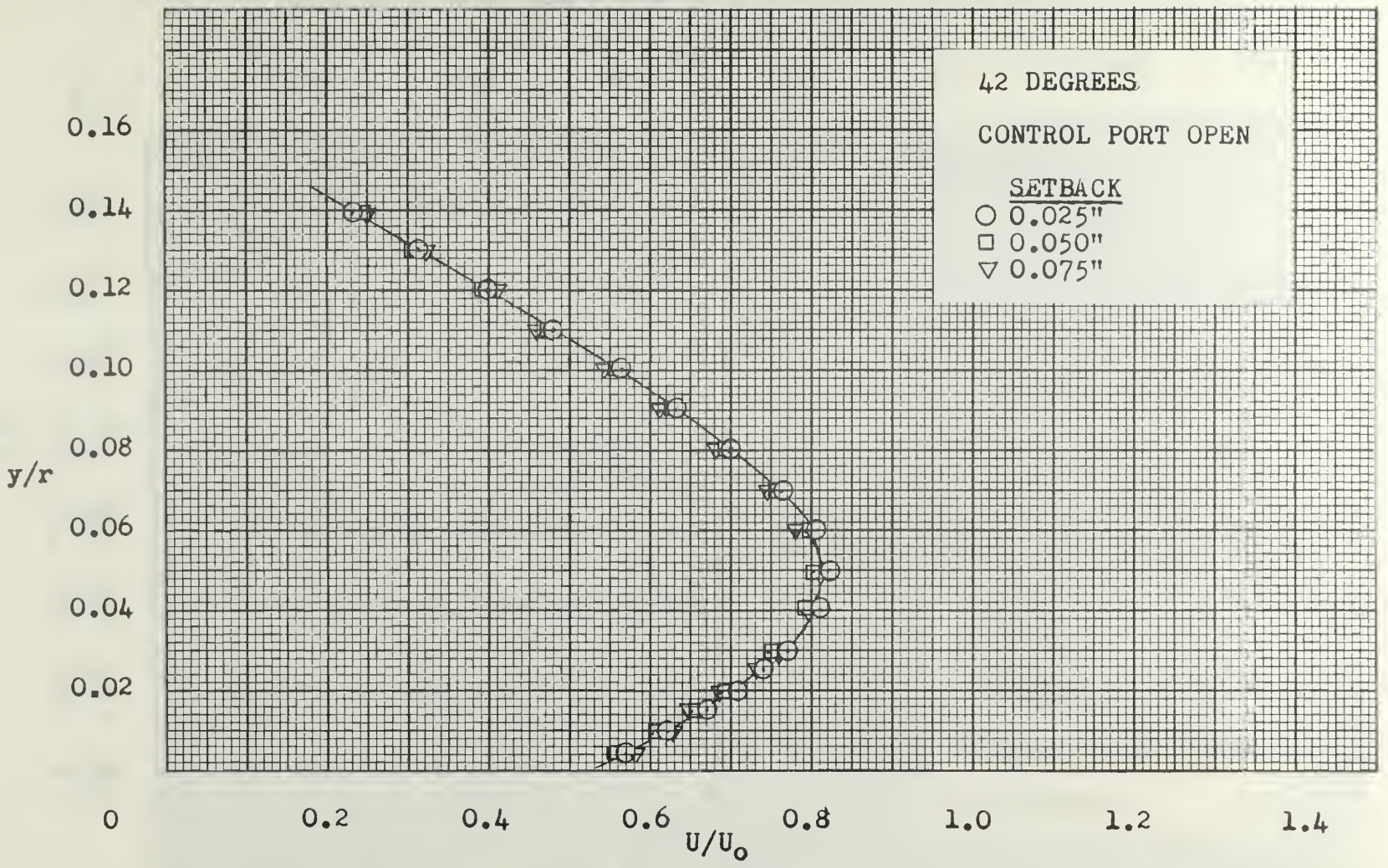

FIGURE 54. NORMALIZED VELOCITY PROFILE - TEST SECTION #1

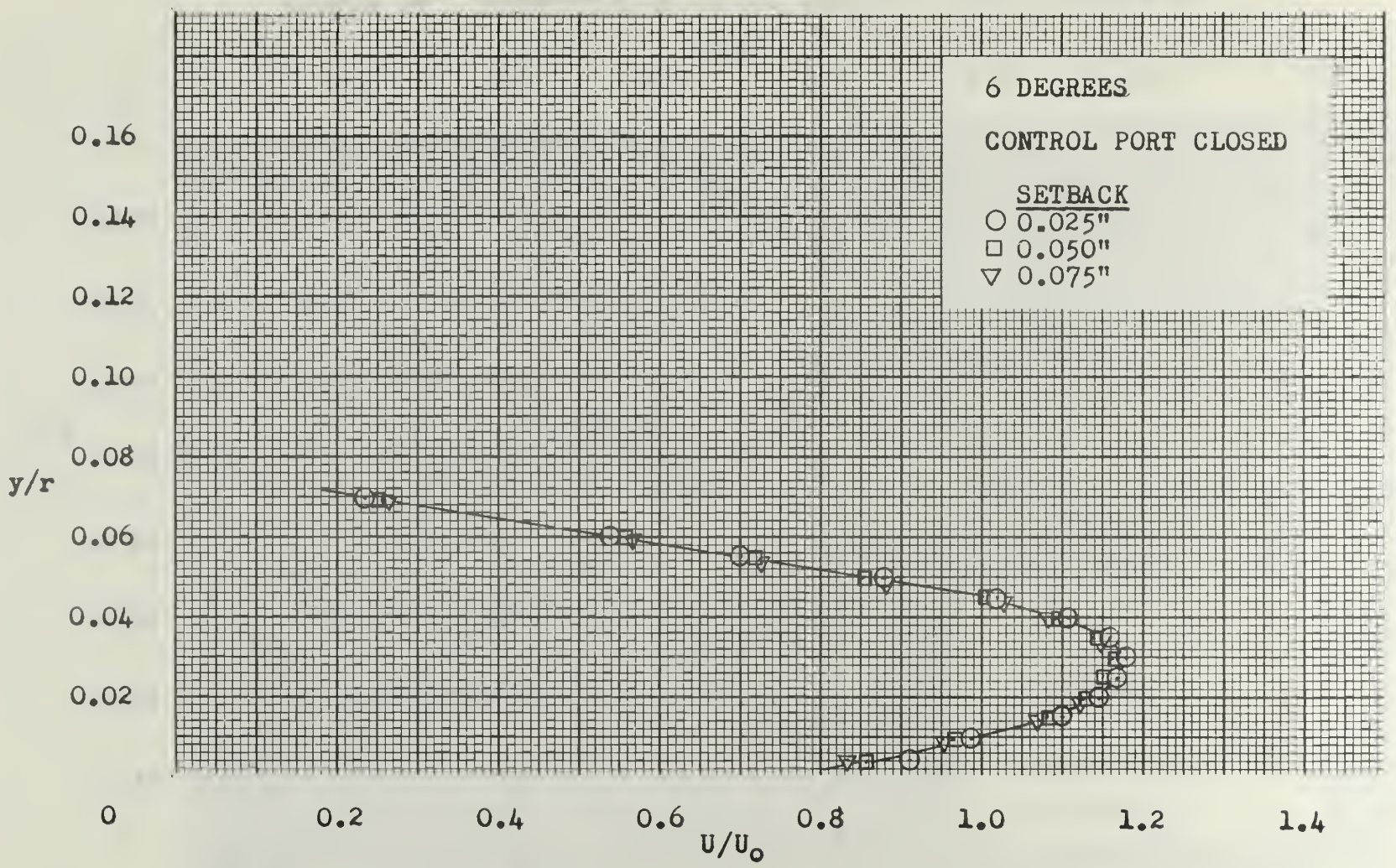

FIGURE 55. NORMALIZED VELOCITY PROFILE - TEST SECTION #1

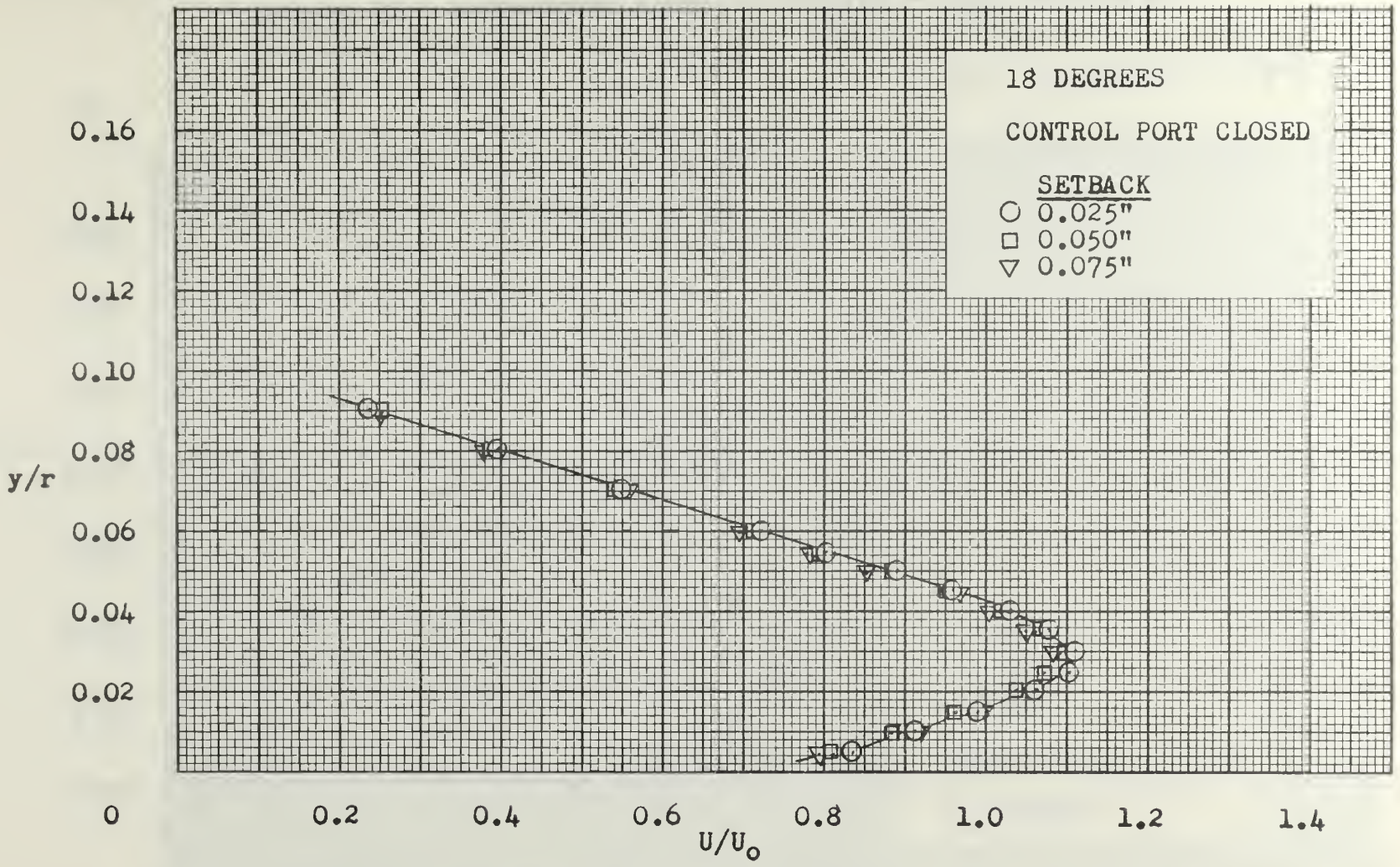

FIGURE 56. NORMALIZED VELOCITY PROFILE - TEST SECTION #1

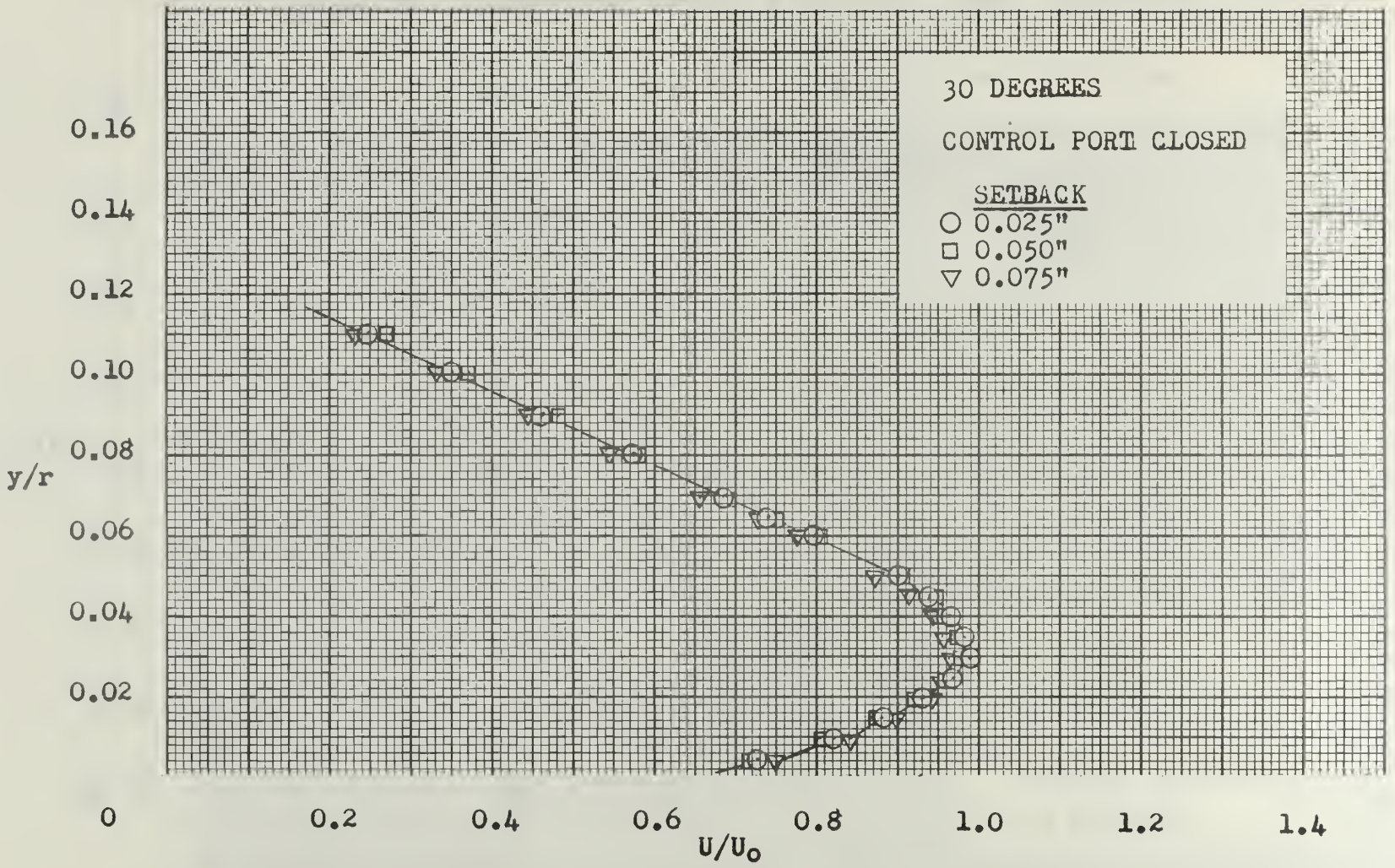

FIGURE 57. NORMALIZED VELOCITY PROFILE - TEST SECTION #1

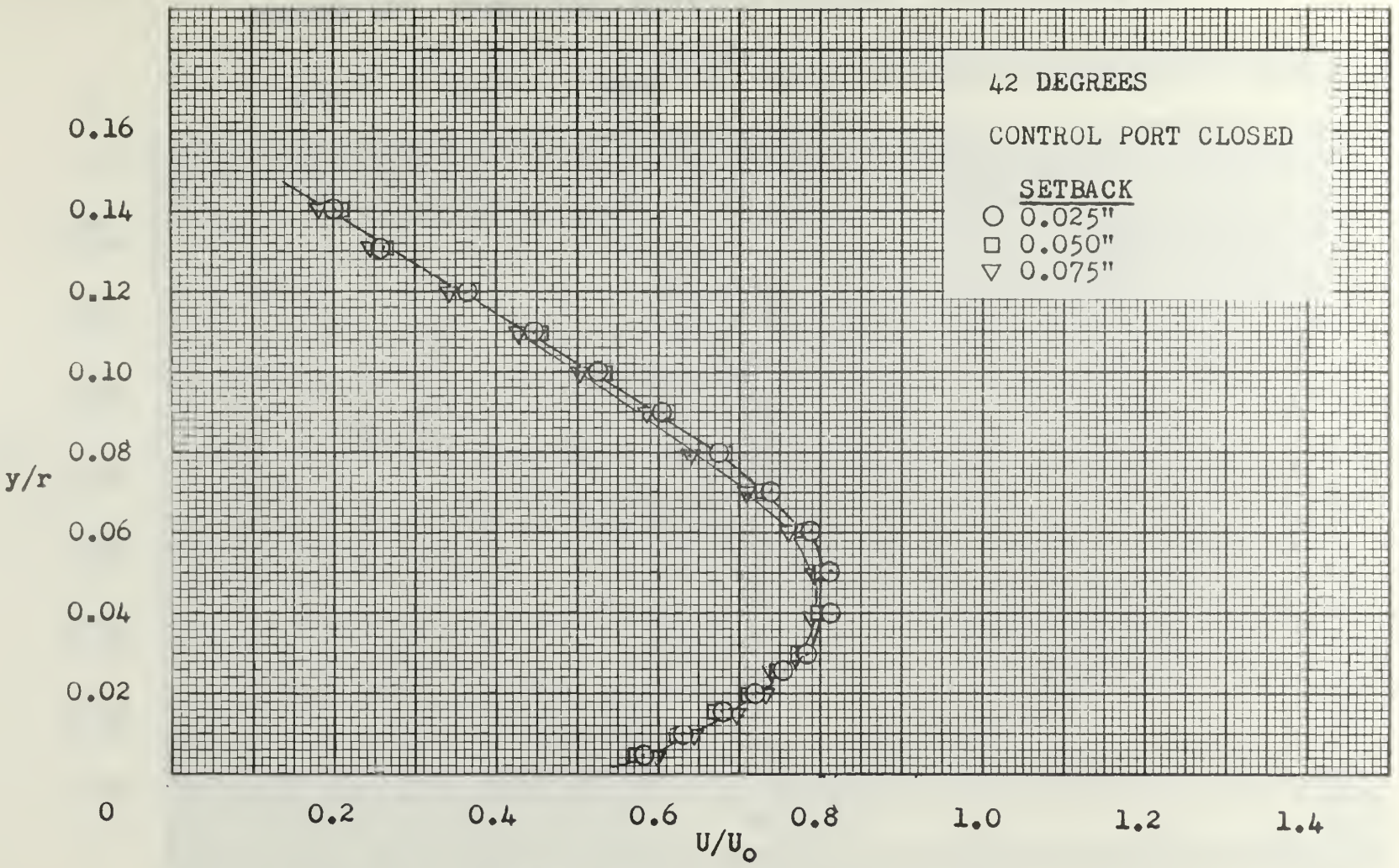

FIGURE 58. NORMALIZED VELOCITY PROFILE - TEST SECTION #1

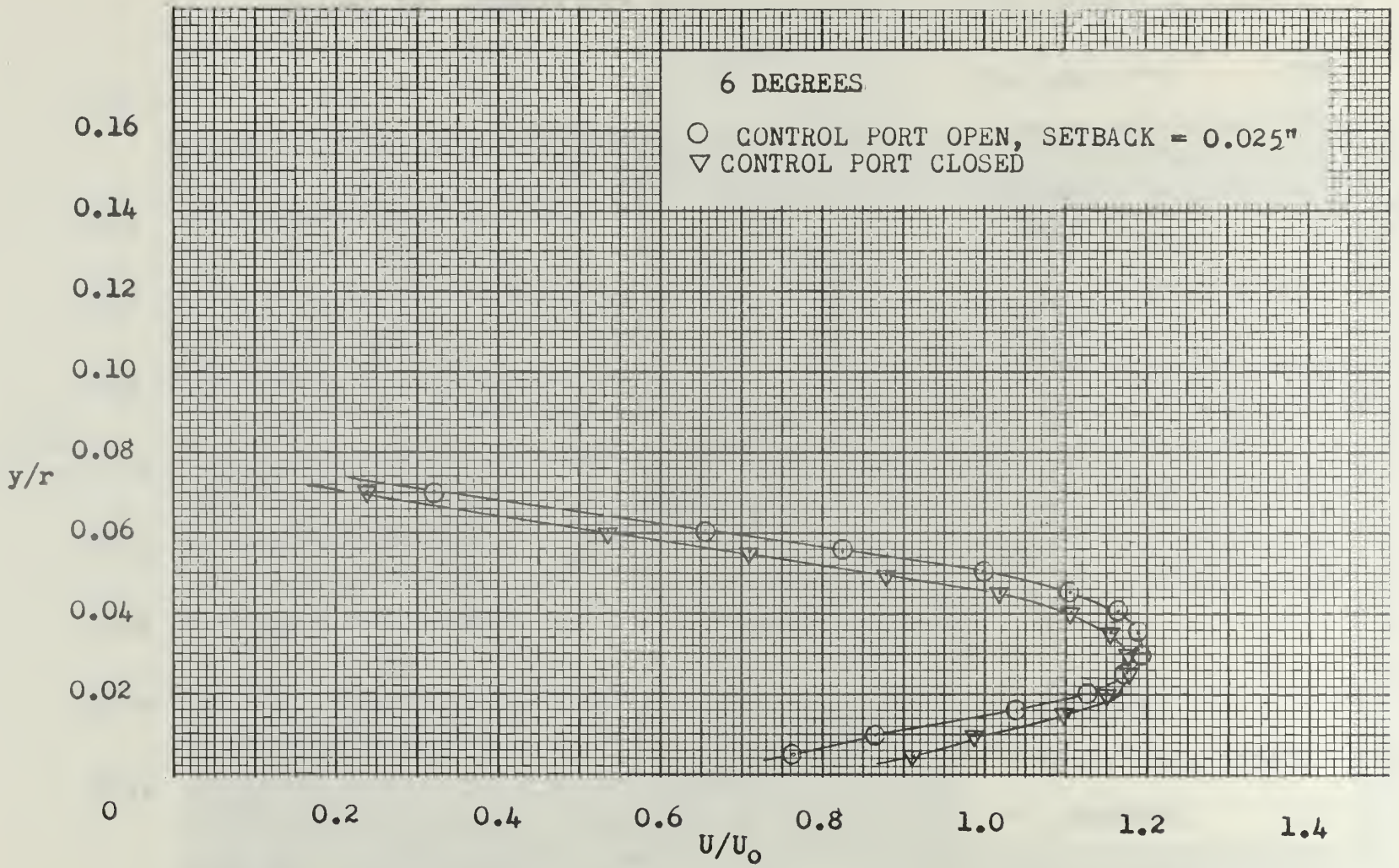

FIGURE 59. NORMALIZED VELOCITY PROFILE - TEST SECTION #1

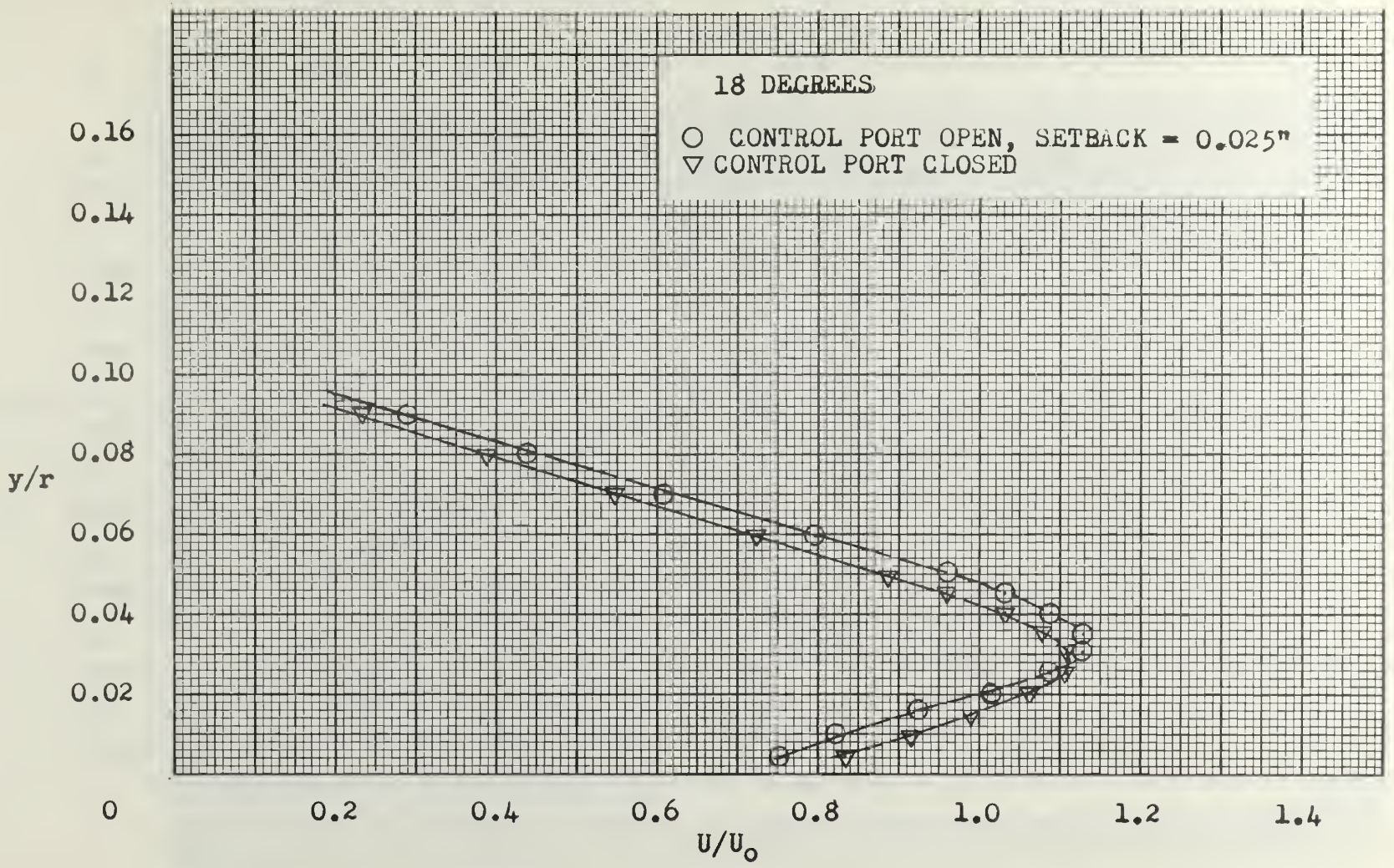

FIGURE 60. NORMALIZED VELOCITY PROFILE - TEST SECTION #1

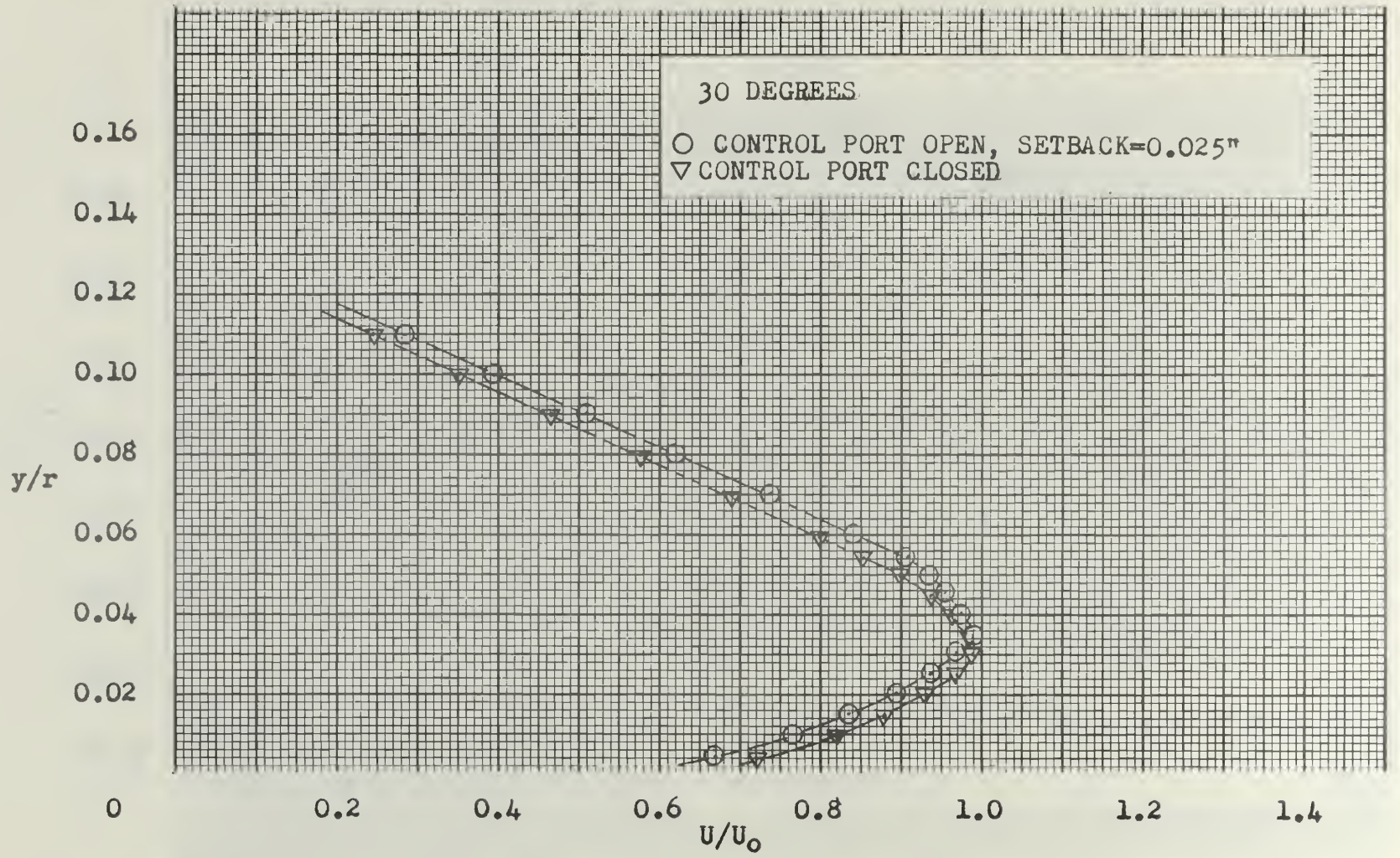

FIGURE 61. NORMALIZED VELOCITY PROFILE - TEST SECTION #1

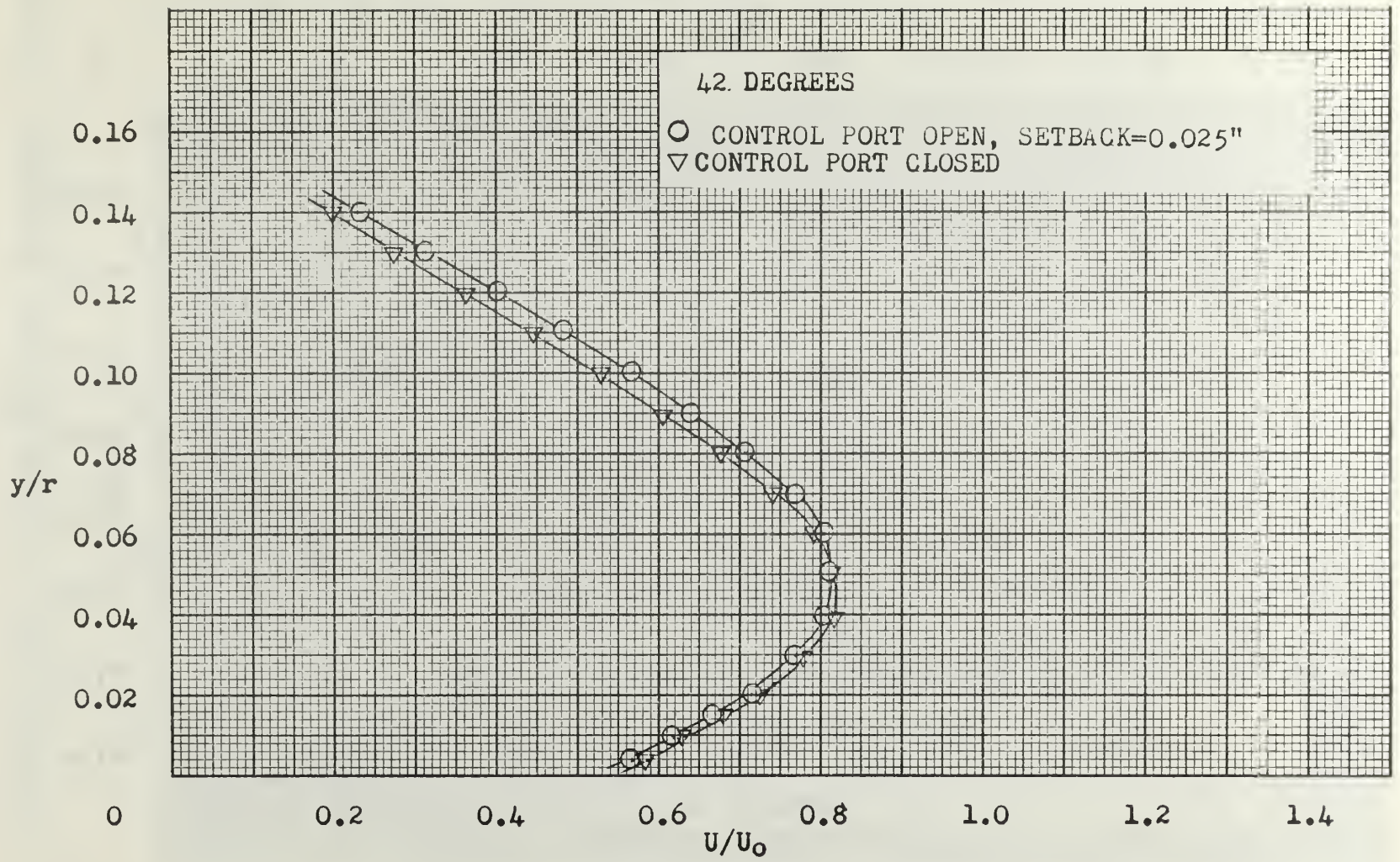

FIGURE 62. NORMALIZED VELOCITY PROFILE - TEST SECTION #1

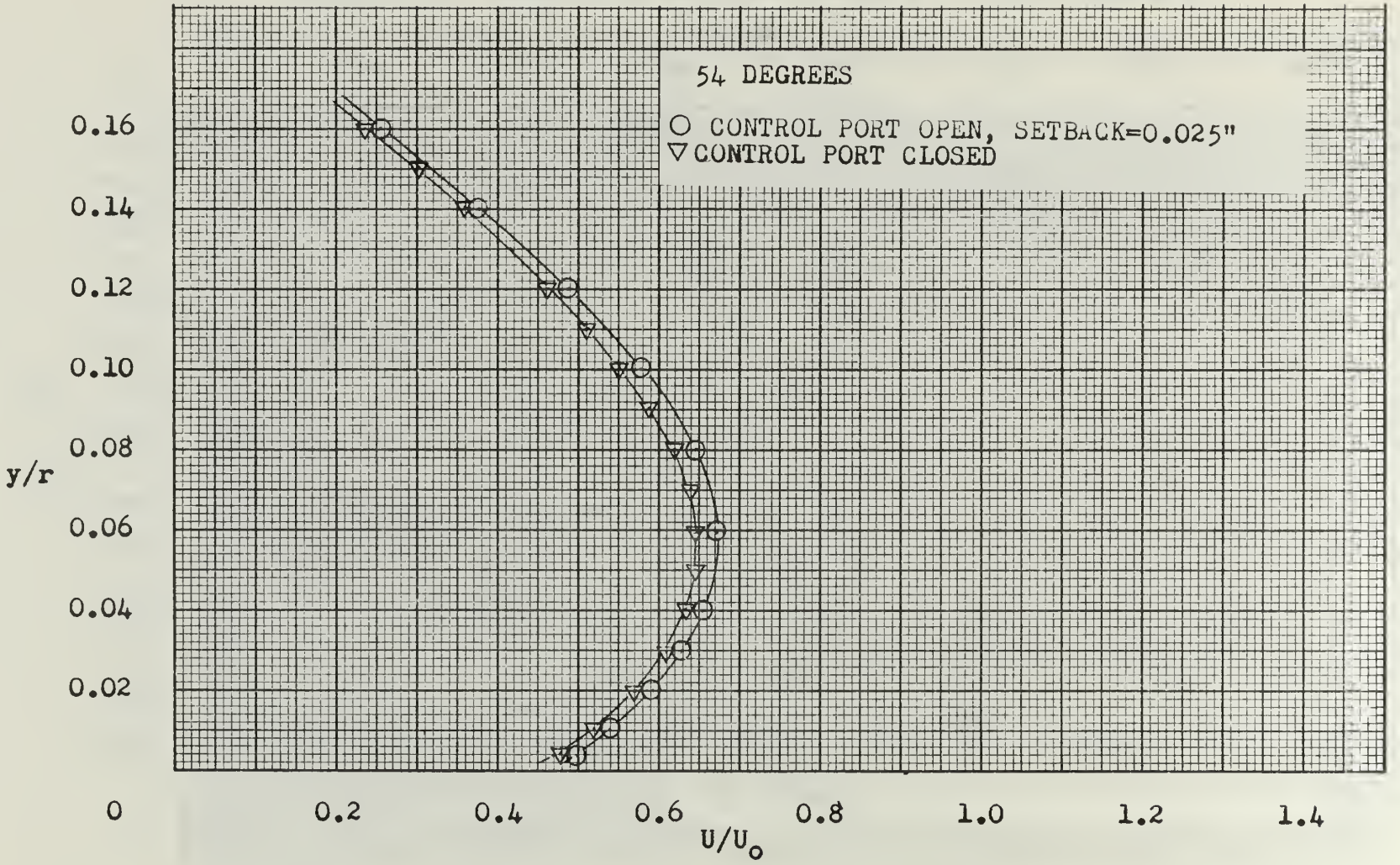

FIGURE 63. NORMALIZED VELOCITY PROFILE - TEST SECTION #1

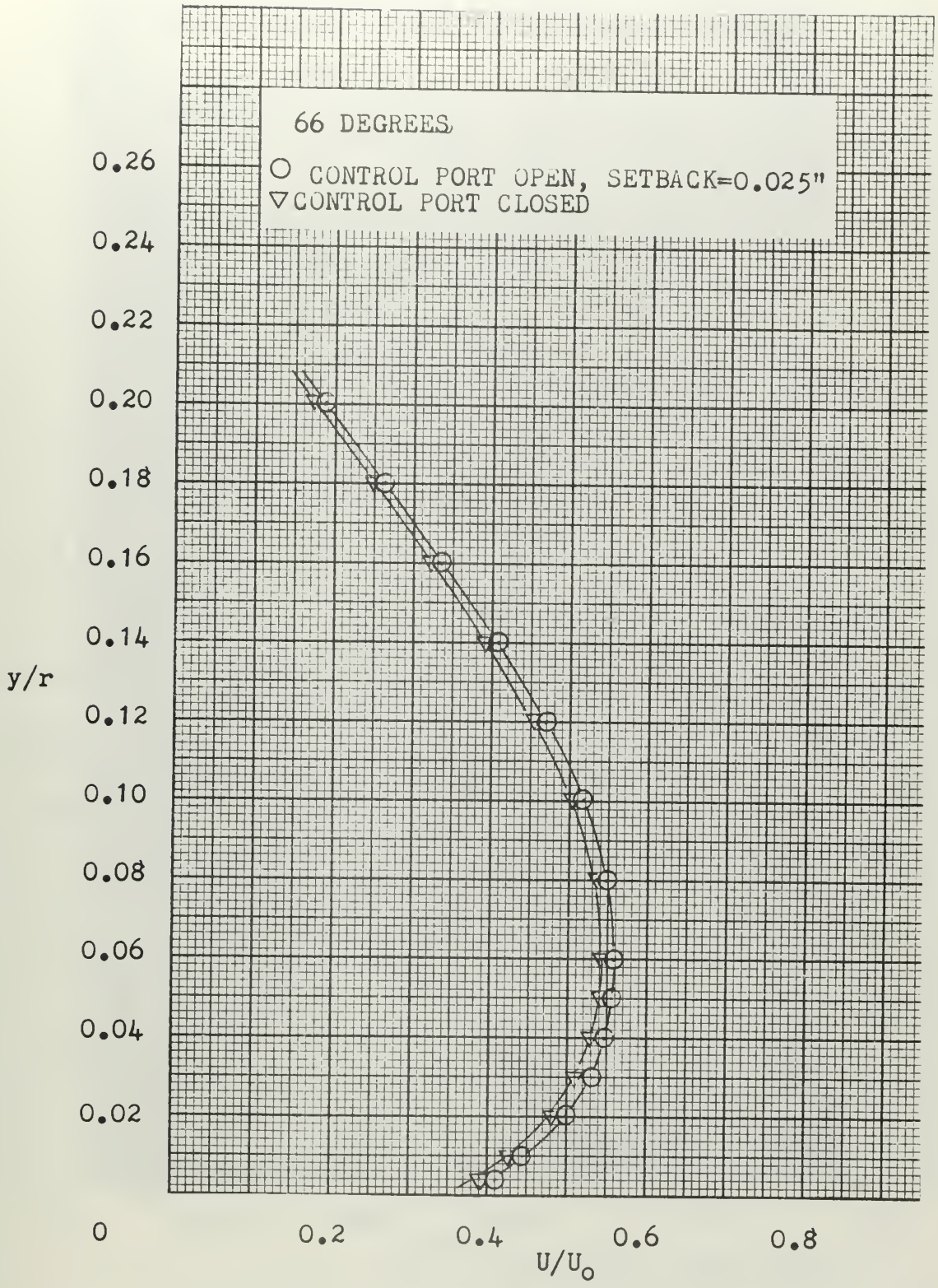

FIGURE 64. NORMALIZED VELOCITY PROFILE - TEST SECTION #1

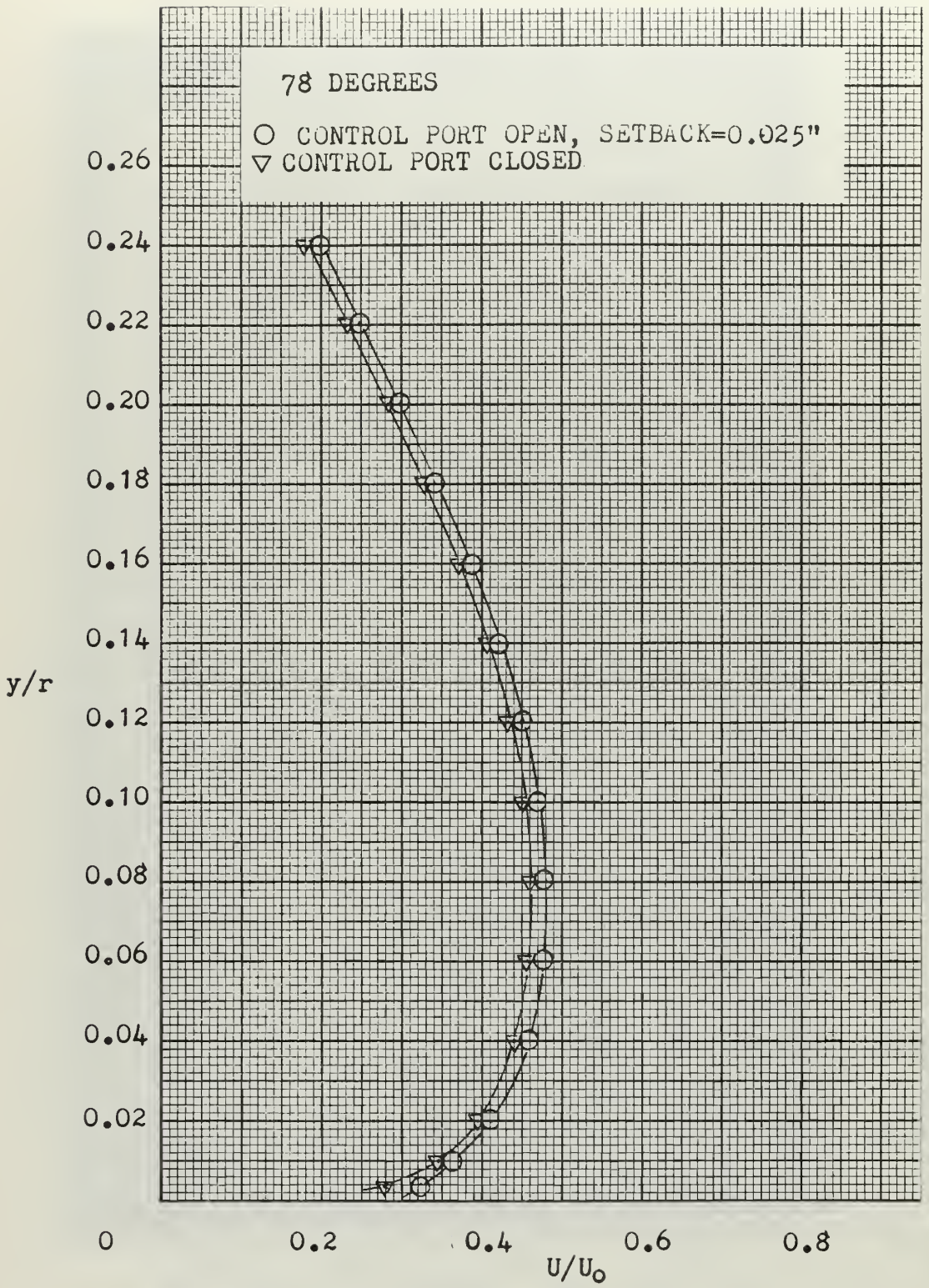

FIGURE 65. NORMALIZED VELOCITY PROFILE - TEST SECTION #1

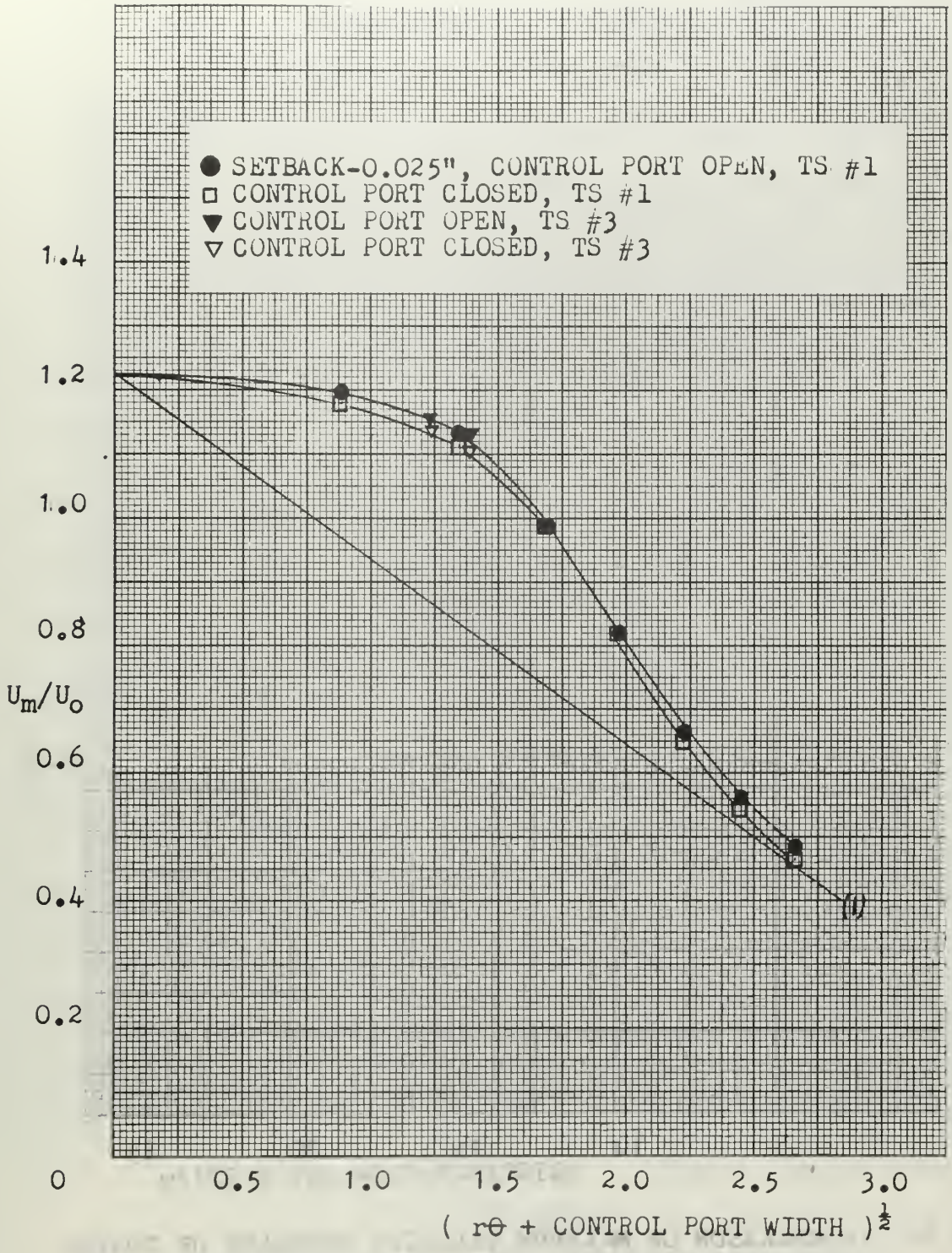

FIGURE 66. DECREASE OF MAXIMUM VELOCITY AROUND CONVEX WALL

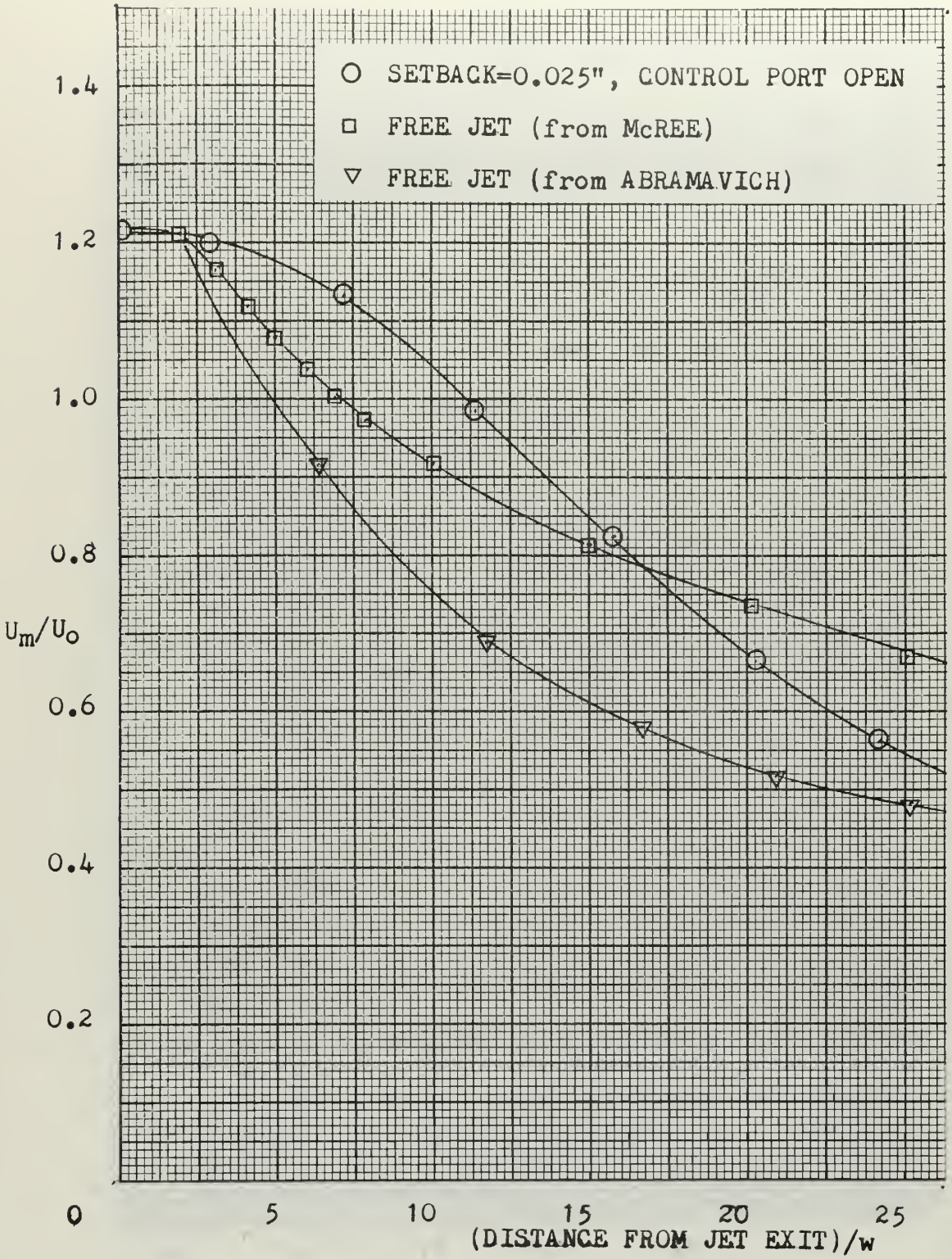

FIGURE 67. COMPARISON OF MAXIMUM VELOCITY DECREASE OF CONVEX WALL FLOW WITH FREE JETS - TEST SECTION #1

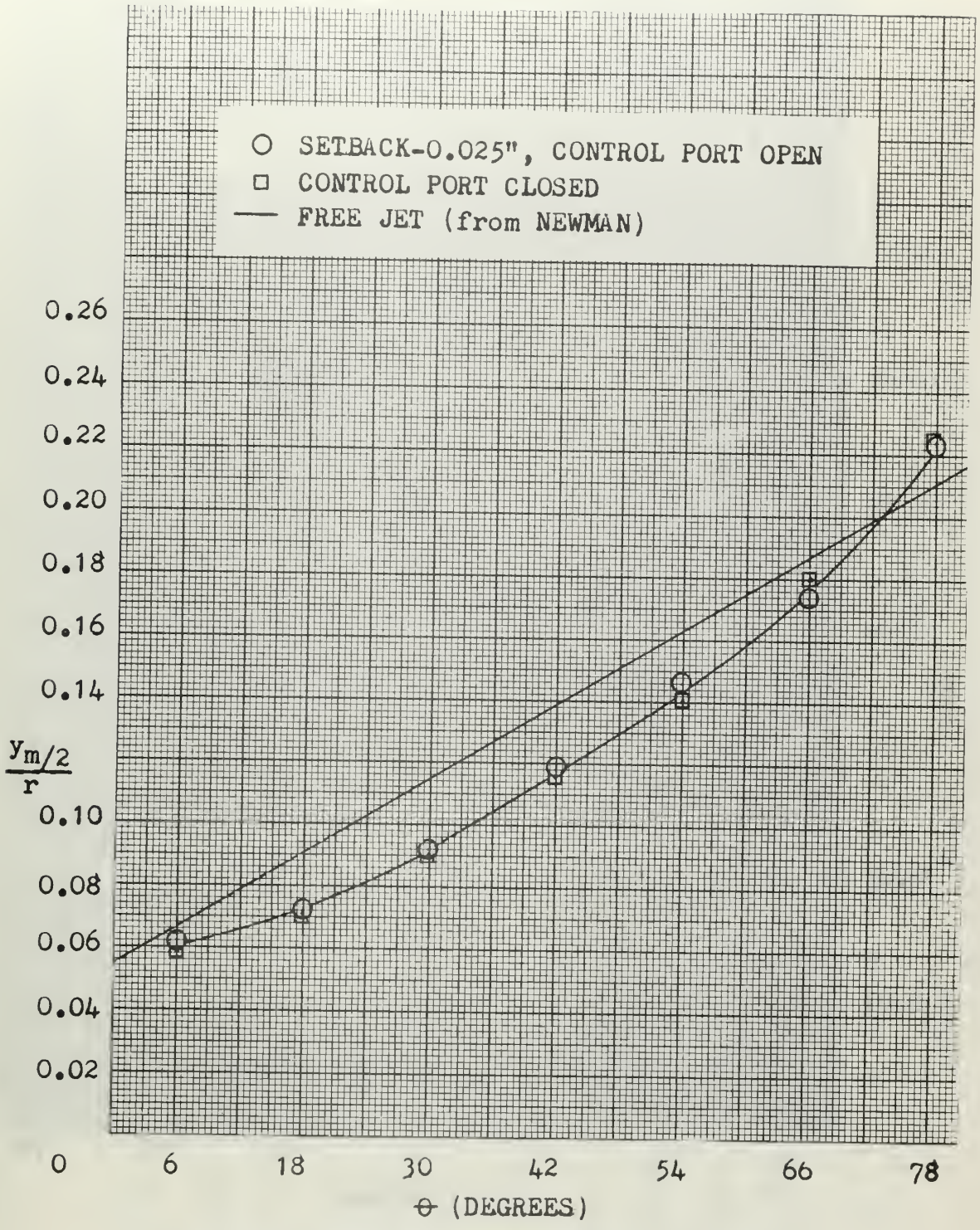

FIGURE 68. GROWTH OF $y_{m/2}$ AROUND CONVEX WALL
TEST SECTION #1

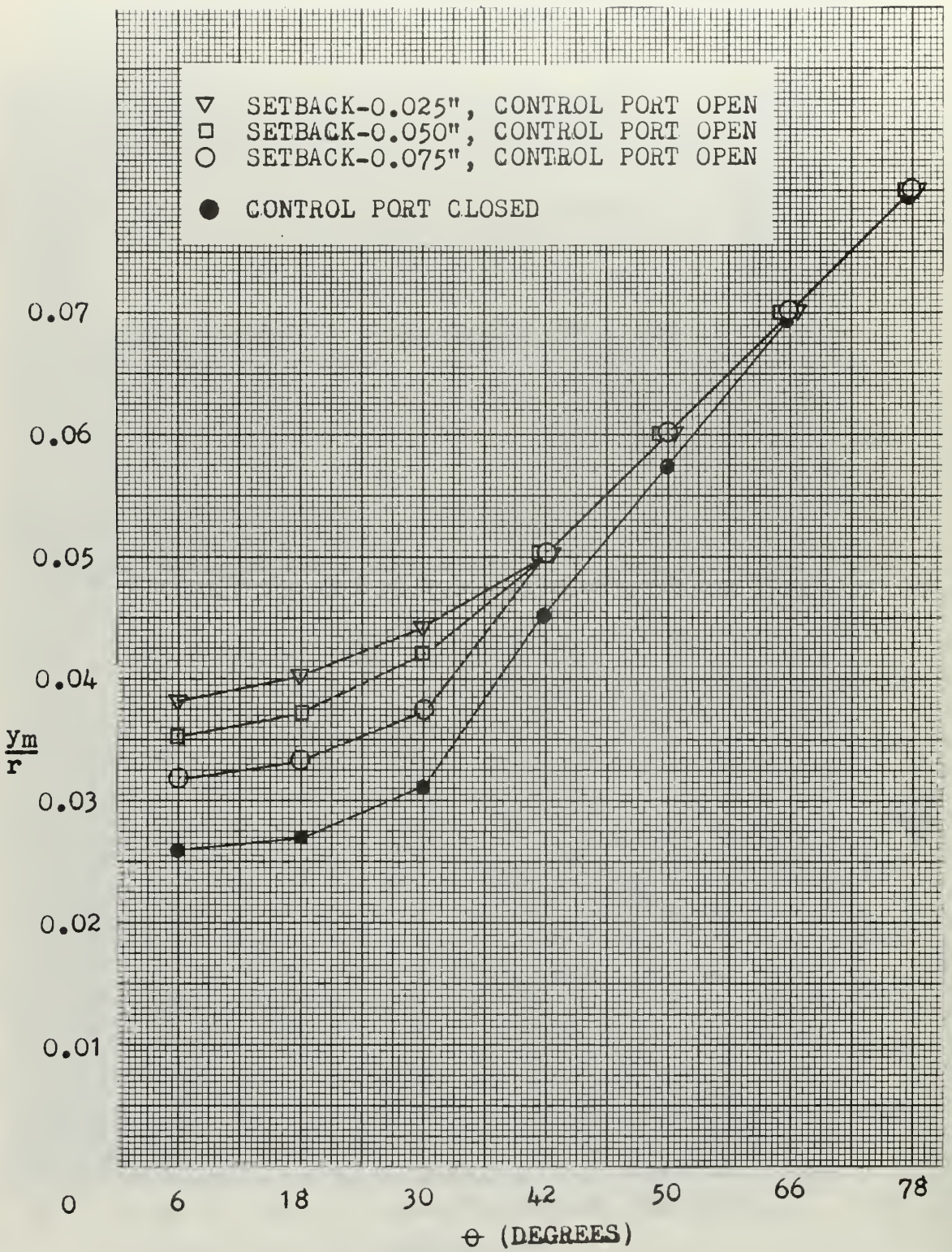

FIGURE 69. GROWTH OF y_m AROUND CONVEX WALL
TEST SECTION #1

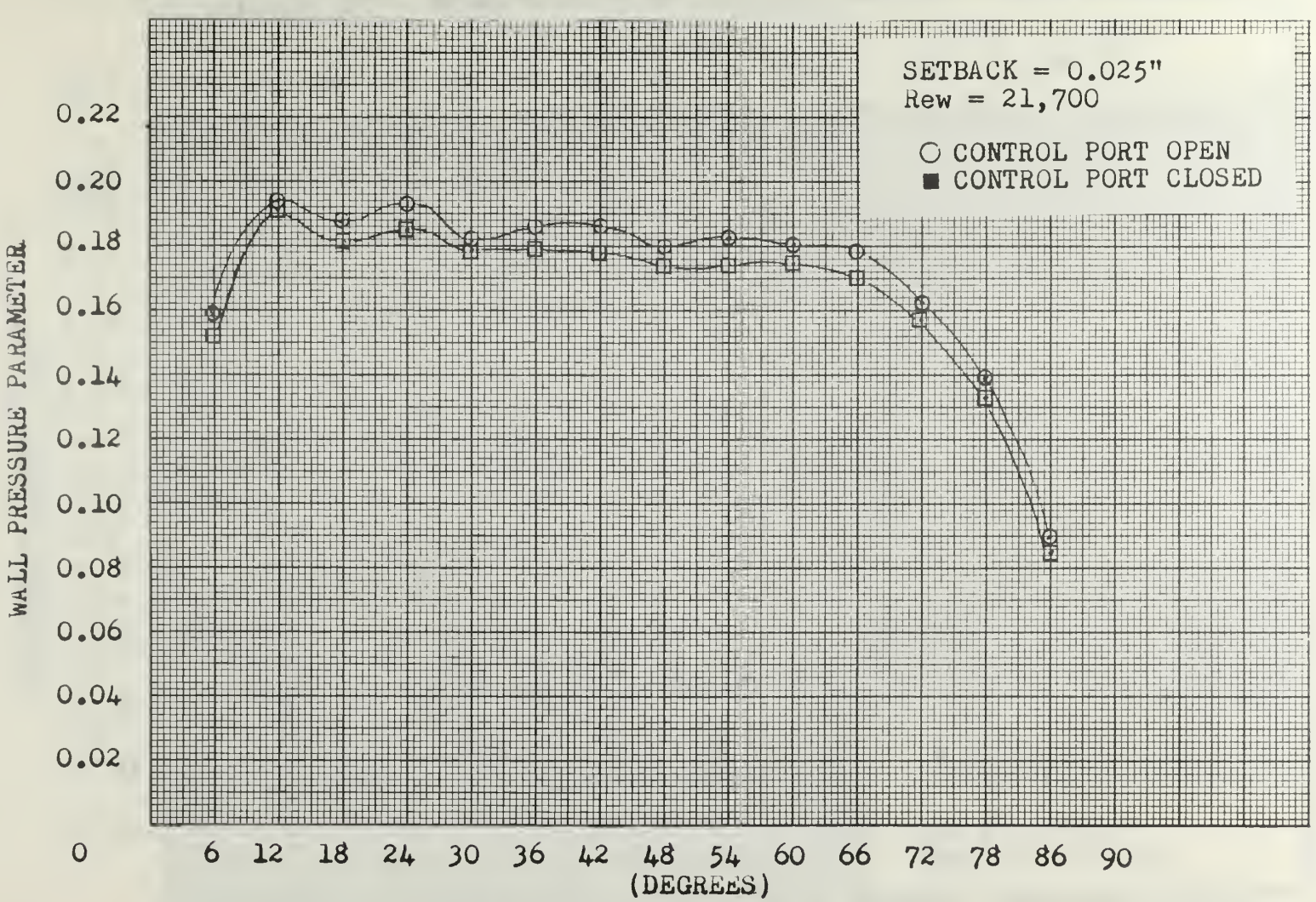

FIGURE 70. NORMALIZED WALL PRESSURE PROFILE - TEST SECTION #1

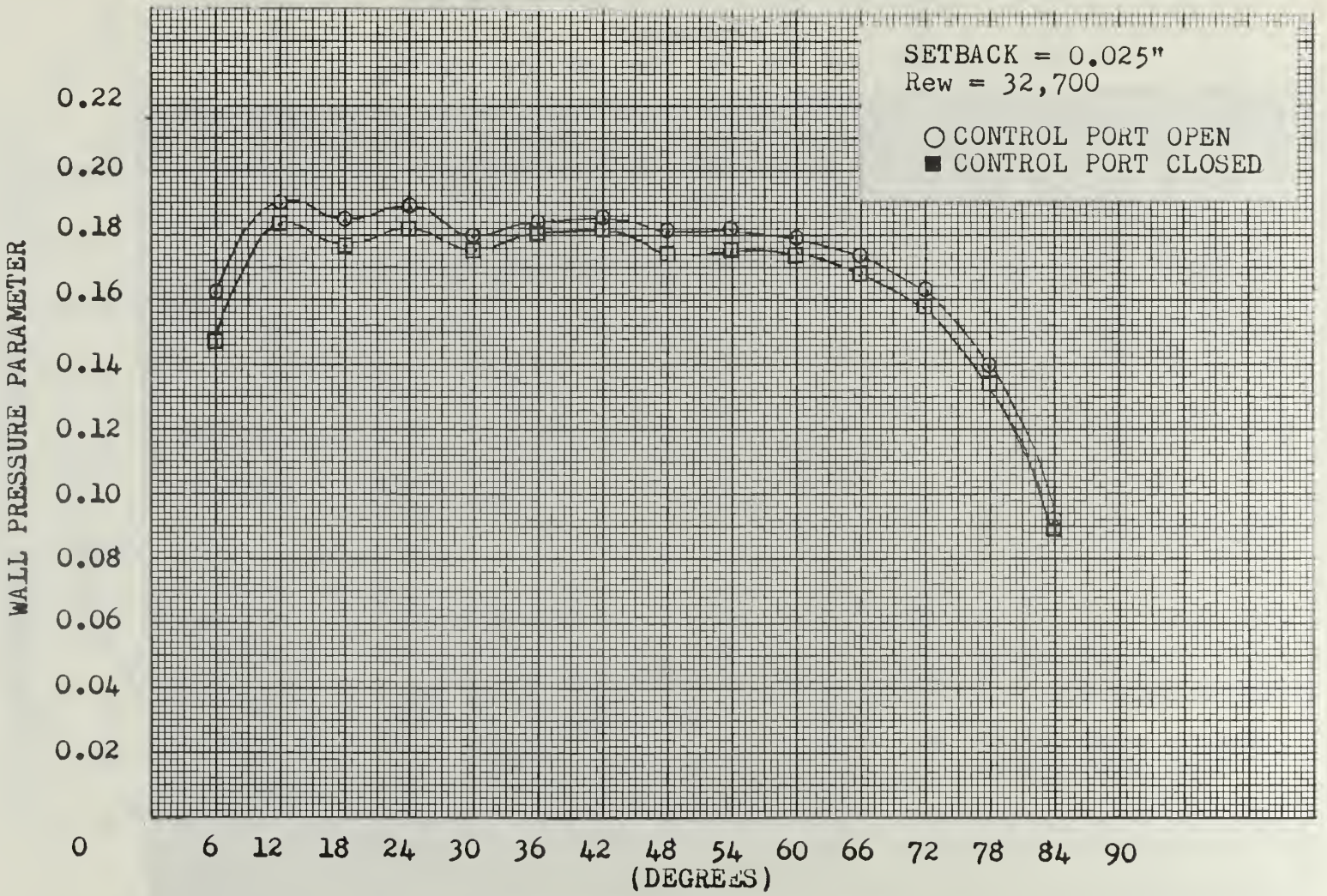

FIGURE 71. NORMALIZED WALL PRESSURE PROFILE - TEST SECTION #1

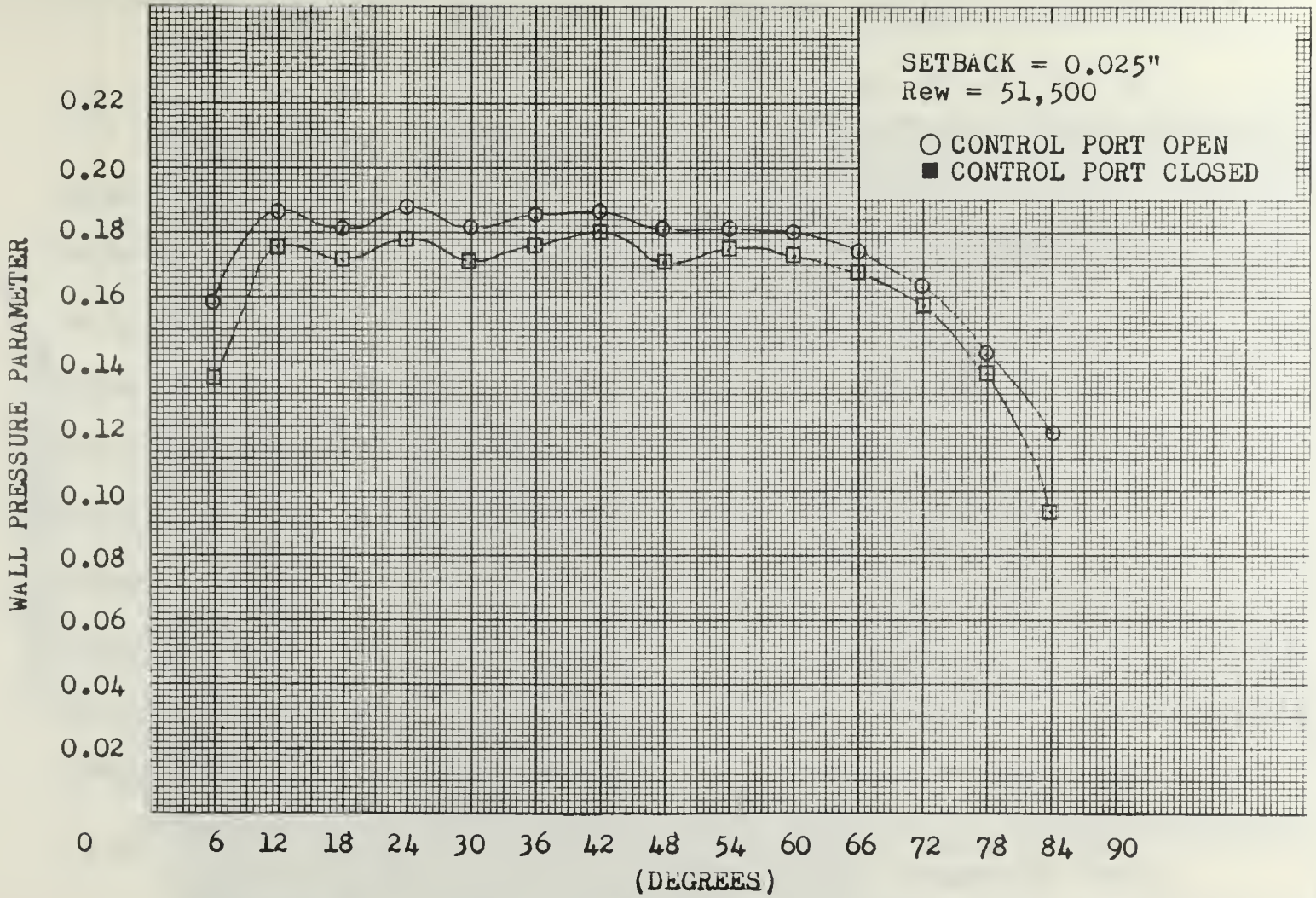

FIGURE 72. NORMALIZED WALL PRESSURE PROFILE - TEST SECTION #1.

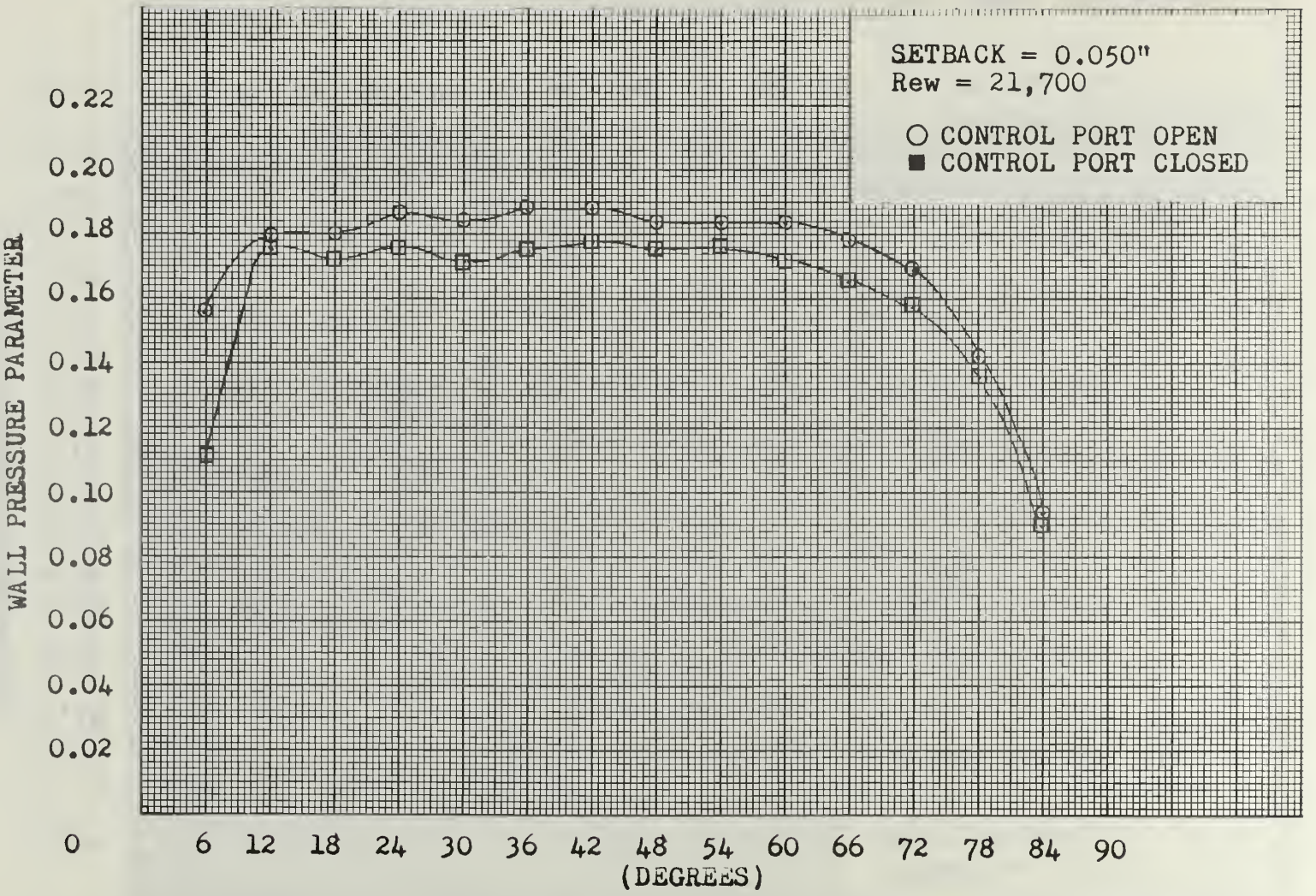

FIGURE 73. NORMALIZED WALL PRESSURE PROFILE - TEST SECTION #1

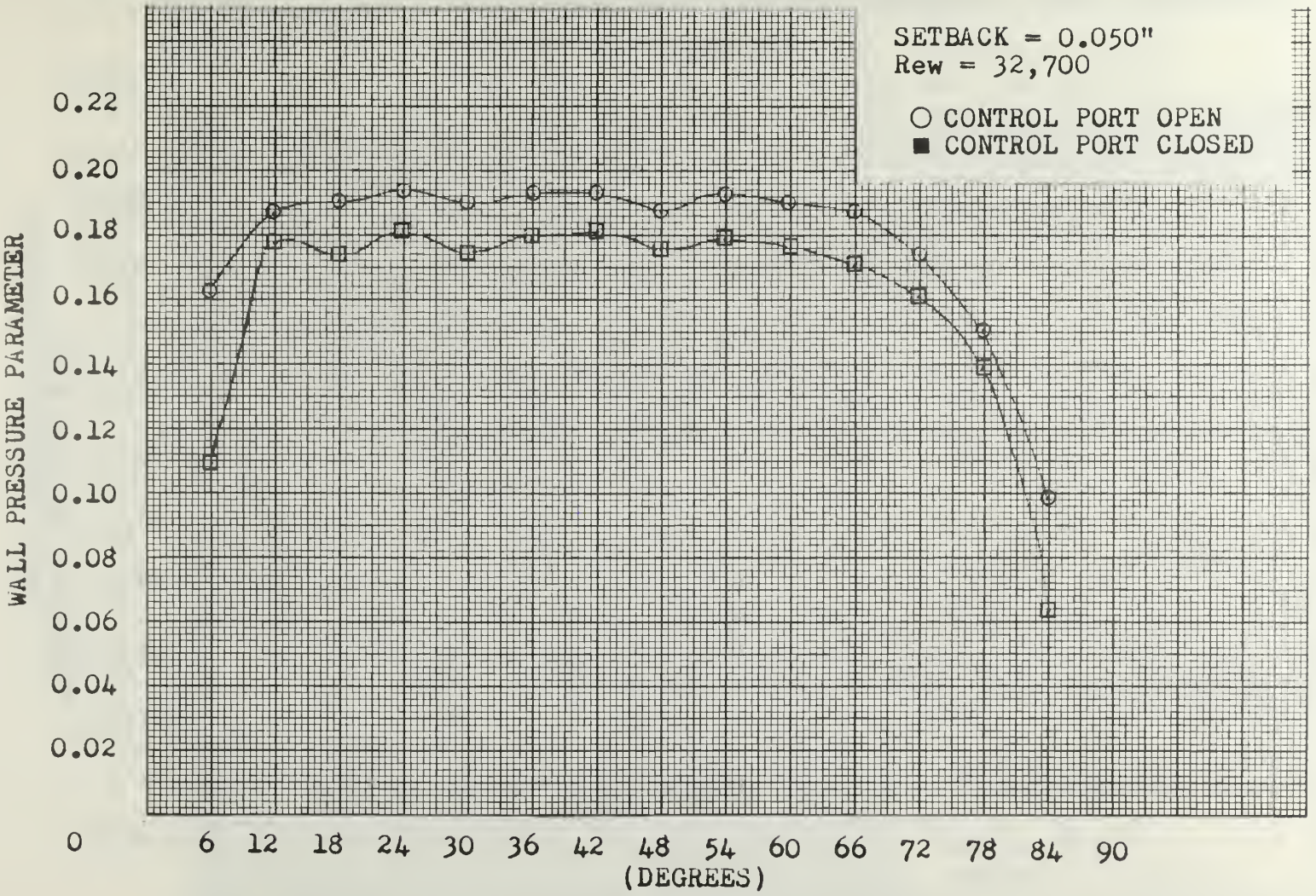

FIGURE 74. NORMALIZED WALL PRESSURE PROFILE - TEST SECTION # 1

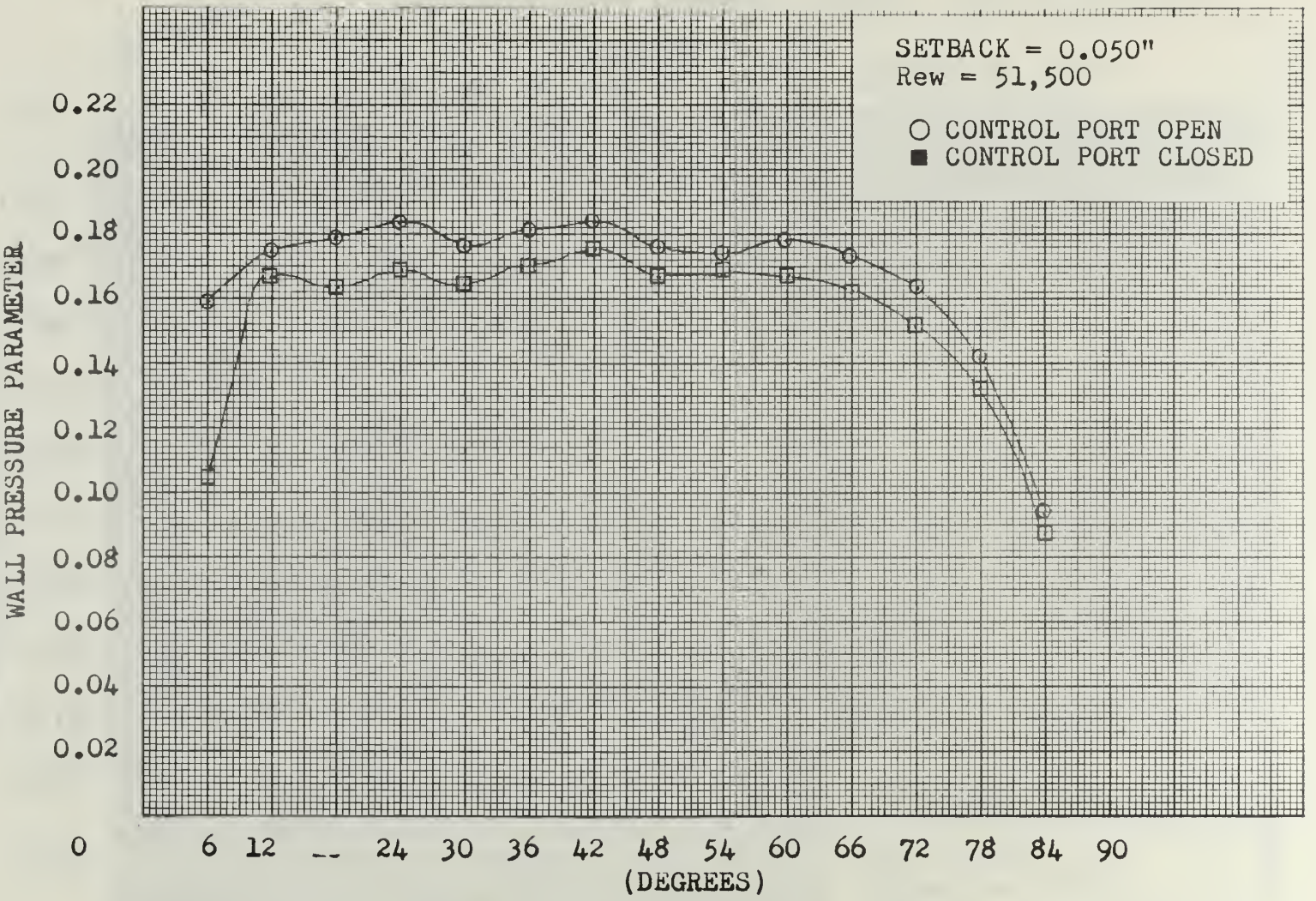

FIGURE 75. NORMALIZED WALL PRESSURE PROFILE - TEST SECTION #1

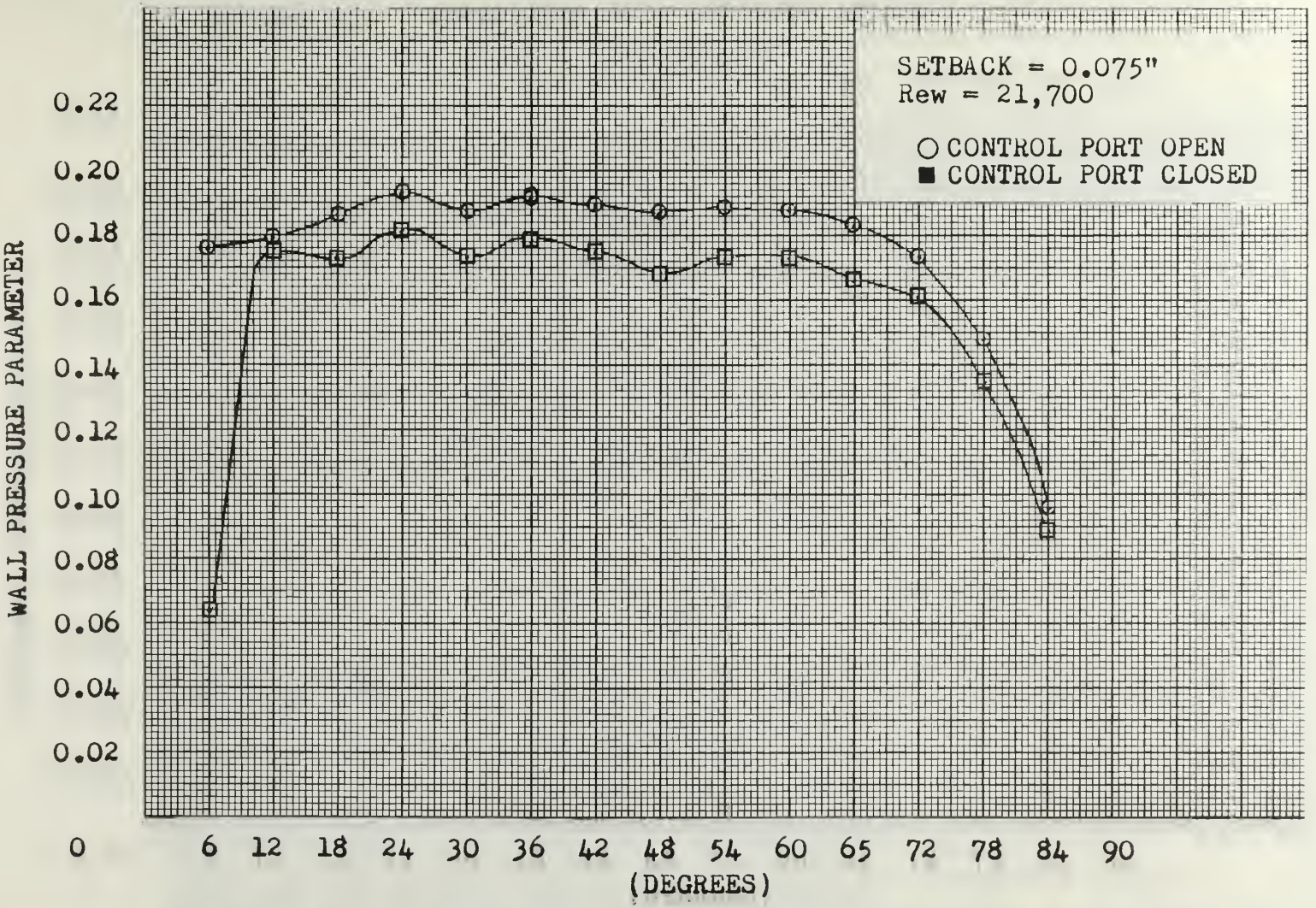

FIGURE 76. NORMALIZED WALL PRESSURE PROFILE - TEST SECTION #1

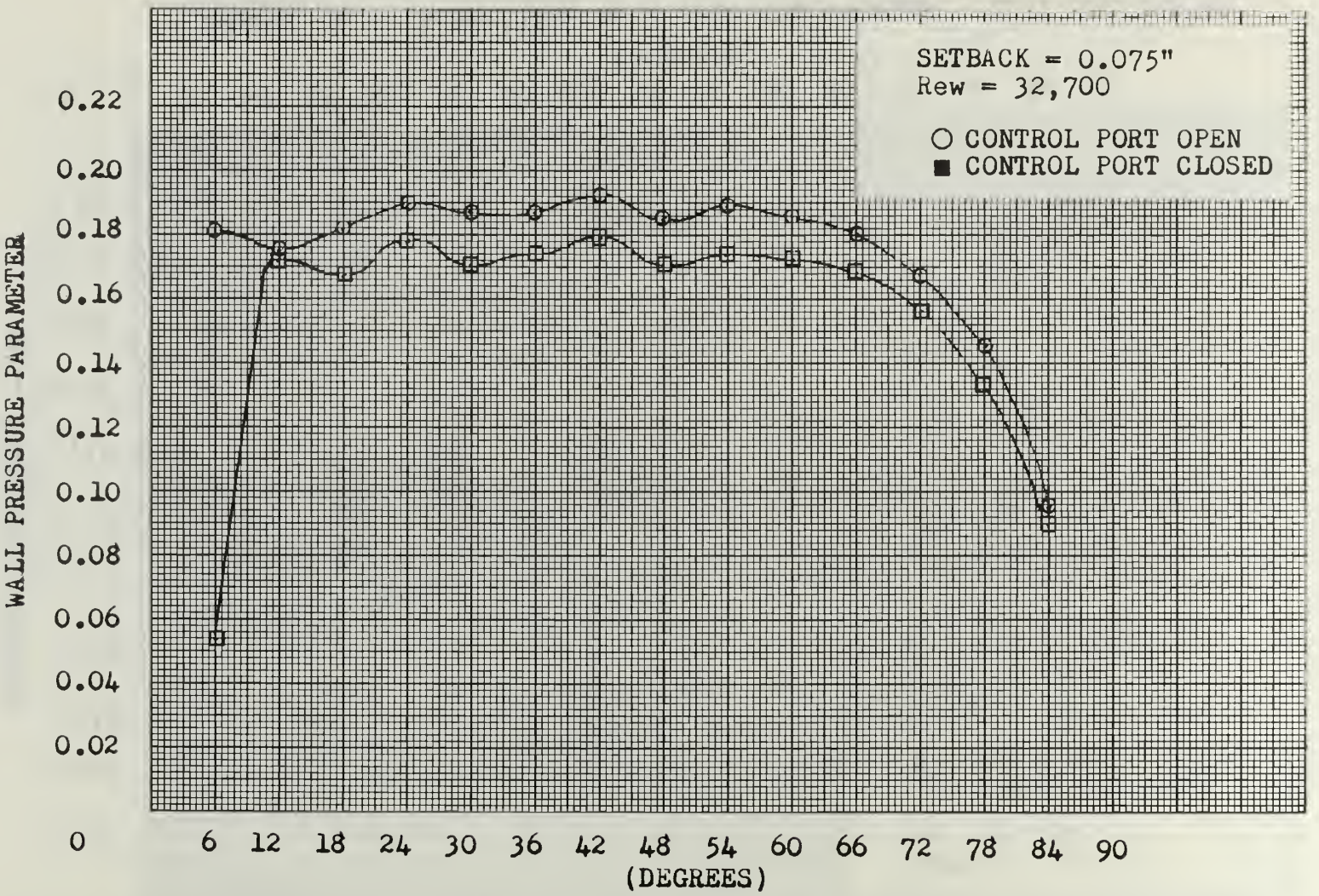

FIGURE 77. NORMALIZED WALL PRESSURE PROFILE - TEST SECTION #1

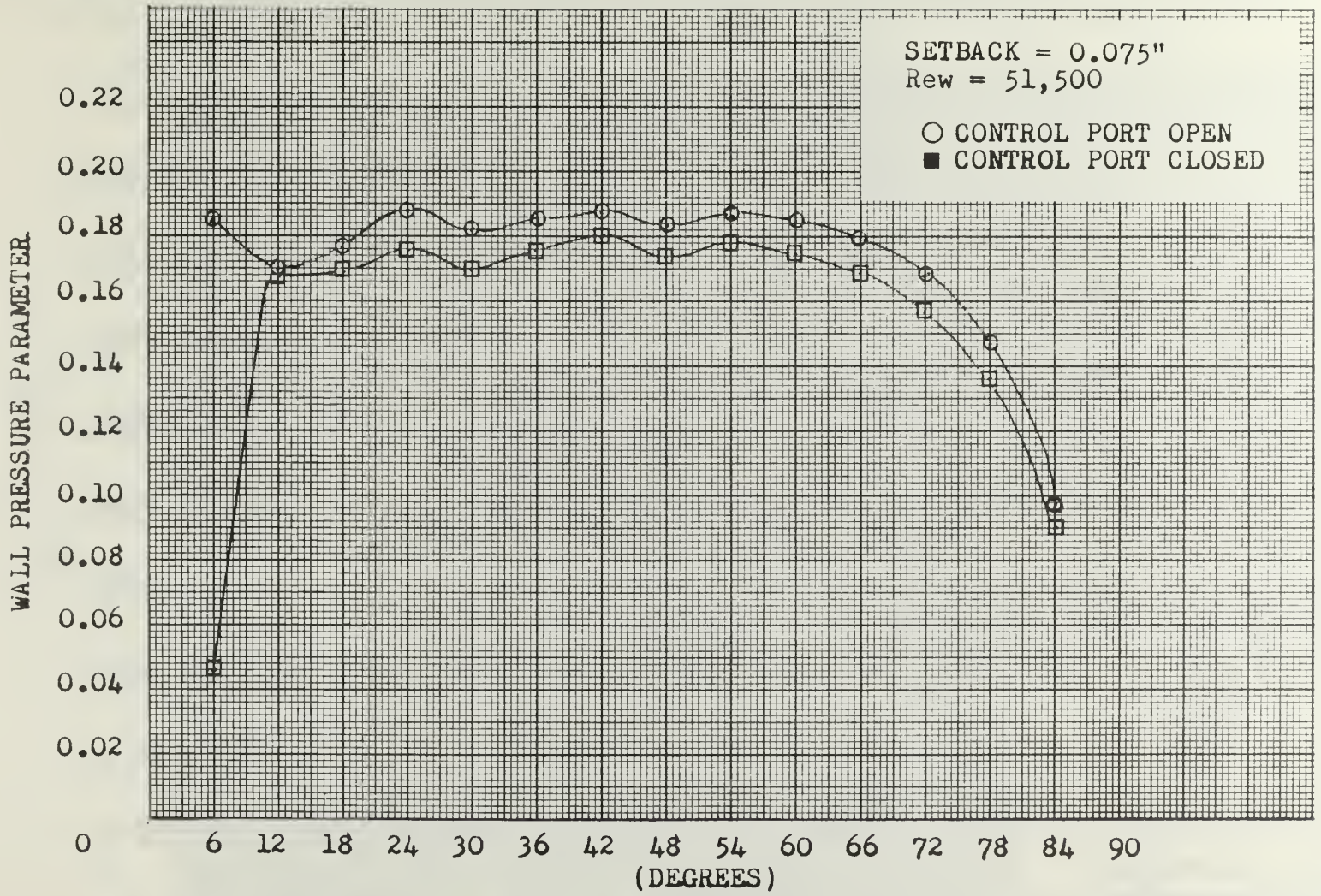

FIGURE 78. NORMALIZED WALL PRESSURE PROFILE - TEST SECTION #1

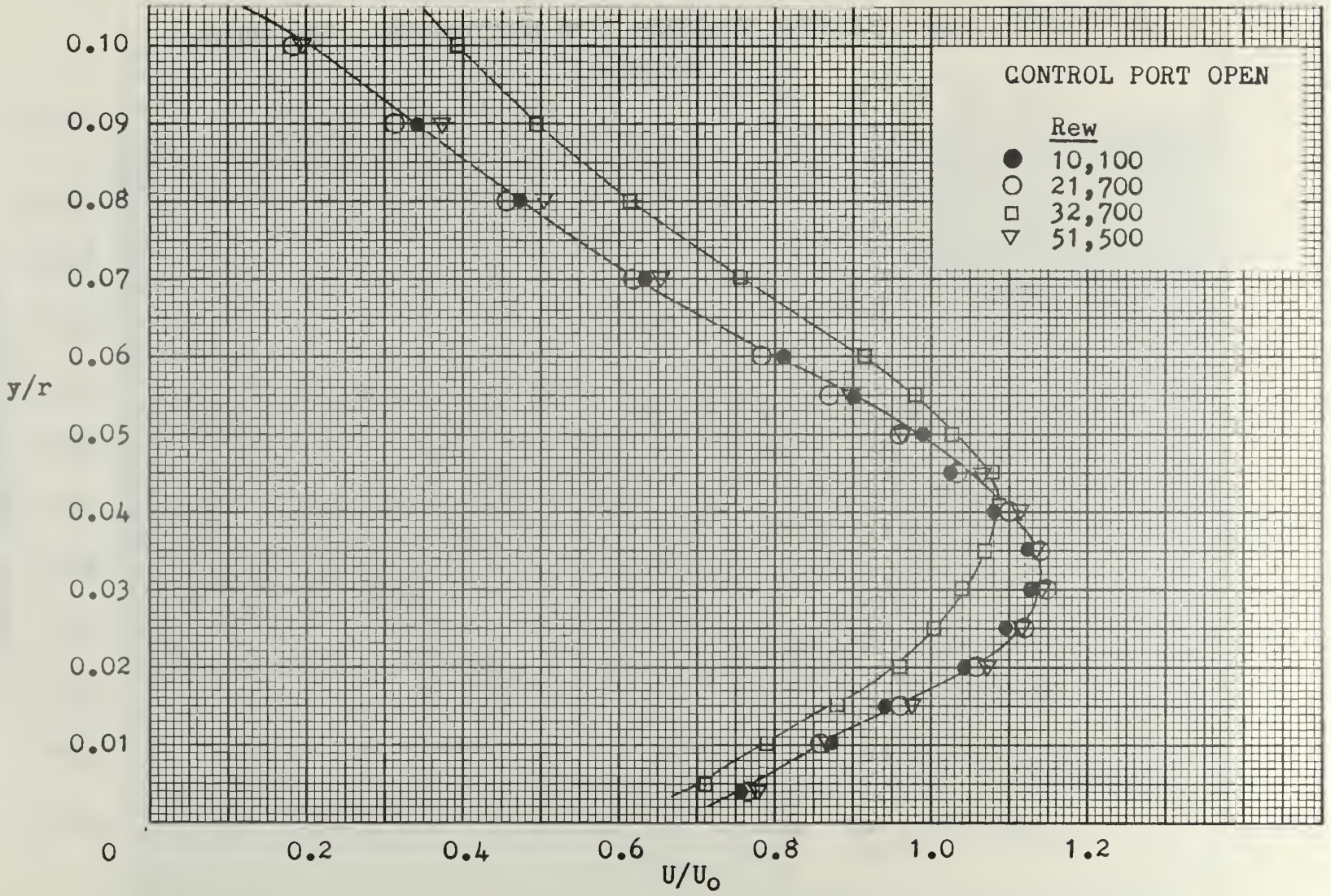

FIGURE 79. NORMALIZED VELOCITY PROFILE - TEST SECTION #3

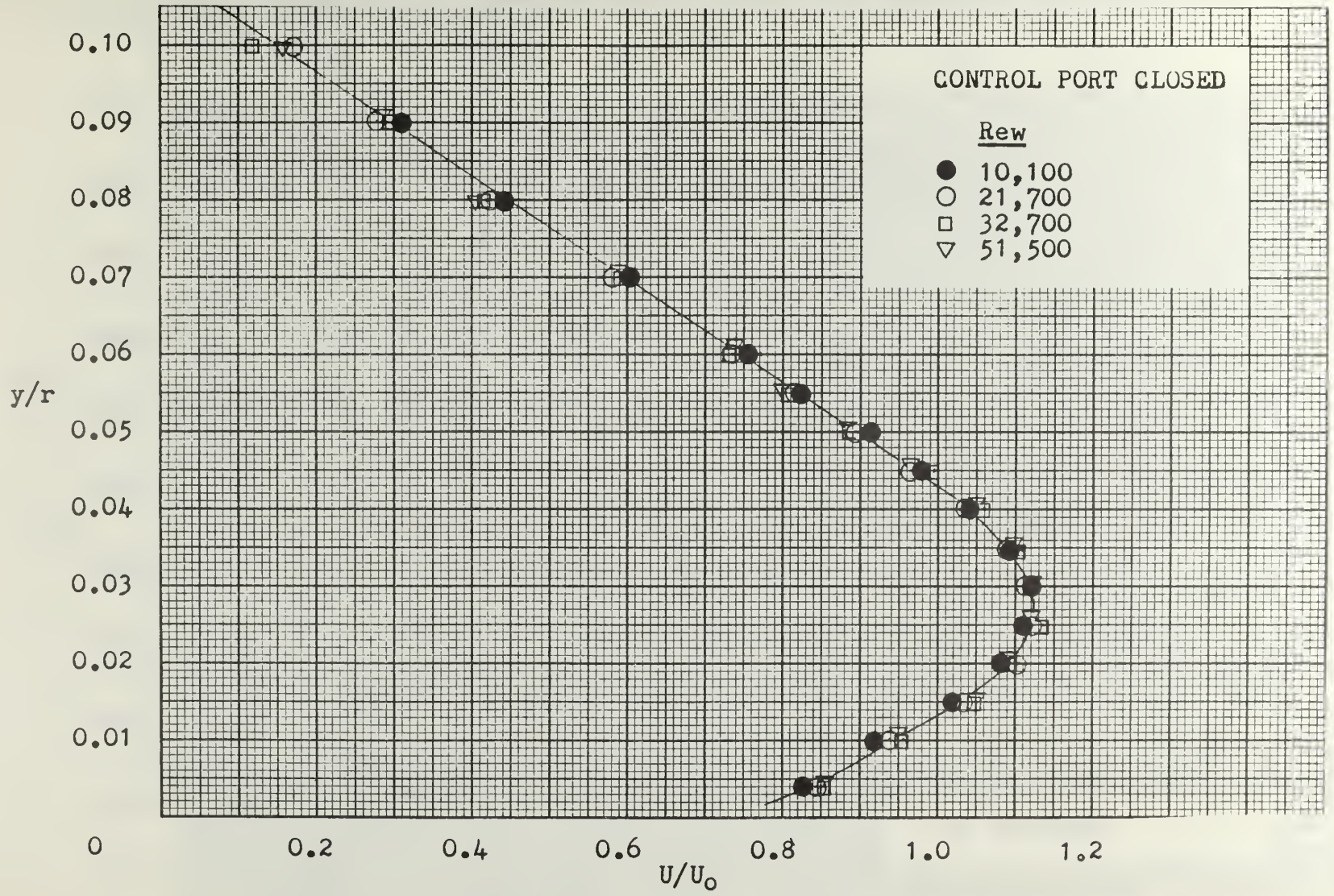

FIGURE 80. NORMALIZED VELOCITY PROFILES - TEST SECTION #3

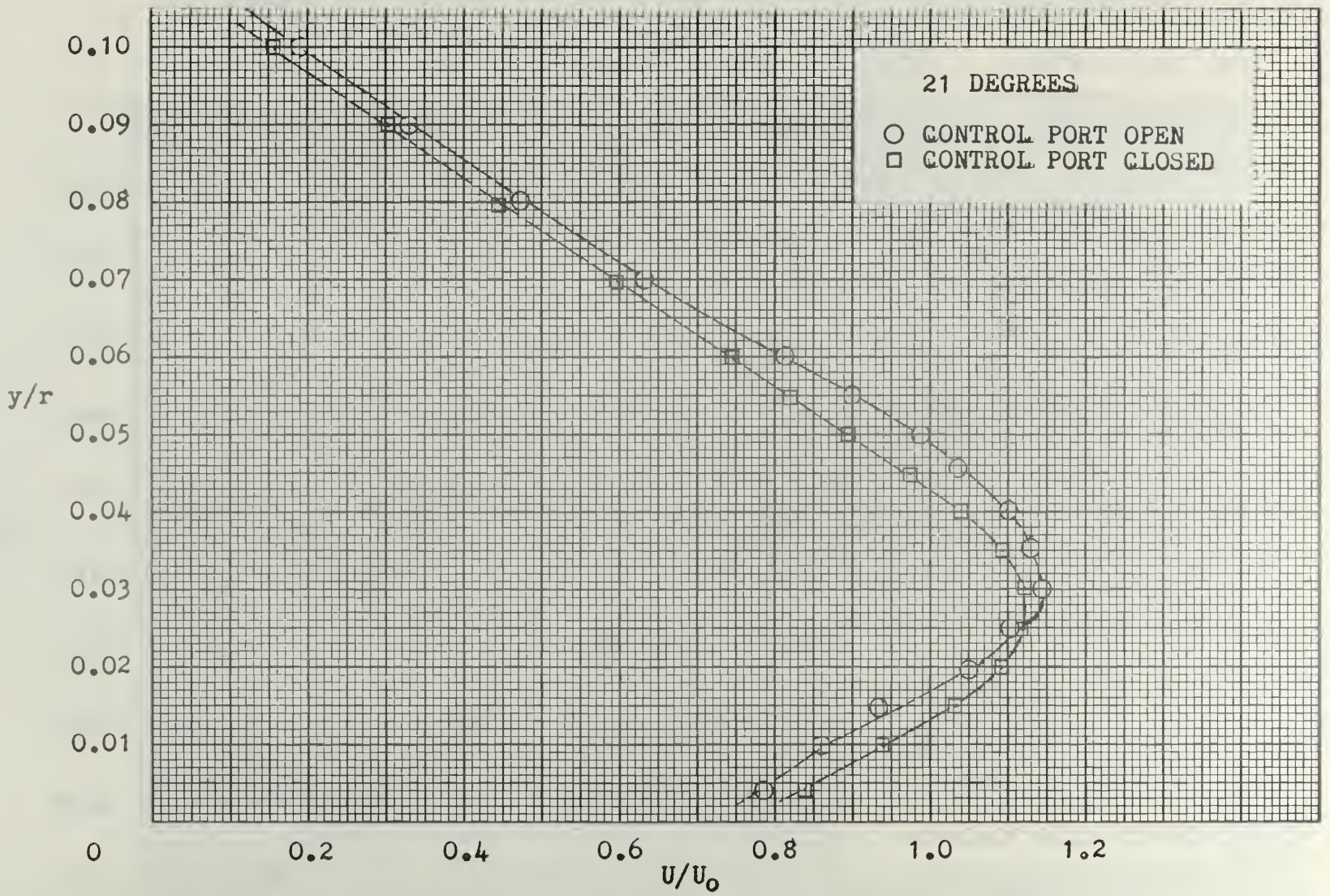

FIGURE 81. NORMALIZED VELOCITY PROFILE - TEST SECTION #3

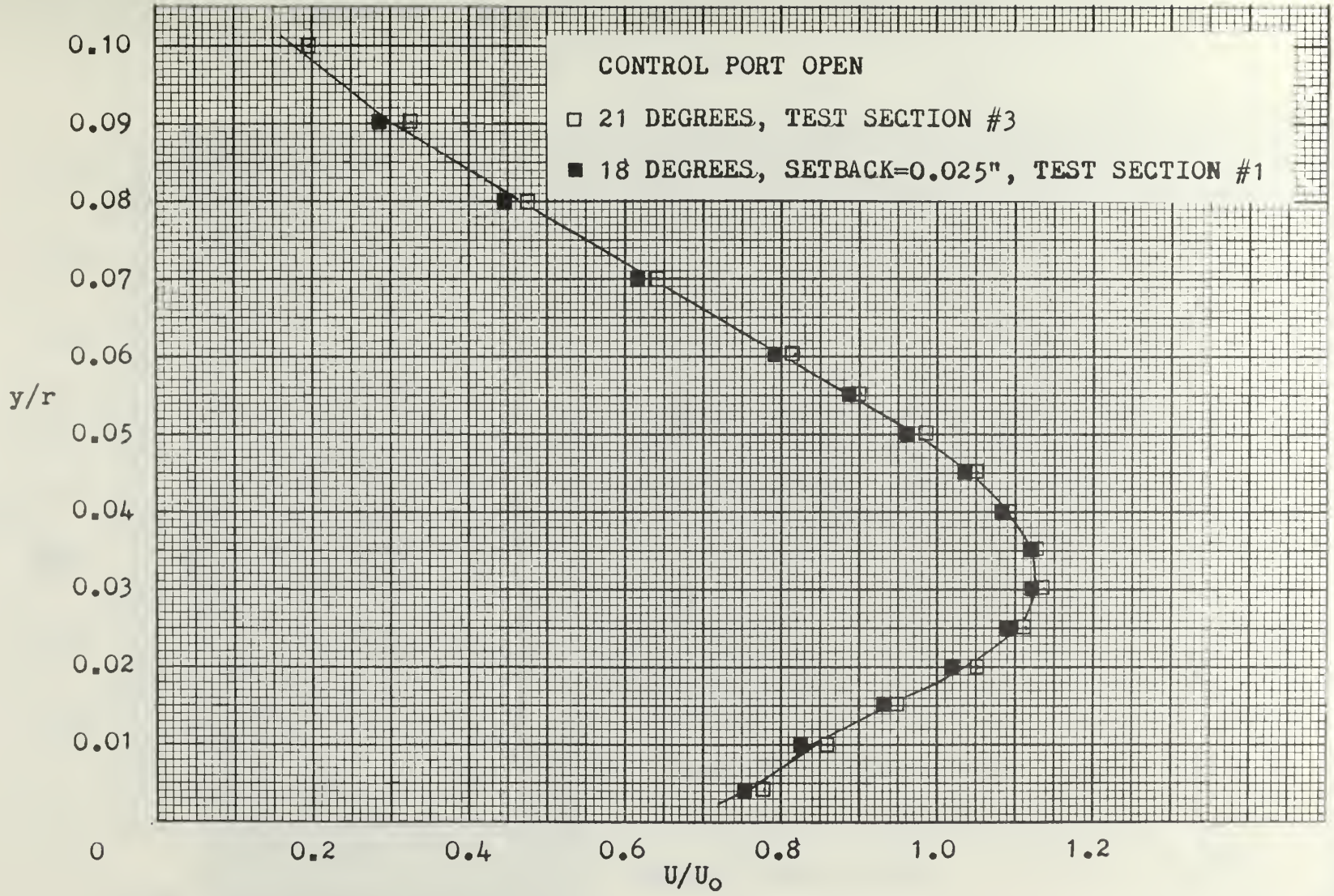

FIGURE 82. NORMALIZED VELOCITY PROFILE - TEST SECTION #3

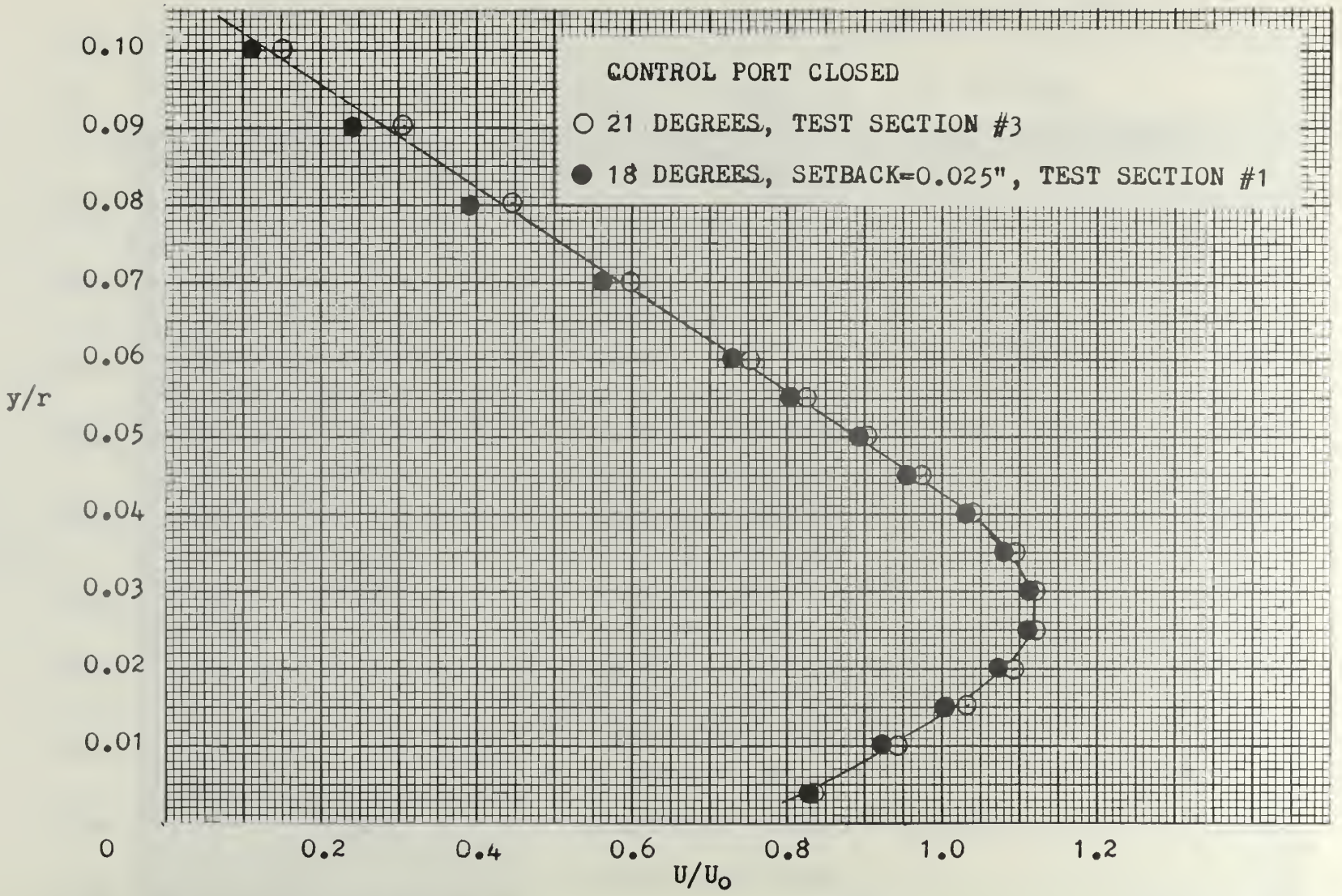

FIGURE 83. NORMALIZED VELOCITY PROFILE - TEST SECTION #3

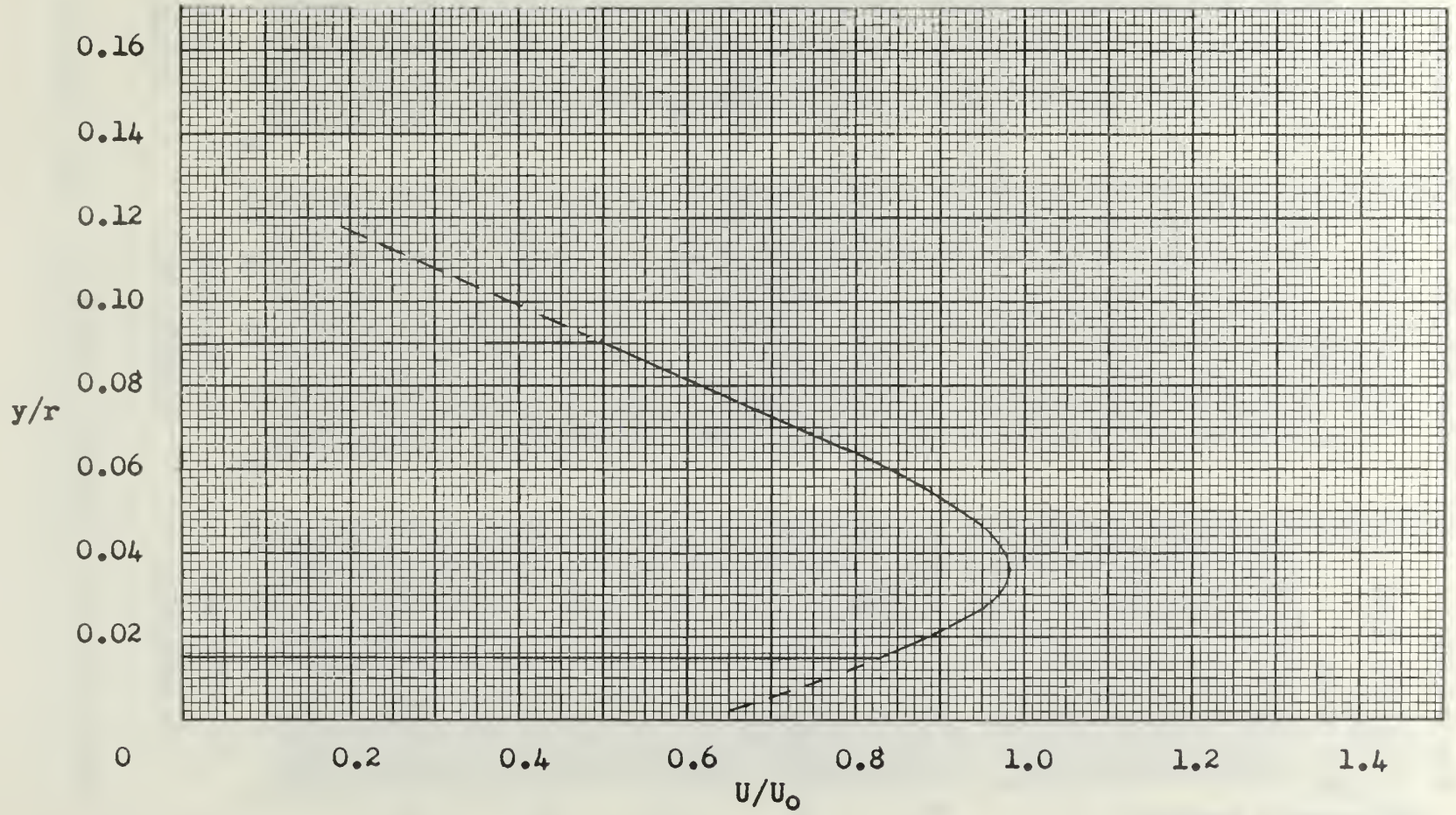

FIGURE 84. NORMALIZED VELOCITY PROFILE -TEST SECTION # 3

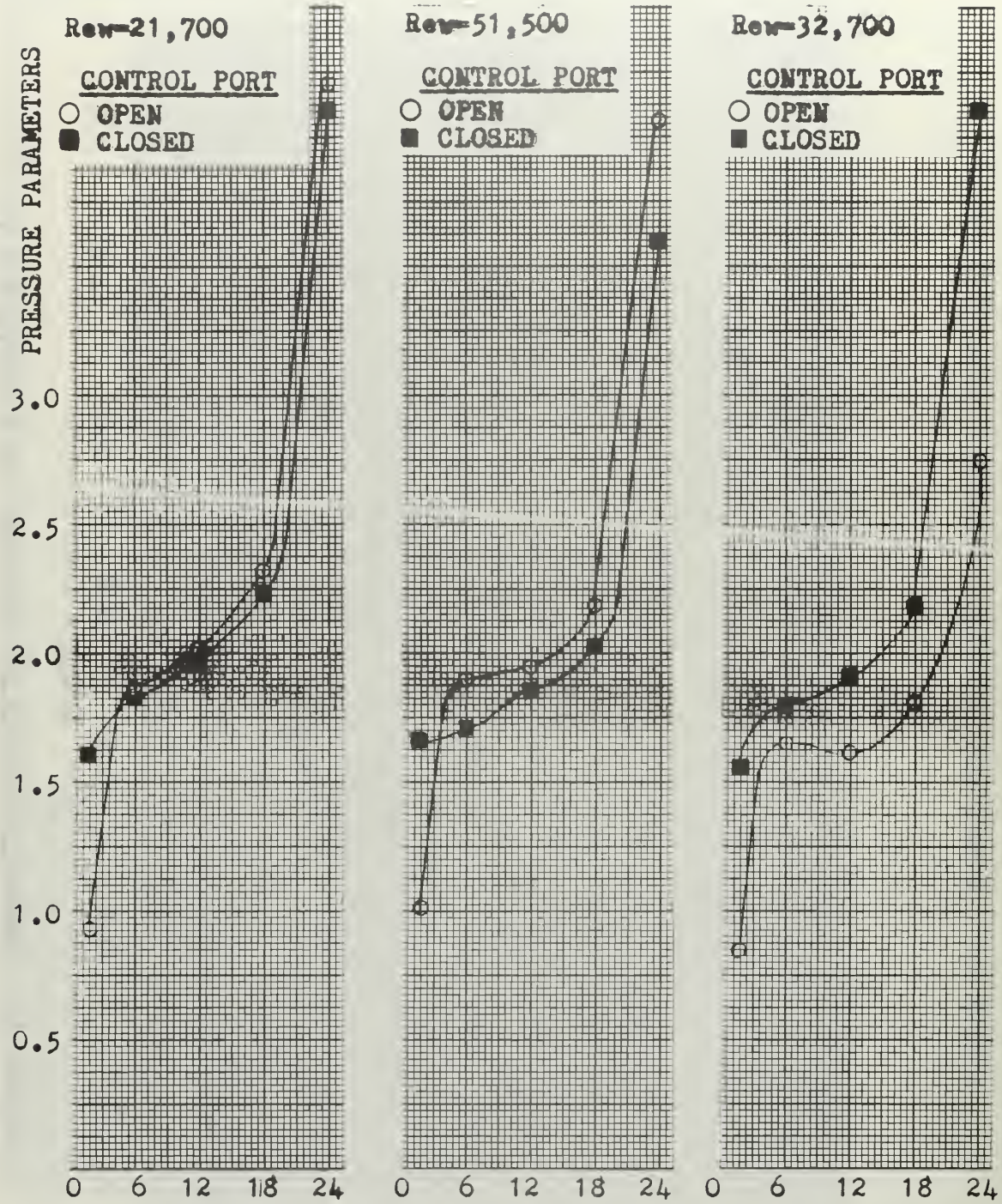

FIGURE 85. FIGURE 86. FIGURE 87.

NORMALIZED WALL PRESSURE PROFILES - TEST SECTION #3

INITIAL DISTRIBUTION LIST

		No. Copies
1.	Defense Documentation Center Cameron Station Alexandria, Virginia 22314	20
2.	Library Naval Postgraduate School Monterey, California 93940	2
3.	Naval Ship Systems Command (Code 2052) Navy Department Washington, D. C. 20360	1
4.	Mechanical Engineering Department Naval Postgraduate School Monterey, California 93940	2
5.	Professor T. Sarpkaya Chairman, Mechanical Engineering Department Naval Postgraduate School Monterey, California 93940	5
6.	LT L. D. Johnson, USN Ship Repair Facility, Guam, M. I. % FPO San Francisco 96630	3

DOCUMENT CONTROL DATA - R & D

Security classification of title, body of abstract and indexing annotation must be entered when the overall report is classified)

1. ORIGINATING ACTIVITY *(Corporate author)*
Naval Postgraduate School
Monterey, California 93940

2a. REPORT SECURITY CLASSIFICATION
Unclassified

2b. GROUP
NA

3. REPORT TITLE
Experimental Investigation of Turbulent Jet Attachment to a Convex Wall

4. DESCRIPTIVE NOTES *(Type of report and, inclusive dates)*
None

5. AUTHOR(S) *(First name, middle initial, last name)*
Larry Dean Johnson

6. REPORT DATE	7a. TOTAL NO. OF PAGES	7b. NO. OF REFS
September 1968	125	16

8a. CONTRACT OR GRANT NO.	9a. ORIGINATOR'S REPORT NUMBER(S)
NA	NA
b. PROJECT NO.	
c.	9b. OTHER REPORT NO(S) *(Any other numbers that may be assigned this report)*
d.	

10. DISTRIBUTION STATEMENT
[redacted]

11. SUPPLEMENTARY NOTES

12. SPONSORING MILITARY ACTIVITY
Naval Postgraduate School
Monterey, California 93940

13. ABSTRACT

The effects of geometry and Reynolds number on the attachment of an air jet to a circular convex wall and the mechanism of high pressure recovery in convex-walled amplifiers are investigated. The results are presented in terms of normalized parameters suitable for comparison with theoretical predictions. Extremely high pressure recoveries are possible in convex-walled amplifiers due to the particular velocity distribution and entrainment characteristics exhibited by flow attached to a convex wall. The wall setback and the condition of the control port have very little influence on the flow downstream of the initial attachment region.

14 KEY WORDS	LINK A		LINK B		LINK C	
	ROLE	WT	ROLE	WT	ROLE	WT
Fluidics						
Coanda Effect						
Fluid Amplifiers						

Gaylord
SHELF BINDER
Syracuse, N. Y.
Stockton, Calif.

thesJ6235
DUDLEY KNOX LIBRARY
3 2768 00414553 2
DUDLEY KNOX LIBRARY